Towards artificial photosynthesis on the lipid bilayer of liposomes

Klein, D.M.

Appendix A

Supporting information of Chapter 1

A.1. Experimental methods for studying photocatalytic vesicles

Table A1. Experimental techniques for the preparation, characterisation, and study of photocatalytic self-assembled membranes.

Experimental techniques	Information obtained	Reference(s)
Nuclear Magnetic Resonance (NMR)	– Nature and purity of membrane-embedded components – Stability of liposomes and membrane-embedded components – Photoproduct analysis and quantification (e.g. formate from CO_2 reduction)* – Position and diffusion of membrane-embedded components (Magic Angle Spinning NMR, MAS NMR)	1–5
Fourier Transform / Attenuated Total Reflectance Infrared Spectroscopy (FT/ATR-IR)	– Confirm presence/immobilisation of membrane components* – Lipid membrane phase transitions	6–9
Mass Spectrometry (MS, native and LC-MS, HPLC-MS)	– Characterisation of the membrane-immobilised components – Determination of reaction products and decomposition by-products of the membrane (lipid degradation)	10
Cryo Transmission Electron Microscopy (TEM), Cryo Scanning Electron Microscopy (SEM), Energy Dispersive X-ray Spectroscopy (EDX)	– Morphology and size of liposomes (cryo TEM, SEM) – Characterisation and quantification of metal-based membrane components (EDX) – Stability studies	11–13
Electron Paramagnetic Resonance (EPR)	– Determination of the physical properties (phase transition, fluidity) of a membrane – Determination of the pH at membranes – Study of oxygen transport in membranes (spin labels) – Study of oxidation of lipids in membranes	14–16

	– Characterisation of paramagnetic membrane-embedded components	
X-ray Photoelectron Spectroscopy (XPS)	– Characterisation and quantification of metal-based membrane components*	17, 18
UV-Vis spectroscopy	– Characterisation of electronic absorption properties of membrane-immobilised components – Characterisation of the filter effect – Stability of liposomes and membrane-embedded components	12, 19–32
Fluorescence/emission spectroscopy	– Characterisation of excited state energy of membrane-embedded components – Stability of liposomes and membrane-embedded components – Transition temperature of heterogenous mixture of lipids/molecules	6, 10, 11, 21, 22, 24, 26–28, 32–35
Time-resolved absorption or emission spectroscopy	– Determination of excited state lifetime of membrane-embedded photoactive components – Analysis of the binding of immobilised components within the liposome assembly – Nature and kinetics of reactive intermediate species during photocatalysis (mechanism)	11, 20, 22, 24, 28, 30, 32, 33, 36, 37
Single-molecule fluorescence microscopy	– Determination of the lipid lateral diffusion in membranes	38
Differential Scanning Calorimetry (DSC) and fluorescence anisotropy	– Determination of the membrane transition temperature	11, 39
Dynamic and static light scattering	– Hydrodynamic diameter of liposomes – Surface charge of liposomes / zeta (ζ) potential – Stability of liposomes and membrane-embedded components	6, 12, 19, 23, 25–29, 32, 34, 40, 41
Nanoparticle tracking analysis	– Concentration and size distribution of liposomes	19
Atomic Force Microscopy (AFM)	– Analysis of the surface of liposomes	13, 42
Inductively Coupled Plasma - Mass Spectrometry (ICP-MS), Atomic Emission Spectroscopy (ICP-AES), Optical Emission Spectroscopy (ICP-OES)	– Quantification of metal content (synthetic molecules and enzymes)	23, 43, 44
Confocal microscopy	– Assessment of membrane-embedding of luminescent components (only in giant unilamellar vesicles)	1, 13, 32, 34, 35

Extrusion kit (syringes, polycarbonate extrusion filters, etc.)	–	Prepare monodispersed liposome solutions	6, 10, 11, 21–23, 25, 29, 32–34, 40, 41, 45
Cyclic voltammetry	–	Electrochemical characterisation of lipid membrane-embedded components (quantification, stability, activity)*	8, 37, 46–49
Sonicator, ultrasonicator	–	Preparation of small unilamellar liposomes	6, 11, 12, 20, 24, 26–28, 45
Rotary evaporator and liquid N_2 Dewar	–	Preparation of liposomes (before hydration/self-assembly) and storage	12, 21–23, 25, 32, 34, 45
Column chromatography (e.g. size exclusion gel filtration, affinity columns, desalting column, etc.)	–	Purification of proteo-liposomes or liposomes after self-assembly with newly immobilised synthetic components	6, 10, 19, 20, 22, 23, 25, 26, 32, 34, 41, 45
Light source (e.g. LED 450 nm for $[Ru(bpy)_3]^{2+}$; sunlight simulator $\lambda > 400$ nm, Xe lamp, 100 mW cm^{-2}, AM 1.5G)	–	Light irradiation for photocatalytic experiments	12, 21, 22, 24–28, 30–32, 35, 37
Fluorescence O_2 probe or Clarke electrode	–	Quantification of O_2	12
Gas Chromatography (GC)	–	Product analyses and quantification (gaseous product e.g. H_2, O_2, CO)	12, 26–28, 30, 31
Ion Chromatography (IC)	–	Product analyses and quantification (charged ions e.g. formate)*	5
Osmometer	–	Determination of osmolarity of buffer solution containing components (for preparing asymmetric liposomes)	12,25

* Universal method, mainly used in homogeneous or heterogeneous systems.

A.2. References

1 D. K. Weber, M.-A. Sani, M. T. Downton, F. Separovic, F. R. Keene and J. G. Collins, *J. Am. Chem. Soc.*, 2016, **138**, 15267–15277.

2 C. Ader, R. Schneider, K. Seidel, M. Etzkorn and M. Baldus, *Biochem. Soc. Trans.*, 2007, **35**, 991–995.

3 H. A. Scheidt and D. Huster, *Acta Pharmacol. Sin.*, 2008, **29**, 35–49.

4 S. F. Rowe, G. Le Gall, E. V Ainsworth, J. A. Davies, C. W. J. Lockwood, L. Shi, A. Elliston, I. N. Roberts, K. W. Waldron, D. J. Richardson, T. A. Clarke, L. J. C. Jeuken, E. Reisner and J. N. Butt, *ACS Catal.*, 2017, **7**, 7558–7566.

5 Q. Wang, J. Warnan, S. Rodríguez-Jiménez, J. J. Leung, S. Kalathil, V. Andrei, K. Domen and E. Reisner, *Nat. Energy*, 2020, **5**, 703–710.

6 L. M. Hays, J. H. Crowe, W. Wolkers and S. Rudenko, *Cryobiology*, 2001, **42**,

88–102.
7 A. F. A. Aisha, A. M. S. A. Majid and Z. Ismail, *BMC Biotechnol.*, 2014, **14**, 23.
8 N. Kornienko, K. H. Ly, W. E. Robinson, N. Heidary, J. Z. Zhang and E. Reisner, *Acc. Chem. Res.*, 2019, **52**, 1439–1448.
9 X. Fang, K. P. Sokol, N. Heidary, T. A. Kandiel, J. Z. Zhang and E. Reisner, *Nano Lett.*, 2019, **19**, 1844–1850.
10 I. O. L. Bacellar, M. C. Oliveira, L. S. Dantas, E. B. Costa, H. C. Junqueira, W. K. Martins, A. M. Durantini, G. Cosa, P. Di Mascio, M. Wainwright, R. Miotto, R. M. Cordeiro, S. Miyamoto and M. S. Baptista, *J. Am. Chem. Soc.*, 2018, **140**, 9606–9615.
11 M. Andersson, L. Hammarström and K. Edwards, *J. Phys. Chem.*, 1995, **99**, 14531–14538.
12 B. Limburg, J. Wermink, S. S. van Nielen, R. Kortlever, M. T. M. Koper, E. Bouwman and S. Bonnet, *ACS Catal.*, 2016, **6**, 5968–5977.
13 B. Ruozi, D. Belletti, A. Tombesi, G. Tosi, L. Bondioli, F. Forni and M. A. Vandelli, *Int. J. Nanomedicine*, 2011, **6**, 557–563.
14 M. A. Voinov, I. Rivera-Rivera and A. I. Smirnov, *Biophys. J.*, 2013, **104**, 106–116.
15 A. Ligeza, A. N. Tikhonov, J. S. Hyde and W. K. Subczynski, *Biochim. Biophys. Acta - Bioenerg.*, 1998, **1365**, 453–463.
16 S. P. Gabbita, D. A. Butterfield, K. Hensley, W. Shaw and J. M. Carney, *Free Radic. Biol. Med.*, 1997, **23**, 191–201.
17 M. K. Baumann, E. Amstad, A. Mashaghi, M. Textor and E. Reimhult, *Biointerphases*, 2010, **5**, 114–119.
18 K. Eleršič, J. I. Pavlič, A. Iglič, A. Vesel and M. Mozetič, *Chem. Phys. Lipids*, 2012, **165**, 120–124.
19 A. Stikane, E. T. Hwang, E. V. Ainsworth, S. E. H. Piper, K. Critchley, J. N. Butt, E. Reisner and L. J. C. Jeuken, *Faraday Discuss.*, 2019, **215**, 26–38.
20 L. Hammarström, H. Berglund and M. Almgren, *J. Phys. Chem.*, 1994, **98**, 9588–9593.
21 A. Perez-Velasco, V. Gorteau and S. Matile, *Angew. Chemie Int. Ed.*, 2008, **47**, 921–923.
22 S. Bhosale, A. L. Sisson, P. Talukdar, A. Fürstenberg, N. Banetji, E. Vauthey, G. Bollot, J. Mareda, C. Röger, F. Würthner, N. Sakai and S. Matile, *Science*, 2006, **313**, 84–86.
23 A. Bahreman, M. Rabe, A. Kros, G. Bruylants and S. Bonnet, *Chem. Eur. J.*, 2014, **20**, 7429–7438.
24 L. Hammarström, T. Norrby, G. Stenhagen, J. Mårtensson, B. Åkermark and M. Almgren, *J. Phys. Chem. B*, 1997, **101**, 7494–7504.
25 B. Limburg, E. Bouwman and S. Bonnet, *Chem. Commun.*, 2015, **51**, 17128–17131.
26 S. Troppmann and B. König, *Chem. Eur. J.*, 2014, **20**, 14570–14574.
27 M. Hansen, F. Li, L. Sun and B. König, *Chem. Sci.*, 2014, **5**, 2683–2687.
28 N. Ikuta, S. Y. Takizawa and S. Murata, *Photochem. Photobiol. Sci.*, 2014, **13**,

691–702.
29 B. Limburg, E. Bouwman and S. Bonnet, *J. Phys. Chem. B*, 2016, **120**, 6969–6975.
30 Y. Amao and I. Okura, *J. Mol. Catal. A Chem.*, 1996, **105**, 125–130.
31 N. Sugiyama, M. Toyoda and Y. Amao, *Colloids Surf A Physicochem. Eng. Asp.*, 2006, **284**–**285**, 384–387.
32 A. Pannwitz, H. Saaring, N. Beztsinna, X. Li, M. A. Siegler and S. Bonnet, *Chem. Eur. J.*, 2021, **27**, 3013-3018.
33 P. Jurkiewicz, L. Cwiklik, A. Vojtíšková, P. Jungwirth and M. Hof, *Biochim. Biophys. Acta - Biomembr.*, 2012, **1818**, 609–616.
34 B. Maherani, E. Arab-Tehrany, A. Kheirolomoom, D. Geny and M. Linder, *Biochimie*, 2013, **95**, 2018–2033.
35 E. Altamura, F. Milano, R. R. Tangorra, M. Trotta, O. H. Omar, P. Stano and F. Mavelli, *Proc. Natl. Acad. Sci. U. S. A.*, 2017, **114**, 3837–3842.
36 M. J. Llansola-Portoles, D. Gust, T. A. Moore and A. L. Moore, *C. R. Chim.*, 2017, **20**, 296–313.
37 R. Becker, T. Bouwens, E. C. F. Schippers, T. van Gelderen, M. Hilbers, S. Woutersen and J. N. H. Reek, *Chem. Eur. J.*, 2019, **25**, 13921–13929.
38 M. J. Murcia, S. Garg and C. A. Naumann, in *Methods in Membrane Lipids*, ed. A. M. Dopico, Humana Press, Totowa, NJ, 2007, pp. 277–294.
39 S. H. C. Askes, P. Brodie, G. Bruylants and S. Bonnet, *J. Phys. Chem. B*, 2017, **121**, 780–786.
40 J. Sabín, G. Prieto, J. M. Ruso, R. Hidalgo-Álvarez and F. Sarmiento, *Eur. Phys. J. E*, 2006, **20**, 401–408.
41 S. Paula, A. G. Volkov, A. N. van Hoek, T. H. Haines and D. W. Deamer, *Biophys. J.*, 1996, **70**, 339–348.
42 J. Flores, B. M. White, R. J. Brea, J. M. Baskin and N. K. Devaraj, *Chem. Soc. Rev.*, 2020, **49**, 4602–4614.
43 I. S. Dovydenko, Y. A. Laricheva, K. V. Korchagina, A. E. Grigoryeva, E. I. Ryabchikova, N. B. Kompankov, D. P. Pischur, A. L. Gushchin, E. K. Apartsin and M. N. Sokolov, *J. Phys. Chem. B*, 2019, **123**, 8829–8837.
44 C. Verdiá-Báguena, A. Alcaraz, V. M. Aguilella, A. M. Cioran, S. Tachikawa, H. Nakamura, F. Teixidor and C. Viñas, *Chem. Commun.*, 2014, **50**, 6700–6703.
45 A. Akbarzadeh, R. Rezaei-Sadabady, S. Davaran, S. W. Joo, N. Zarghami, Y. Hanifehpour, M. Samiei, M. Kouhi and K. Nejati-Koshki, *Nanoscale Res. Lett.*, 2013, **8**, 102.
46 G. R. Heath, M. Li, H. Rong, V. Radu, S. Frielingsdorf, O. Lenz, J. N. Butt and L. J. C. Jeuken, *Adv. Funct. Mater.*, 2017, **27**, 1606265.
47 L. N. Pelster and S. D. Minteer, *ACS Catal.*, 2016, **6**, 4995–4999.
48 T. Laftsoglou and L. J. C. Jeuken, *Chem. Commun.*, 2017, **53**, 3801–3809.
49 Ó. Gutiérrez-Sanz, P. Natale, I. Márquez, M. C. Marques, S. Zacarias, M. Pita, I. A. C. Pereira, I. López-Montero, A. L. De Lacey and M. Vélez, *Angew. Chemie Int. Ed.*, 2016, **55**, 6216–6220.

Appendix B

Supporting information of Chapter 2

B. 1. Material and methods

Materials and reagents: All reagents were obtained from Sigma-Aldrich and used as received unless stated otherwise. Fmoc-L-Ala-Wang TentaGel S resin was obtained from Iris Biotech GmbH. DPPC was obtained from Avanti Polar Lipids and stored at −20 °C. NaDSPE-PEG2K was purchased from Lipoid and stored at −20 °C. 4-(bromomethyl)-4'-methyl-2,2'-bipyridine (97%) was obtained from TCI chemicals. Copper(II) nitrate hemi(pentahydrate) was obtained from Riedel-de Haën. [Re(bpy-(C_{15})$(CO)_3$Cl] (**ReC$_{15}$**, bpy-(C_{15})$_2$ = 4,4'-di-pentadecane-2,2'-bipyridine) was available in our group from previous work.[1] Fmoc-protected amino acids: alanine, glycine, leucine, Boc-protected tryptophan, and N-(9H-Fluoren-9-ylmethoxycarbonyloxy)succinimide were obtained from NovaBioChem. DMF (peptide synthesis grade), piperidine, acetic anhydride, pyridine, TFA, and MeCN were purchased from Biosolve. DIPEA and Oxyma were obtained from Carl Roth. DCM and Et_2O were supplied by Honeywell. Sephadex LH-20 was purchased from VWR International B.V. The Avanti Mini-Extruder including polycarbonate extrusion filter (pore size = 200 nm, diameter 19 mm) and filter supports (10 mm) was purchased from Avanti Polar Lipids. Phosphate buffer (1 L, 0.1 M, pH = 7.8) was prepared by dissolving $NaH_2PO_4 \cdot 2H_2O$ (12 g) in Milli-Q water (500 mL), adjusting the pH with NaOH (≈ 90 mL, 1 M), and diluting further with Milli-Q water up to 1 L. $K_3[Fe(C_2O_4)_3] \cdot 3H_2O$ for actinometry was prepared following a literature procedure[2], kept in the dark, and used within 24 h after preparation.

Instrumentation: ^{1}H and ^{13}C NMR spectra were recorded on a Bruker AV-400 MHz spectrometer. Chemical shift values (δ) are indicated in ppm relative to tetramethylsilane, measured using a residual solvent peak. HRMS was measured via direct injection on a Thermo Finnagan LTQ Orbitrap with

electrospray ionisation. UV-Vis absorption spectra were measured on a Varian Cary60 spectrophotometer equipped with a single cell Peltier temperature controller at 25 °C using a 3 mL cuvette. Emission spectra were measured on a FLS900 spectrometer from Edinburgh Instruments Ltd. in a 3 mL cuvette at 22 °C using 380 nm as excitation source for Re and 450 nm as excitation source for Ru complexes. Luminescence lifetimes were measured using an in-house assembled setup.[3] The emission intensity versus time was modelled by a biexponential decay using Glotaran.[4] The osmolarity of aqueous solutions was measured on a Micro-Osmometer Autocal Type 13 from Roebling. The size distribution of the hydrodynamic diameter (Z_{ave}) and the polydispersity index (PDI) of liposomes were measured at 25 °C on a Zetasizer Nano-S from Malvern operating at 632.8 nm with a scattering angle of 173°. Elemental analysis was performed by Mikroanalytisches Laboratorium Kolbe in Oberhausen, Germany. LED optical power was measured by OPHIR Nova-display laser power meter.

B. 2. Peptide design (preliminary studies)

The x, y, z coordinates of α-helical WALPn peptides (acetyl-GWWL(AL)$_n$WWA-amide, with G = glycine, W = tryptophan, A = alanine, and L = leucine) were initially generated using PyMol. YASARA (Yet Another Scientific Artificial Reality Application) was then used as a modelling program to replace two alanine amino acids by two unnatural bipyridyl alanine amino acids (A_{bpy}) at the desired positions within the peptide sequence.[5] Coordination of the metal to the A_{bpy} fragments was achieved by manually inserting a bond between the nitrogen atoms of the A_{bpy} fragments and the metal. We initially used Ca^{2+} as the coordinated metal center instead of Ru^{2+} or Re^{+}, because YASARA is not able to model Ru^{2+} or Re^{+}. We also added two extra bipyridine (bpy) ligands to Ca^{2+}; to make it resemble the photosensitiser $[Ru(bpy)_3]^{2+}$. The generated structures were optimised by energy minimisation (using the YASARA force field) and analysed with YASARA to evaluate the Ca-Ca distance.

We chose to synthesise **WALP23-M_2** with the A_{bpy} in positions 7 and 17 (Figure B1, Table B1). By positioning the A_{bpy} at these intermediate positions, the length of the hydrophobic central part ($L(AL)_4$ = 2.55 nm; length ≈ 0.15 nm per amino acid in an ideal α-helix) matched well with the expected hydrophobic thickness of the lipid bilayer (DPPC bilayer = 2.65 nm)[6]. Furthermore, of all the peptide molecules considered, it has the shortest Ca-Ca distance, which will be important for its electron transfer purposes. Moreover, **WALP23-M_2** with the A_{bpy} in positions 7 and 17 is nearly-symmetrical, e.g. the location of the metals is at the same position from either end of the peptide. Finally, a shorter peptide (WALP23-M_2) would be easier to synthesise than a longer peptide (WALP27-M_2), because the overall yield obtained after solid-phase peptide synthesis (Section B.3) will decrease with every amino acid added to the peptide sequence (i.e. 98% yield at every coupling step would result in a maximum yield of 0.98^{23} × 100% = 62.8% for WALP23-M_2 and 0.98^{27} = 58.0% for WALP27-M_2).

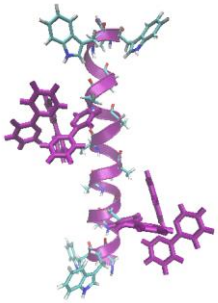

Figure B1. Molecular model of **WALP23-Ca_2** with A_7 and A_{17} substituted by A_{bpy}.

Table B1. Chemical design of metallopeptides that were considered for this work.

WALPn-M_2 (A_x and A_y)[a]	Peptide length (nm)[b]	Ca-Ca distance (nm)	Symmetrical
WALP23-M_2 (A_5 and A_{19})	3.45	2.1	Yes
WALP23-M_2 (A_7 and A_{17})	3.45	1.6	Yes
WALP25-M_2 (A_5 and A_{21})	3.75	3.0	Yes
WALP25-M_2 (A_7 and A_{21})	3.75	2.4	No
WALP27-M_2 (A_5 and A_{23})	4.05	3.4	Yes
WALP27-M_2 (A_7 and A_{21})	4.05	1.9	Yes
WALP27-M_2 (A_9 and A_{19})	4.05	1.9	Yes

[a] n equals the number of amino acids within the WALPn peptide and A_x and A_y are the locations of the alanine amino acid residues that were substituted by bipyridyl alanine.[b] It is assumed that each amino acid has a length of 0.15 nm in an ideal α-helix.[7]

B. 3. Synthesis of WALP23-Ru$_2$, WALP23-Re$_2$, and RuC$_{15}$

General considerations: The full synthesis scheme of **WALP23-Ru$_2$** and **WALP23-Re$_2$** is depicted in Scheme B1. In short, **Fmoc-A$_{bpy}$** was prepared from L-2-amino-3-(4'-methyl-2,2'-bipyridin-4-yl) propanoic acid by the addition of the Fmoc protecting group. Automated solid-phase peptide synthesis in combination with manual coupling of **Fmoc-A$_{bpy}$** at the desired positions within the peptide chain afforded **WALP23-bpy$_2$** (Ac-GWWLALA$_{bpy}$LALALALALA$_{bpy}$LALWWA-**X** with **X** = ethanolamine or NH_2). Finally, formation of **WALP23-Ru$_2$** and **WALP23-Re$_2$** was achieved by reaction between **WALP23-bpy$_2$** with either *cis*-[Ru(bpy)$_2$Cl$_2$] · 2 H_2O or [Re(bpy)(CO)$_5$Cl]. L-2-amino-3-(4'-methyl-2,2'-bipyridin-4-yl) propanoic acid and *cis*-[Ru(bpy)$_2$Cl$_2$] · 2 H_2O were prepared following literature procedures.[8–10] [Re(bpy)(CO)$_5$Cl] was obtained from Sigma Aldrich. [Ru(bpy)$_2$(bpy-(C$_{15}$)$_2$)]Cl$_2$ (**RuC$_{15}$**, bpy = 2,2'-bipyridine; bpy-(C$_{15}$)$_2$ = 4,4'-di-pentadecane-2,2'-bipyridine) was available as a crude product in our group from previous work and required further work-up as described below.[1]

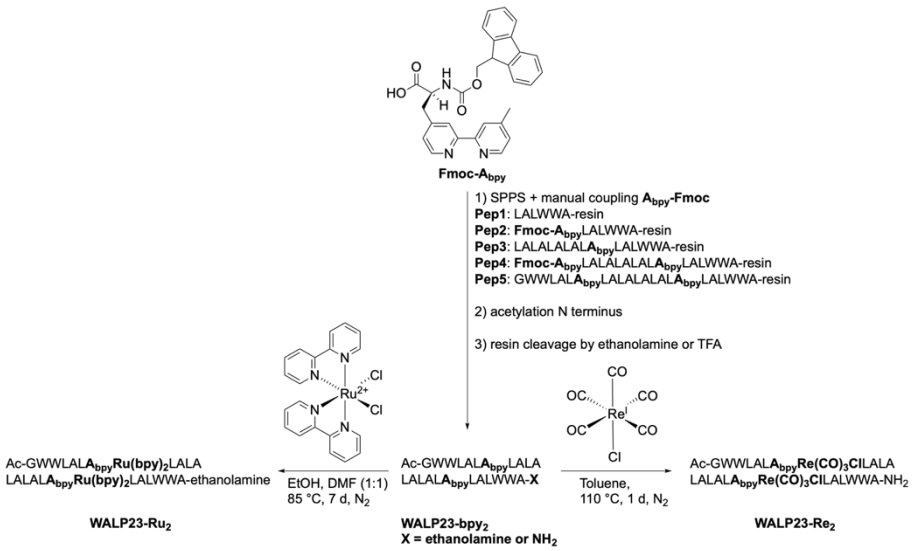

Scheme B1. Synthetic route for the metallopeptides **WALP23-Ru$_2$** and **WALP23-Re$_2$**. A = alanine, Ac = acetyl, G = glycine, L = leucine, and W = tryptophan.

Fmoc-A_{bpy}: (S)-1-carboxy-2-(4'-methyl-[2,2'-bipyridin]-4-yl)ethan-1-aminium chloride (103 mg, 0.35 mmol) was dissolved in a sodium bicarbonate solution (126 mg, 1.19 mmol, 2 mL). To this solution was added dropwise a dioxane solution containing N-(9H-Fluoren-9-ylmethoxycarbonyloxy)succinimide (138 mg, 0.41 mmol, 2 mL). The reaction mixture was stirred at room temperature for 2.5 h. Afterwards, Et_2O (20 mL) was added to the mixture and the mixture was extracted with water (3 x 20 mL). The combined aqueous layers were cooled down to 0 °C and concentrated HCl (≈ 1 mL, 37%) was then added until pH < 2, resulting in the formation of a pink precipitate. The aqueous layers were divided over 4 corning tubes (15 mL) and centrifuged (Jouan Br4i centrifuge, 4000 rpm, 20 min, RT). After removal of the supernatant, the pellets were redissolved in MeOH. After removal of MeOH under reduced pressure and vacuum drying, the product **Fmoc-A_{bpy}** was obtained as a pink-purple powder (75 mg, 0.16 mmol, 45%). ^{1}H NMR (400 MHz, DMSO-d6): δ = 8.55 (d, *J* = 5.0 Hz, 1H), 8.49 (d, *J* = 4.9 Hz, 1H), 8.33 (s, 1H), 8.20 (s, 1H), 7.85 (d, *J* = 7.6 Hz, 2H), 7.80 (s, 1H), 7.57 (dd, *J* = 15.1, 7.5 Hz, 2H), 7.36 (m, 3H), 7.22 (m, 3H), 4.28 (t, *J* = 11.5 Hz, 1H), 4.16 (m, 3H), 3.20 (dd, *J* = 13.9, 4.3 Hz, 1H), 2.99 (t, *J* = 13.7, 10.6 Hz, 1H), 2.39 (s, 3H). ^{1}H NMR (400 MHz, MeOD): δ = 8.73 (d, *J* = 5.2 Hz, 1H), 8.56 (d, *J* = 5.8 Hz, 1H), 8.37 (d, *J* = 8.4 Hz, 2H), 7.81 (m, 1H), 7.69, (m, 4H), 7.46 (m, 2H), 7.33 (m, 3H), 7.18 (m, 2H), 4.69 (m, 1H), 4.28 (m, 2H), 4.03 (t, *J* = 7.2 Hz, 1H), 3.58 (dd, *J* = 14.1, 4.9 Hz, 1H), 3.25 (m, 1H), 2.53 (s, 3H). ^{13}C NMR (75 MHz, MeOD): δ = 173.88 (C_q), 172.79 (C_q), 160.20 (C_q), 159.99 (C_q), 158.27 (C_q), 154.37 (C_q), 149.10 (C_q), 148.92 (C_q), 148.02 (CH), 146.19 (C_q), 144.84 (C_q), 144.35 (C_q), 142.33 (CH), 129.08 (CH), 128.81 (CH), 128.38 (CH), 128.12 (CH), 128.05 (CH), 127.90 (CH), 126.08 (CH), 125.36 (CH), 124.86 (CH), 120.90 (CH), 120.73 (CH), 67.84 (CH_2), 55.11 (CH), 48.18 (CH_2), 37.89 (CH), 22.17 (CH_3). HRMS (ESI) *m/z* found (calcd): 480.19139 (480.19178, $[M+H]^+$), 494.20695 (494.20743, $[M+CH_3]^+$, methyl ester instead of carboxylic acid).

WALP23-bpy_2: Solid-phase peptide synthesis was performed using a Liberty Blue microwave assisted automated peptide synthesiser for the coupling of the natural amino acids (A, W, L, and G). For the coupling of the unnatural amino acid **A_{bpy}**, we performed a manual coupling, see below. Synthesis was performed on the solid-phase, at a 0.1 mmol scale, using Fmoc-L-Ala-Wang

TentaGel resin (90 µm, 0.20 – 0.25 mmol/g) as the solid support. Fmoc deprotection was achieved using 20% piperidine in DMF, and coupling was facilitated with DIC as activator and Oxyma as base using a double deprotection, double coupling procedure. Peptide synthesis was performed twice; the first batch was cleaved with ethanolamine and used for the synthesis of **WALP23-Ru$_2$**, whereas the second batch was cleaved with TFA and used for the synthesis of **WALP23-Re$_2$**.

The synthesis of **WALP23-bpy$_2$** was started by the automated synthesis of LALWWA-resin (**Pep1**). Afterwards, the contents of the reaction vessel were transferred to a 10 mL syringe with a filter and washed with DMF (3 x 5 mL). In the next step, a solution of **Fmoc-A$_{bpy}$** (52.7 mg, 0.11 mmol), HCTU (45.5 mg, 0.11 mmol), and DIPEA (0.11 mmol, 0.019 mL) in DMF (2 mL) was added to the syringe containing LALWWA-resin and left to react on a rocking platform at RT for 24 h. The reaction mixture was washed with DMF (3 x 5 mL), resulting in a color change of the resin from yellow to purple. **Fmoc-A$_{bpy}$**LALWWA-resin (**Pep2**) was added back to the reaction vessel of the peptide synthesiser and the sequence LALALALAL was coupled to it, resulting in a yellow residue, due to the deprotection of the Fmoc group of **Fmoc-A$_{bpy}$**, which was responsible for the purple color. Afterwards, the contents of the reaction vessel were transferred to a 10 mL syringe with a filter and washed three times with DMF (3 x 5 mL). In the next step, a solution of **Fmoc-A$_{bpy}$** (52.7 mg, 0.11 mmol), HCTU (45.5 mg, 0.11 mmol), and DIPEA (0.11 mmol, 0.019 mL) in DMF (2 mL) was added to the syringe containing LALALALALA$_{bpy}$LALWWA-resin (**Pep3**) and left to react on a rocking platform at RT for 24 h. The reaction mixture was washed with DMF (3 x 5 mL), resulting again in a color change of the resin from yellow to purple. **Fmoc-A$_{bpy}$**LALALALALA$_{bpy}$LALWWA-resin (**Pep4**) was added back to the reaction vessel of the peptide synthesiser and the sequence GWWLAL was coupled to it, resulting in a yellow residue. The resin-bound peptide was suspended in DMF (5 mL), transferred to a 10 mL syringe with a filter, and washed with DMF (3 x 5 mL). Afterwards, acetic anhydride (10 drops) and pyridine (11-12 drops) in DMF (5 mL) were added to the syringe and the mixture was left to react on a rocking platform at RT for 1 h to acetylate the N-terminus of the peptide. Then, the syringe was drained and washed with DMF (3 x 5 mL) and

with DCM (3 x 5 mL). At this stage, two methods of cleavage, previously reported for WALP23[7,11], were performed for two different batches of **WALP23-bpy$_2$**; either with 1) ethanolamine or 2) TFA, as described below:

1) Ethanolamine (0.8 mL) and DCM (4.2 mL) were added to the resin and left to react on a rocking platform at RT for 48 h to facilitate peptide cleavage. The solution was filtered and the resin was washed with DCM (10 mL), TFE (5 mL), a mixture of DCM/TFE (1:1, 5 mL), and finally with DCM again (10 mL). The solutions were combined and solvents were evaporated until only ethanolamine was left. Afterwards, a minimum amount of DCM (1 mL) was added and the solution was transferred to a 50 mL conical tube. Water (35 mL) was added and the solution was left in the fridge (4 °C) for 2.5 h, resulting in a suspension. Centrifugation (Thermo IEC CL10 centrifuge, 30 min, 4000 rpm, RT) of the suspension led to a yellowish precipitate. After freeze-drying for 1 day, **WALP23-bpy$_2$** with **X** = ethanolamine (151.4 mg, 52.5%) was obtained as a white solid that was characterised and, due to its very high hydrophobicity, used without further purification.

2) TFA (3 mL), water (5 drops), and TIPS (6 drops) were added to the resin and left to react on a rocking platform at RT for 3 h to cleave the peptide. The reaction mixture was drained into ice-cold Et_2O (30 mL) resulting in a suspension. Centrifugation (Thermo IEC CL10 centrifuge, 10 min, 4000 rpm, RT) of the suspension led to a yellowish-brown precipitate. The precipitate was redissolved in a mixture of tert-butanol (2 mL) and water (6 mL). After freeze-drying for 1 day, **WALP23-bpy$_2$** with **X** = NH_2 (41.6 mg, 14.6%) was obtained as a white solid that was characterised and, due to its very high hydrophobicity, used without further purification.

All intermediate peptides were analysed by LC-MS to monitor the progress of peptide synthesis using the following protocol. After finishing a peptide fragment by either solid-phase or manual synthesis, a test cleavage was performed by transferring a few mg of the resin to a 5 mL syringe with filter. The resin was washed with DCM (3 x 2 mL) and afterwards TFA (1 mL), TIPS (2 drops), and water (2 drops) were added. After cleavage (2 h on a rocking platform), the contents of the syringe were added into 20 mL ice-cold Et_2O

and after centrifugation (Thermo IEC CL10 centrifuge, 10 min, 4000 rpm, RT) a solid would remain on the bottom of the centrifuge tube. The supernatant was removed and the residue was typically dissolved in a mixture of H_2O:CH_3CN:tBuOH (1:1:1) for LC-MS analysis on either a C_{18} column (**Pep1** and **Pep2**) or a diphenyl column (**Pep3**, **Pep4** and **WALP23-bpy$_2$**), depending on the hydrophobicity of the peptide. In case no precipitation was observed after centrifugation, all solvents were evaporated under a stream of N_2, resulting in a solid residue that was dissolved and analysed as described above.

LC-MS (ESI) *m/z* found (calcd) for **Pep1**: 759.33 (759.42, [*M*+H]$^+$). LC-MS (ESI) *m/z* found (calcd) for **Pep2**: 1220.53 (1220.59, [*M*+H]$^+$. LC-MS (ESI) *m/z* found (calcd) for **Pep3**: 924.75 (925.05, [*M*+2H]$^{2+}$, 1847.67 (1849.10, [*M*+H]$^+$). LC-MS (ESI) *m/z* found (calcd) for **Pep4**: 1155.6 (1155.64, [*M*+2H]$^{2+}$, 1177.2 (1176.15, [*M*+ACN+2H]$^{2+}$. LC-MS (ESI-TOF) *m/z* found (calcd) for **WALP23-bpy$_2$** with **X** = NH_2: 952.9425 (952.87, [M+3H]$^{3+}$), 1428.8895 (1428.80, [*M*+2H]$^{2+}$). HRMS (ESI) *m/z* found (calcd) for **WALP23-bpy$_2$** with **X** = NH_2: 952.87025 (952.87092, [M+3H]$^{3+}$), 1428.80237 (1428.80274, [*M*+2H]$^{2+}$).

WALP23-Ru$_2$: DMF and EtOH were dried overnight on molecular sieves (3 – 5Å) and degassed for 15 min with N_2 before use. **WALP23-bpy$_2$** with **X** = ethanolamine (70.0 mg, 0.024 mmol) and *cis*-[Ru(bpy)$_2$Cl$_2$] · 2 H_2O (52.0 mg, 0.100 mmol) were dissolved in a mixture of DMF (2 mL) and EtOH (2 mL). The reaction mixture was heated at 85 °C for 7 days under N_2. Afterwards, the reaction mixture was concentrated under reduced pressure by co-evaporation with toluene (3 x 20 mL). The crude product was purified by size exclusion chromatography (Sephadex LH-20 as packing material) using MeOH as the eluent. The orange band, which was red phosphorescent under UV-light, was collected. After evaporation under reduced pressure, the product was obtained as a red solid (55.4 mg, 0.014 mmol, 59%). Elemental analysis for $C_{193}H_{244}N_{40}O_{25}Ru_2Cl_4$ · 4 H_2O: (calcd.): C, 58.83; H, 6.45; N, 14.22; (exp.): C, 58.93; H, 6.57; N, 14.23. LC-MS (ESI-TOF) *m/z* found (calcd) for **WALP23-Ru$_2$**: 929.0564 (927.93, [*M*-4Cl-OH]$^{4+}$), 1238.4000 (1236.91, [*M*-4Cl-OH-H]$^{3+}$. LC-MS on a diphenyl column (ESI) *m/z* found (calcd) for **WALP23-Ru$_2$**: 928.67 (927.93, [*M*-4Cl-OH]$^{4+}$), 1237.75 (1236.91, [*M*-4Cl-OH-H]$^{3+}$,

1856.08 (1854.35, [*M*-4Cl-OH-2H]$^{2+}$). UV-Vis (MeOH): λ_{max} (ε): 454 nm (1.59 x 10^4 mol^{-1}dm^{3}cm^{-1}).

WALP23-Re$_2$: **WALP23-bpy$_2$** with **X** = NH_2 (17.6 mg, 6.2 µmol) and [Re(CO_5)Cl] (15.9 mg, 44 µmol) were dissolved in dry toluene (5 mL) and refluxed for 24 h under N_2. The formed precipitate was collected by filtration, washed with toluene (3 x 10 mL), and dried on vacuum overnight. Afterwards, the precipitate was purified by size-exclusion chromatography (Sephadex LH-20 as packing material) using acetone as eluent. The yellowish band, which was yellowish-orange phosphorescent under UV-light, was collected. After evaporation under reduced pressure, the product was obtained as a yellowish brown solid (9.6 mg, 2.8 µmol, 45%). Elemental analysis for $C_{157}H_{207}Cl_2N_{31}O_{31}Re_2 \cdot 2\ H_2O$: (calcd.): C, 53.82; H, 6.07; N, 12.39; (exp.): C, 53.72; H, 6.06; N, 12.37. LC-MS (ESI-TOF) *m/z* found (calcd) for **WALP23-Re$_2$**: 1160.2767 (1159.84, [*M*-2Cl+2ACN]$^{3+}$, 1428.8831 (1428.80, [*M*-2[Re(CO_3Cl]+2H]$^{2+}$, unreacted starting material or degradation due to the conditions necessary for dissolving the sample; H_2O:ACN:tBuOH 1:1:1 with few drops of FA), 1739.9296 (1739.76, [*M*-2Cl+2ACN]$^{2+}$. UV-Vis ($CHCl_3$): λ_{max} (ε): 380 nm (3.97 x 10^3 mol^{-1}dm^{3}cm^{-1}).

RuC$_{15}$: The crude product [Ru(bpy)$_2$(bpy-(C_{15})$_2$)]$Cl_2 \cdot$ x NaCl] (258.4 mg, 0.243 mmol, 56.2% yield) was obtained as described in literature[1]. To remove excess salts, the crude product (61.0 mg, 0.057 mmol) was purified by size-exclusion chromatography (Sephadex LH-20 as packing material) using methanol as eluent. After evaporation under reduced pressure, the product was obtained as a red solid (34.8 mg, 0.033 mmol). R_f = 0.1 (SiO_2, acetone:water:brine (8:4:1)). ^{1}H NMR (400 MHz, CD_3OD): δ = 8.71 (d, *J* = 8.2 Hz, 4H), 8.63 (d, *J* = 1.9 Hz, 2H), 8.11 (tt, *J* = 8.0, 1.5 Hz, 4H), 7.82 (td, *J* = 5.7, 1.8 Hz, 4H), 7.63 (d, *J* = 5.8 Hz, 2H), 7.49 (dq, *J* = 7.0, 5.5, 1.3 Hz, 4H), 7.34 (dd, *J* = 5.9, 1.7 Hz, 2H), 2.85 (t, *J* = 7.8 Hz, 4H), 1.73 (q., *J* = 8.0 Hz, 4H), 1.28 (m, 48H), 0.89 (t, *J* = 6.6 Hz, 6H). ^{13}C NMR (100 MHz, CD_3OD): δ = 158.62 (C_q), 158.58 (C_q), 158.17 (C_q), 156.55 (C_q), 152.63 (CH), 152.49 (CH), 151.87 (CH), 139.05 (CH), 128.87 (CH), 125.62 (CH), 36.24 (CH_2), 33.07 (CH_2), 31.35 (CH_2), 30.79 (CH_2), 30.75 (CH_2), 30.72 (CH_2), 30.61 (CH_2), 30.47 (CH_2), 30.44 (CH_2), 30.41 (CH_2), 23.74 (CH_2), 14.46 (CH_3). Elemental analysis for $C_{60}H_{84}N_6Cl_2Ru \cdot$ x

NaCl (before size-exclusion chromatography): (calcd.): C, 67.90; H, 7.98; N, 7.92; (exp.): C, 44.76; H, 7.40; N, 5.12. Elemental analysis for $C_{60}H_{84}N_6Cl_2Ru$ + 1 H_2O (after size-exclusion chromatography): (calcd.): C, 66.77; H, 8.03; N, 7.79; (exp.): C, 66.98; H, 8.12; N, 7.79. HRMS (ESI) *m/z* found (calcd): 495.29007 (495.29032, [**RuC$_{15}$**-2Cl]$^{2+}$).

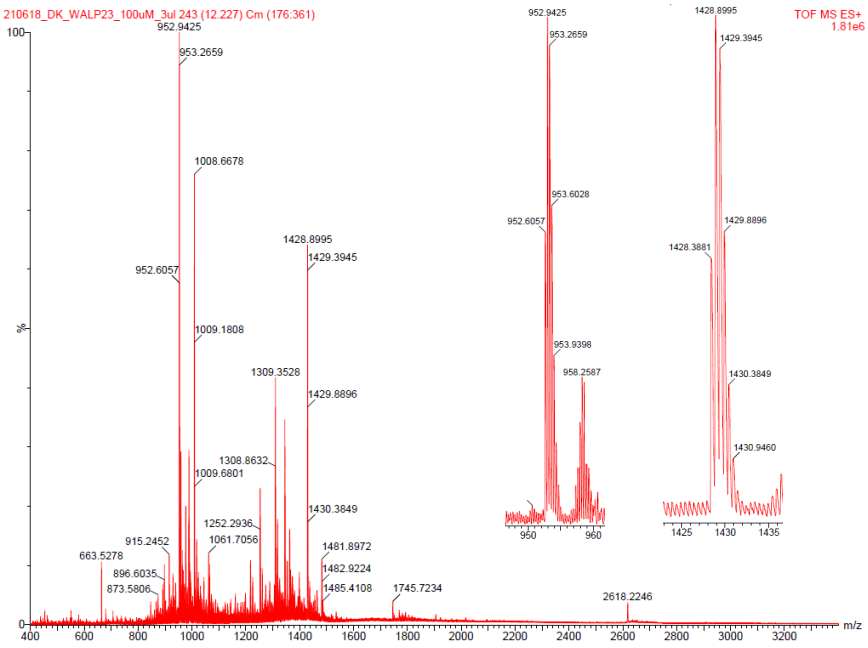

Figure B2. ESI-TOF spectrum of **WALP23-bpy$_2$**.

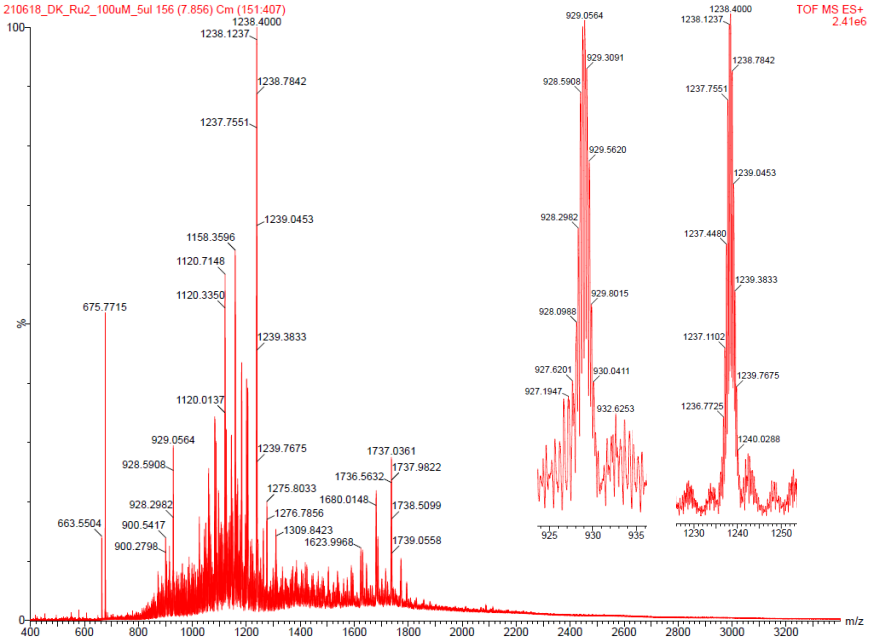

Figure B3. ESI-TOF spectrum of **WALP23-Ru$_2$**.

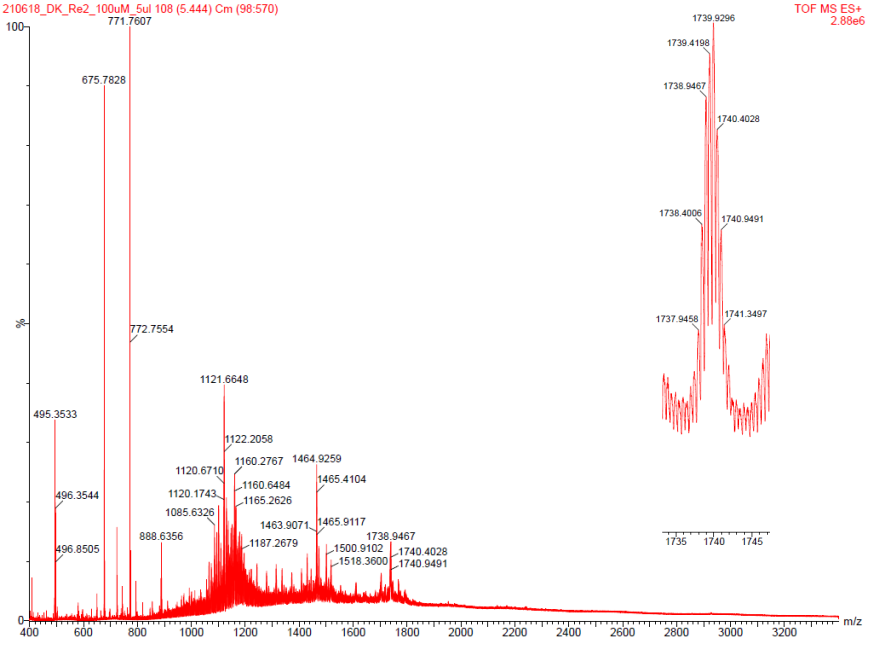

Figure B4. ESI-TOF spectrum of **WALP23-Re$_2$**.

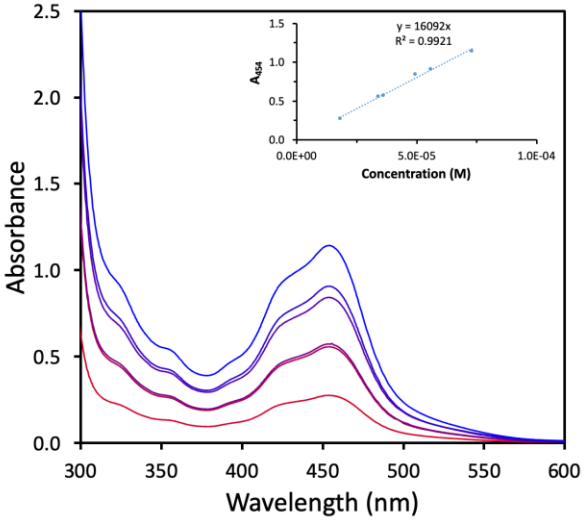

Figure B5. UV-Vis spectra of six samples of **WALP23-Ru$_2$** with different concentrations, measured in 3 mL MeOH in a cuvette (l = 1 cm) at 298 K. Inset: determination of the molar absorption coefficient of **WALP23-Ru$_2$**; ε = 1.61 × 10^4 M^{-1} cm^{-1} at λ = 454 nm. For [Ru(bpy)$_3$Cl$_2$], ε = 1.46 × 10^4 M^{-1} cm^{-1} at λ = 453 nm in MeOH.[12]

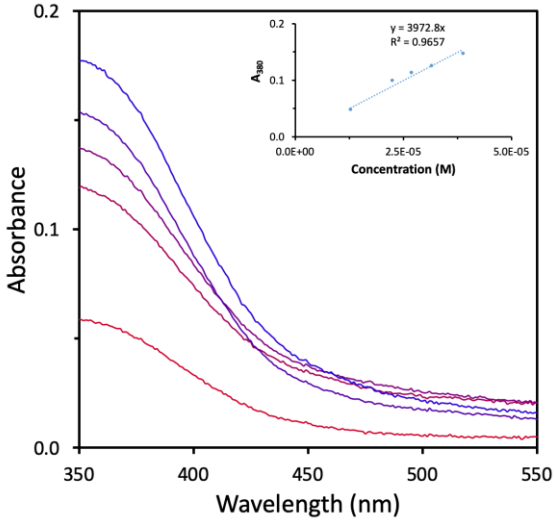

Figure B6. UV-Vis spectra of five samples of **WALP23-Re$_2$** at different concentrations, measured in 3 mL $CHCl_3$ in a cuvette (l = 1 cm) at 298 K. Inset: determination of the molar absorption coefficient of **WALP23-Re$_2$**; ε = 3.97 × 10^3 M^{-1} cm^{-1} at λ = 380 nm. For [Re(dmb)(CO)$_3$Cl] (dmb = 4,4'-dimethyl-2,2'-bipyridine), ε = 3.5 × 10^3 M^{-1} cm^{-1} at λ = 383 nm in $CHCl_3$.[13]

B. 4. Molecular Dynamics

Computational methods: All MD simulations were performed using Gromacs 2018[14] with periodic boundary conditions applied along all Cartesian dimensions. Both metal peptide complexes were treated with the AMBER99SB force field.[15] We adopted two different methods to incorporate the metal complex residue. The Ru-complex residue was optimised using DFT calculations (B3LYP/def2-TZVP level), and the atomic point-charge parameters were obtained according to the charge model 5 (CM5).[16] Following a bonded model approach, six Ru–N bonds were added to keep about 0.21 nm coordination distance between Ru and N. The Lennard-Jones non-bonded parameters of Ru were taken from Brandt's work.[17] The Re-complex residue was parameterised using the MCPB.py tool[18] with B3LYP/6-31G(d)-LanL2DZ level DFT calculations. All the DFT calculations were performed using the Gaussian16 software.[19] The force field parameters of DPPC were obtained from Lyubartsev's work,[20] which are compatible with the Amber force fields. For water molecules, the TIP3P model was used.[21]

For each system, we sequentially performed energy minimisation, NVT and NPT relaxation simulation, and NPT production simulation (100 ns anisotropic pressure coupling and another 100 ns semi-isotropic pressure coupling). The target temperature and pressure are set to 300 K and 1 Bar. The velocity-rescale thermostat was used with a coupling constant of 0.1 ps.[22] Anisotropic pressure coupling was applied using the Berendsen scheme with a coupling constant of 1.0 ps.[23] In semi-isotropic pressure coupling simulations, a Parrinello-Rahman barostat with a coupling constant of 2.0 ps was also used.[24,25] Bond lengths were constrained using the LINCS algorithm and simulations were run with a 2.0 fs time step. The van der Waals interactions were calculated using a cut-off of 1.0 nm, with the potential energy shifted to be zero at the cut-off. The electrostatic interactions were calculated using the PME method.[26]

Spontaneous aggregation simulation. We performed spontaneous aggregation simulations on two systems: 1 molecule of **WALP23-Ru$_2$** or 1

molecule of **WALP23-Re$_2$** and 128 DPPC lipid molecules for the membrane. Both systems were solvated by water molecules in a cubic box (about 7.0 nm edge length) and the overall charge of the system containing **WALP23-Ru$_2$** was neutralised by the addition of 4 Cl^- ions.

Our simulation protocol was adapted from previous research.[27] After energy minimisation, 10 ps NVT and 40 ps NPT (isotropic pressure control) simulations were conducted with position constraints on the heavy atoms of the metallopeptide. A consequential 100 ns production NPT simulation allowed the system to evolve freely under anisotropic pressure coupling. At the end, an extra 100 ns NPT simulation using semi-isotropic pressure coupling was performed to further equilibrate the formed membrane. As the semi-isotropic pressure coupling in Gromacs is suitable for membranes that align with their normal vectors along the z-axis, the membrane formed from the anisotropic simulation had to be oriented accordingly before the last 100 ns NPT simulation.

To guarantee the randomness, in each simulation instance the lipid molecules were inserted into the box via the *gmx insert-molecules* command, using a unique seed. We note that sometimes the anisotropic pressure coupling led to "unsuccessful" simulations, in which the simulation box became over-stretched, and we discarded such results. We obtained a total of 13 successful trajectories of **WALP23-Ru$_2$** and 16 of **WALP23-Re$_2$** showing the formation of a proper lipid membrane, and we visually checked the trans-membrane status of the metallopeptide in addition to the automated analysis. The total simulation time for all proper cases was 5.8 µs.

The immersion ratio (φ, see main text) and the angle between the metal-metal vector and the normal vector of the lipid membrane (ϑ, see main text) were derived from the final orientation of the molecules in the system at the last frame of each MD simulation trajectory. To calculate φ, we used the following equation:

$$\varphi = \frac{N_{DPPC}}{N_{total}} \qquad \text{Equation B1}$$

In Equation B1, N_{DPPC} are the amount of non-hydrogen atoms from DPPC molecules and N_{total} are the total amount of non-hydrogen atoms from DPPC, water, and/or Cl^- ions that surround the metal residue of the metallopeptide within a cut-off range of 0.35 nm. To calculate the angle between the metal-metal vector and the normal vector of the lipid membrane (ϑ, see main text), we used the following equation:

$$\cos(\theta) = \frac{\vec{V}_{memb}\vec{V}_{M-M}}{|\vec{V}_{memb}||\vec{V}_{M-M}|} \qquad \text{Equation B2}$$

In Equation B2, $\vec{V}_{memb}$ is the normal vector of the lipid membrane and $\vec{V}_{M-M}$ is the vector joining the two metals centers (Ru-Ru or Re-Re) of the metallopeptides.

Mass density profiles. The mass density of grouped atoms was determined along the z-axis, which in all simulations is defined as the normal vector of the lipid membrane ($\vec{V}_{memb}$). The atom groups are defined as shown in Figure B7. The densities are centered on the last carbon beads of both tails of the DPPC lipids, since on average this can be defined as the center of the bilayer. The density plots were obtained with Gromacs, using the *gmx density* command, from the last 20 ns of the simulations that formed bilayers, and they were averaged over 1000 frames (Figure B8 and Figure B9).

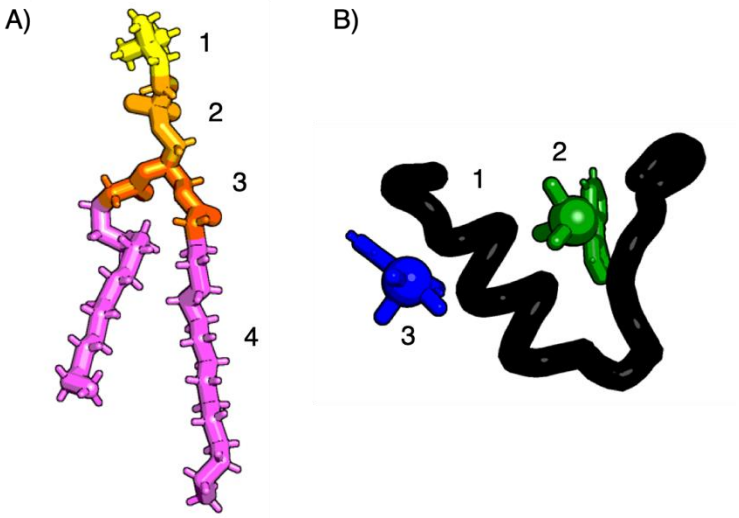

Figure B7. The grouping used for the mass density profiles. (A) A schematic representation of the DPPC lipid. The groups are choline (1), phosphor oxygen (2), glycerol groups (3), and the hydrophobic tails (4). (B) A schematic representation of the WALP23-peptide with the metal atoms including its ligands (three bipyridines in the case of **WALP23-Ru$_2$**, and one bipyridine, three CO, and one Cl in the case of **WALP23-Re$_2$**). Here the groups are defined as WALP23-peptide (1), one metal atom including its ligands (2), and the other metal atom including its ligands (3).

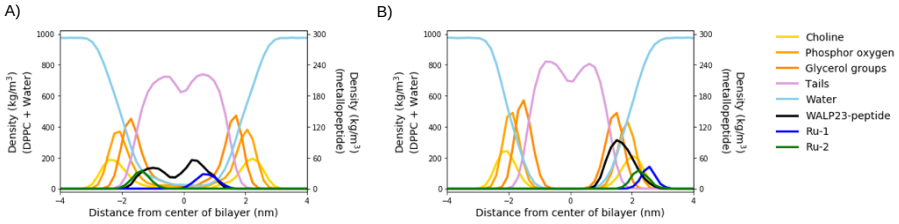

Figure B8. Representative mass density profiles of DPPC, water, and the metallopeptide **WALP23-Ru$_2$**. In the transmembrane configuration (A) **WALP23-Ru$_2$** is located within the hydrophobic region of the lipid bilayer (tails). In the parallel configuration (B) **WALP23-Ru$_2$** is located on one side of the lipid bilayer at the lipid-water interface (choline, phosphor oxygen, and glycerol groups).

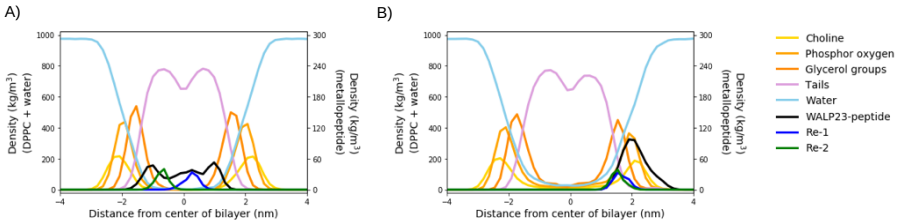

Figure B9. Representative mass density profiles of DPPC, water, and the metallopeptide **WALP23-Re$_2$**. In the transmembrane configuration (A) **WALP23-Re$_2$** is located within the hydrophobic region of the lipid bilayer (tails). In the parallel configuration (B) **WALP23-Re$_2$** is located on one side of the lipid bilayer at the lipid-water interface (choline, phosphor oxygen, and glycerol groups).

The metal-metal distance. The distances between the metal atoms (Re or Ru) were calculated with Gromacs using the *gmx distance* command. For each transmembrane peptide the distance was averaged over the last 20 ns of the simulation with 1000 frames, resulting in the distances given in Table B2 and an average distance of 1.999 ± 0.300 for Ru-Ru and 2.090 ± 0.584 for Re-Re.

Table B2. Distances between both metal atoms in all transmembrane configurations of the WALP23-peptide MD model in a DPPC membrane.

Metallopeptide	Distance (nm)	Standard dev (nm)
WALP23-Ru$_2$	2.299	0.159
WALP23-Ru$_2$	1.698	0.204
WALP23-Re$_2$	1.026	0.055
WALP23-Re$_2$	2.710	0.101
WALP23-Re$_2$	2.501	0.077
WALP23-Re$_2$	2.211	0.084
WALP23-Re$_2$	2.002	0.061
WALP23-Ru$_2$ average	1.999	0.300
WALP23-Re$_2$ average	2.090	0.584

B. 5. Liposome characterisation

Preparation of liposomes for characterisation: DPPC lipids in chloroform, NaDSPE-PEG2K in chloroform, and one of the (metallo)peptides in chloroform (**WALP23-bpy$_2$** and **WALP23-Re$_2$**) or methanol (**WALP23-Ru$_2$**) were added to a pressure resistant tube. The organic solvents were evaporated under reduced pressure and the resulting film was dried for at least 1 h in *vacuo* to remove residual solvent. The film was then hydrated with NH_4OAc buffer (1 mL, pH = 7.0, p = 0.42 Osm), followed by 10 freeze-thaw cycles between liquid N_2 and a 50 °C water bath. Subsequently, the vesicles were extruded 11× with an Avanti Polar Lipids mini-extruder through a 0.2 µm polycarbonate membrane at 55 °C. Assuming no losses during preparation, the resulting liposome stock solutions consisted of DPPC:NaDSPE-PEG2K:(metallo)peptide in the ratio 100:1:1 with bulk concentrations of 12.5 mM DPPC, 0.125 mM NaDSPE-PEG2K, and 0.125 mM (metallo)peptide. Liposome samples were stored at RT and used within two days. The liposome solutions were analysed the same day with DLS and the next day with UV-Vis, emission, and time-resolved fluorescence spectroscopy. For the spectroscopy experiments, the liposome stock solutions were diluted 5× with NH_4OAc.

Preparation of giant vesicles for confocal microscopy: DPPC lipids in chloroform and **WALP23-Ru$_2$** in methanol were added to a pressure resistant tube. The organic solvents were evaporated under reduced pressure and the resulting film was dried for at least 1 h in *vacuo* to remove residual solvent. The film was then hydrated with NaH_2PO_4 buffer (1 mL, 0.1 M, pH = 7.8, p = 0.43 Osm), followed by 3 freeze-thaw cycles between liquid N_2 and a 50 °C water bath. Assuming no losses during preparation, the resulting giant vesicles solution consist of DPPC:**WALP23-Ru$_2$** in the ratio 100:0.4 with bulk concentrations of 25 mM DPPC and 0.1 mM **WALP23-Ru$_2$**. For confocal microscopy, 150 µL of NaH_2PO_4 buffer (0.1 M, pH = 7.8, p = 0.43 Osm) and 50 µL of giant vesicles solution was added to one of the wells of a chambered coverslip with 8 wells (µ-slide 8 well glass bottom from Ibidi). Confocal microscopy images were taken on a Nikon Eclipse Ti microscope with 20×

objective (0.75 NA, 1.00 WD) and confocal imaging with 488 nm laser and 640 – 680 nm detection wavelength. Images were processed with the Fiji version of Image J2.

Table B3. Z_{ave} and PDI (polydispersity index) of liposomes prepared from DPPC, NaDSPE-PEG2K, and (metallo)peptide in a ratio of 100:1:1, which were used for characterisation studies.

Sample[a]	**Z_{ave} (nm)**[b]	**PDI**[b]
WALP23-bpy_2	137.0	0.089
WALP23-Ru_2	135.6	0.077
WALP23-Re_2	123.0	0.091

[a] Experimental conditions: [DPPC] = 12.5 mM, [NaDSPE-PEG2K] = 0.125 mM, [**WALP23-bpy_2**, **WALP23-Ru_2** or **WALP23-Re_2**] = 0.125 mM. [b] The liposome size is considered to be uniformly distributed when PDI < 0.2.

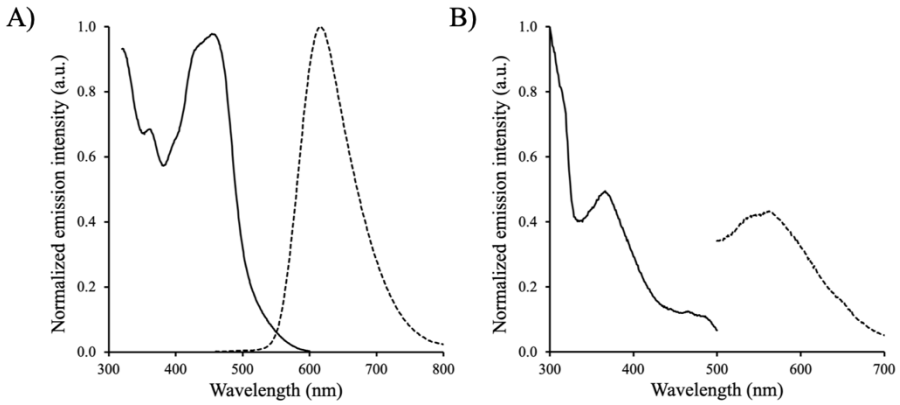

Figure B10. The excitation (solid line, λ_{em} = 620 nm for Ru and 550 nm for Re) and emission spectrum (dashed line, λ_{exc} = 450 nm for Ru and 380 nm for Re) of (A) **WALP23-Ru_2** and (B) **WALP23-Re_2** embedded within DPPC liposomes. Experimental conditions: [DPPC] = 2.5 mM, [NaDSPE-PEG2K] = 25 μM, [**WALP23-Ru_2** or **WALP23-Re_2**] = 25 μM in 0.1 M NH_4OAc (pH = 7.0) under an Ar atmosphere. Excitation spectra were measured instead of absorption spectra, because lipid scattering obscured UV-Vis absorption bands.

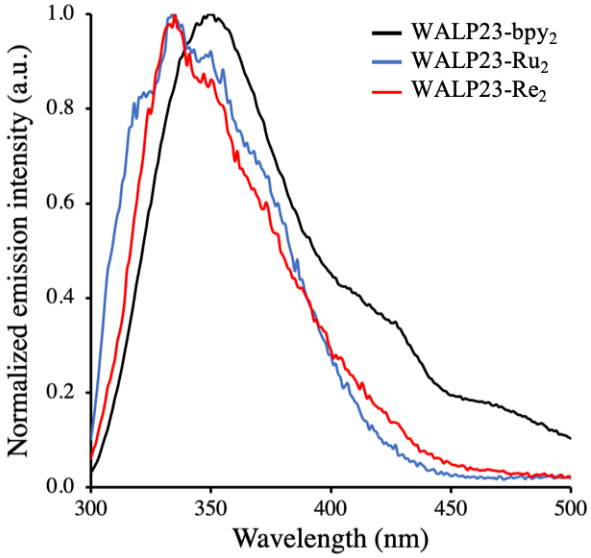

Figure B11. The emission spectrum (λ_{exc} = 280 nm) of the tryptophan (W) amino acids of **WALP23-bpy₂**, **WALP23-Ru₂** **WALP23-Re₂** embedded within DPPC liposomes. Experimental conditions: [DPPC] = 2.5 mM, [NaDSPE-PEG2K] = 25 µM, [**WALP23-bpy2**, **WALP23-Ru₂** or **WALP23-Re₂**] = 25 µM in 0.1 M NH_4OAc (pH = 7.0) under an air atmosphere.

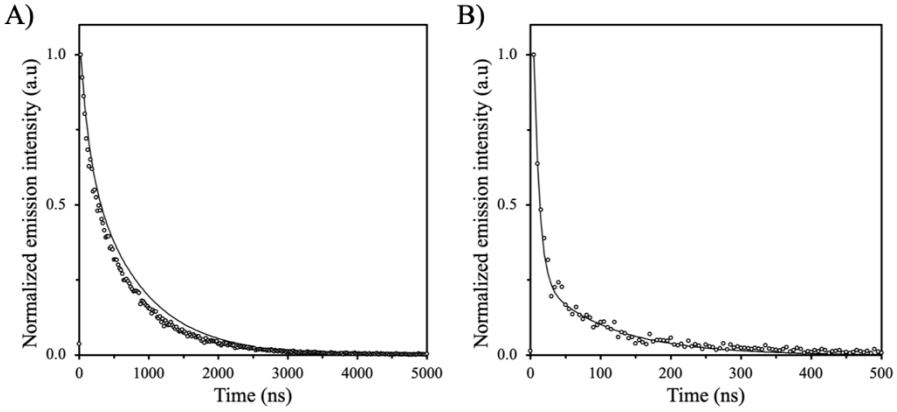

Figure B12. Normalised photoluminescence decays of (A) **WALP23-Ru₂** (λ_{exc} = 450 nm, 3.5 mJ/pulse, λ_{em} = 616 nm) or (B) **WALP23-Re₂** (λ_{exc} = 380 nm, 3.5 mJ/pulse, λ_{em} = 562 nm) embedded within DPPC liposomes. The data (circles) were fitted by a biexponential decay (solid line) using Glotaran; yielding for **WALP23-Ru₂** τ_1 = 123 ns and τ_2 = 787 ns and for **WALP23-Re₂** τ_1 = 8 ns and τ_2 = 103 ns. Experimental conditions: [DPPC] = 2.5 mM, [NaDSPE-PEG2K] = 25 µM, [**WALP23-Ru₂** or **WALP23-Re₂**] = 25 µM in 0.1 M NH_4OAc (pH = 7.0) under an Ar atmosphere.

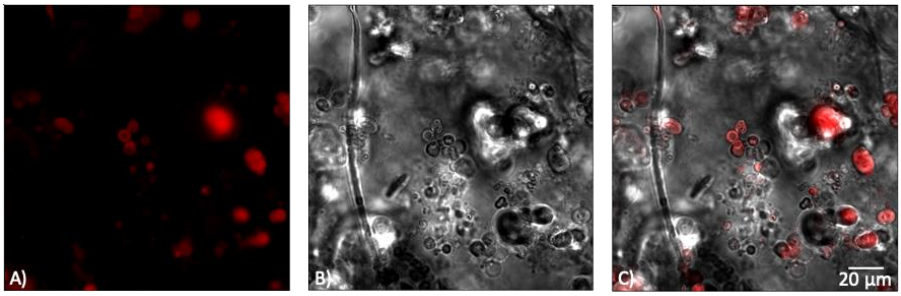

Figure B13. Confocal microscopy of DPPC giant vesicles containing 0.4% **WALP23-Ru$_2$** in NaH_2PO_4 buffer (0.1 M, pH = 7.8, p = 0.43 Osm). Figure B13A is the fluorescence image, Figure B13B is the transmission image, and Figure B13C is the overlay. Images were taken with a Nikon Ti2 microscope at 80x total zoom, 488 nm excitation, and 640 – 680 nm emission.

B. 6. Photoirradiation experiments

Preparation of asymmetric liposomes for irradiation experiments: DPPC lipids in chloroform, NaDSPE-PEG2K in chloroform, and one of the (metallo)peptides or one of the mononuclear metal complexes in either methanol (**WALP23-Ru$_2$** and **RuC$_{15}$**) or chloroform (**WALP23-bpy$_2$**, **WALP23-Re$_2$**, or **ReC$_{15}$**) were added to a pressure-resistant tube. The organic solvents were evaporated under reduced pressure and the resulting film was dried for at least 1 h in *vacuo* to remove residual solvent. The film was then hydrated with a Na_3HEDTA buffer (2 mL, 0.125 M, pH = 8.2, p = 0.42 Osm), followed by 10 freeze-thaw cycles between liquid N_2 and a 50 °C water bath. Subsequently, the vesicles were extruded 11× with an Avanti Polar Lipids mini-extruder through a 0.2 µm polycarbonate membrane at 55 °C. After extrusion, the liposomes were purified over a size-exclusion column (GE Healthcare Illustra™ NAP™-25 size exclusion chromatography cartridges) using an isotonic NH_4OAc buffer (pH = 7.0, p = 0.42 Osm). The liposome fraction was then separated from the Na_3HEDTA fraction (Na_3HEDTA eluted from 3.6 mL and further, as visualised by complexometry as described elsewhere[28]). Assuming no losses during preparation, the resulting liposome stock solutions consisted of DPPC:NaDSPE-PEG2K:(metallo)peptide or metal complex in the ratio 100:1:1 with bulk concentrations of 12.5 mM DPPC, 0.125 mM NaDSPE-PEG2K, and 0.125 mM (metallo)peptide or metal

complex. Liposome samples were stored at RT and used the same day. For irradiation experiments, the liposome stock solutions were diluted 5× (see below). DLS was performed on the liposome stock solutions as well as on the diluted liposome samples after irradiation and the irradiation experiments were followed by UV-Vis spectroscopy.

Photoreactions studied by UV-Vis: A cuvette (3 mL) was filled with a mixture of the asymmetric liposome solution (2.5 mM DPPC, 25 µM NaDSPE-PEG2K, and 25 µM (metallo)peptide or metal complex), a solution of $WST1^-$ (0.33 mM) in NH_4OAc buffer (pH = 7.0, p = 0.42 Osm), and/or a solution of $ZnSO_4$ or $Zn(OAc)_2$ (5 mM) in NH_4OAc buffer (pH = 7.0, p = 0.42 Osm). When mixing these solutions, it was critical to make sure all solutions were at the same osmolality of 0.42 Osm, to avoid osmotic stress on the membrane and the associated leakage of Na_3HEDTA encapsulated inside the liposomes. Each sample was deaerated by gently bubbling N_2 through the solution for 15 min under constant stirring. A blue LED (λ_{irr} = 410 or 385 nm for Re and λ_{irr} = 450 nm for Ru obtained from OSRAM Opto Semiconductors) with water cooling was then fitted to the top of the cuvette. The time evolution of the absorbance of the solution was recorded horizontally (optical pathway 1 cm) on a Varian Cary60 spectrophotometer at 25 °C under constant stirring, first in the dark for 30 min, then under light irradiation for 2.5 h (vertical beam, optical pathway 3 cm). The cuvette contained a small hole in the top, which was either left open to air or used to purge the system under N_2 depending on the experimental conditions.

Actinometry: The photon fluxes (in mol/s) of the different LEDs (λ = 385, 410, and 450 nm) used in this work were determined by ferrioxalate actinometry using a standard protocol.[2,29,30] In short, the cuvette used for the photoreactions was charged with a solution of freshly prepared $K_3[Fe(C_2O_4)_3]\cdot 3H_2O$ (3 mL, 150 mM in 0.05 M H_2SO_4). The reaction mixture was stirred for 2 min, followed by irradiation (vertical beam, optical pathway 3 cm) with one of the LEDs for a given time (Figure B14). Afterwards, a fraction of the irradiated solution (1 mL) was transferred to a vial containing a solution of 1,10-phenanthroline (2 mL, 5.55 mM in water), a buffer solution (0.5 mL from a solution prepared from 36.03 g glacial acetic acid, 25.57 g

Na_2SO_4 in 100 mL water and 240 mL 1 M NaOH), and water (1.5 mL). The resulting $[Fe(phen)_3]^{2+}$ (phen = 1,10-phenanthroline) solution (3 mL) was transferred to a cuvette and its absorption spectrum measured by UV-Vis spectroscopy. The absorbance at 510 nm was used to calculate (using the molar absorption coefficient ε = 11110 M^{-1} cm^{-1} in water for $[Fe(phen)_3]^{2+}$ [29]) how much Fe^{2+} was formed during irradiation for a given time ($\frac{dn_{Fe^{2+}}}{dt}$), which is the slope in Figure B14. The following equation was then used to calculate the photon flux (Φ_0) of the respective LED:

$$\frac{dn_{Fe^{2+}}}{dt} = \Phi_0 \left(1 - 10^{-A_{ref}}\right) \varphi_{ref} \qquad \text{Equation B3}$$

In Equations B3, $\left(1 - 10^{-A_{ref}}\right)$ is the probability of photon absorption by the solution and φ_{ref} is the known quantum yield of the ferrioxalate actinometer for the generation of Fe^{2+} at the irradiated wavelength.[2,30] In this particular system, A_{ref} equals A'_{ref} × 3 (as the vertical beam has an optical pathway of 3 cm), where A'_{ref} is the absorption of the non-irradiated solution of $K_3[Fe(C_2O_4)_3]\cdot 3H_2O$ (3 mL, 150 mM in 0.05 M H_2SO_4) at the irradiation wavelength of the LED, measured with a 1 cm pathlength cuvette.[31] Using Equation B3, Φ_0 was 13.1 nmol/s for the 385 nm LED (P = 7.3 mW), 30.4 nmol/s for the 410 nm LED (P = 8.9 mW), and 39.1 nmol/s for the 450 nm LED (P = 15.8 mW).

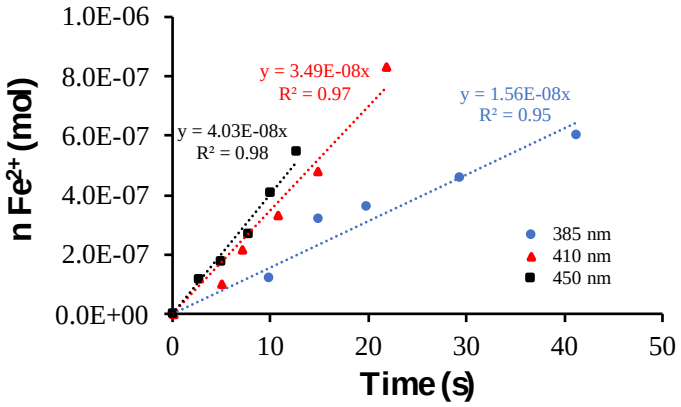

Figure B14. Ferrioxalate actinometry was performed to determine Φ_0 of the used LEDs within the photoirradiation setup.

Transmembrane photoelectron transfer quantum yield determination: The quantum yield (QY) of the photoinduced electron transfer from EDTA to $WST1^-$ through the DPPC membrane functionalised with 1 mol% of a light-activatable metallopeptide was obtained using the following equation:

$$QY = \frac{\#\ \text{photoinduced electron transfer}}{\#\ \text{photons absorbed by photoactive molecule}} = \frac{k_e\, n_e}{\Phi_0\,(1-10^{-A_{ref}})} \quad \text{Equation B4}$$

In Equation B4, k_e is the rate of electron transfer in s^{-1} and n_e is the number of electrons transferred from EDTA to $WST1^-$ in nmol, Φ_0 the photon flux of the LED in nmol/s (see section on actinometry), and $(1 - 10^{-A_{ref}})$ equals the probability of photon absorption by the liposome solution at the irradiation wavelength. The difference in absorption at 438 nm (the molar absorption coefficient ε = 37000 M^{-1} cm^{-1} at 438 nm for $Fz1^{2-}$ in water [32]) after a chosen irradiation time (t = 1 h) was used to calculate the amount of formazan produced, hence $k_e \times n_e$, taking into account that two electrons must be transferred for the formation of one $Fz1^{2-}$ molecule. In this particular system, A_{ref} was not measured experimentally but calculated using the molar absorption coefficients of **WALP23-Ru$_2$** ($\varepsilon = 1.59 \times 10^4$ M^{-1} cm^{-1} at λ = 450 nm in MeOH) and **WALP23-Re$_2$** ($\varepsilon = 3.70 \times 10^3$ M^{-1} cm^{-1} at λ = 385 nm in $CHCl_3$), a pathlength of 3 cm, and the bulk concentration (25 µM) of the metallopeptide, because the absorption measured experimentally has a significant lipid scattering deviation from the Beer-Lambert law generated by the liposomes, in particular in the near-UV domain.[1] Using these values, the QY for electron transfer was determined to be 1.5×10^{-4} for **WALP23-Ru$_2$** and 2.7×10^{-4} for **WALP23-Re$_2$** after 1 h of irradiation.

Table B4. Z_{ave} and PDI of liposomes prepared from DPPC, NaDSPE-PEG2K, and (metallo)peptide or metal complex in a ratio of 100:1:1, which were used for the irradiation experiments.

Sample[a]	**Z_{ave} (nm)**[b]	**PDI**[b]
WALP23-Ru_2 stock before irradiation[c]	135.6 ± 0.8	0.066 ± 0.015
WALP23-Ru_2 after irradiation (no Zn)[c]	134.3 ± 4.9	0.107 ± 0.038
WALP23-Ru_2 after irradiation ($Zn(OAc)_2$)[c]	137.3 ± 3.3	0.116 ± 0.036
WALP23-Ru_2 after irradiation ($ZnSO_4$)	138.0	0.123
WALP23-Re_2 stock before irradiation[c]	123.9 ± 0.5	0.132 ± 0.005
WALP23-Re_2 after irradiation (no Zn)[c]	120.0 ± 1.0	0.126 ± 0.012
WALP23-Re_2 after irradiation ($Zn(OAc)_2$)[c]	121.5 ± 1.0	0.147 ± 0.004
WALP23-bpy_2 stock before irradiation	162.7	0.116
RuC_{15} stock before irradiation	148.1	0.123
RuC_{15} after irradiation (no Zn)	145.3	0.114
RuC_{15} after irradiation ($ZnSO_4$)	146.9	0.119
ReC_{15} stock before irradiation	117.0	0.125
ReC_{15} after irradiation (no Zn)	114.8	0.103
ReC_{15} after irradiation ($Zn(OAc)_2$)	116.3	0.116

[a] Experimental conditions for liposome stock solutions: [DPPC] = 12.5 mM, [NaDSPE-PEG2K] = 125 μM, [**WALP23-Ru_2** or **WALP23-Re_2**] = 125 μM, [$HEDTA^{3-}$] = 0.125 M (before SEC column) in 0.1 M NH_4OAc (pH = 7.0, p = 0.42 Osm). Experimental condition for diluted liposomes solutions after irradiation: [DPPC] = 2.5 mM, [NaDSPE-PEG2K] = 25 μM, [**WALP23-Ru_2** or **WALP23-Re_2**] = 25 μM, [$HEDTA^{3-}$] = 0.125 M (before SEC column), [$WST1^{-}$] = 0.33 mM, and with or without [$Zn(OAc)_2$ or $ZnSO_4$] = 5 mM in 0.1 M NH_4OAc (pH = 7.0, p = 0.42 Osm). [b] The liposome size is considered to be uniformly distributed when PDI < 0.2. [c] Samples were prepared in duplicate (to perform the photoreaction experiments under air and under N_2). The errors correspond to the average deviation from the mean.

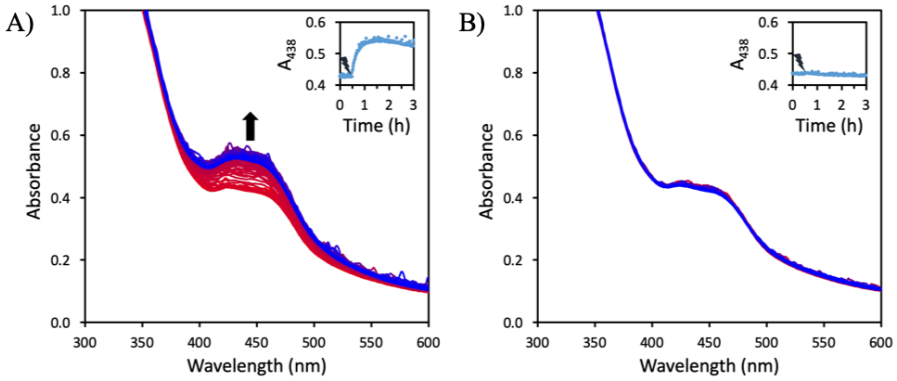

Figure B15. The change in absorbance due to the conversion of $WST1^{-}$ versus irradiation time for liposomes prepared from DPPC:NaDSPE-PEG2K:**WALP23-Ru$_2$** (100:1:1) in absence (A) or in presence (B) of added $Zn(OAc)_2$ (5 mM). Experimental conditions: [DPPC] = 2.5 mM, [NaDSPE-PEG2K] = 25 µM, [**WALP23-Ru$_2$**] = 25 µM, [$HEDTA^{3-}$] = 0.125 M (before SEC column), [$WST1^{-}$] = 0.33 mM, [$Zn(OAc)_2$] = 0 or 5 mM in 0.1 M NH_4OAc (pH = 7.0), under an air atmosphere, and blue light irradiation (λ_{irr} = 450 nm, P = 15.8 mW, Φ_0 = 39.1 nmol/s).

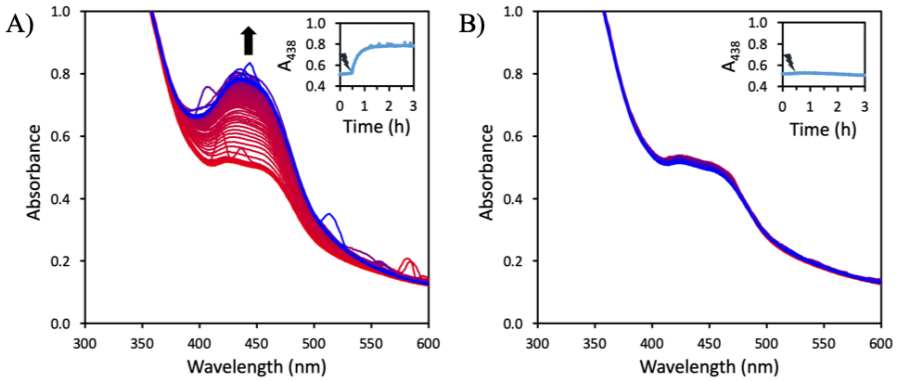

Figure B16. The change in absorbance due to the conversion of $WST1^{-}$ versus irradiation time for liposomes prepared from DPPC:NaDSPE-PEG2K:**WALP23-Ru$_2$** (100:1:1) in absence (A) or in presence (B) of added $Zn(OAc)_2$ (5 mM). Experimental conditions: [DPPC] = 2.5 mM, [NaDSPE-PEG2K] = 25 µM, [**WALP23-Ru$_2$**] = 25 µM, [$HEDTA^{3-}$] = 0.125 M (before SEC column), [$WST1^{-}$] = 0.33 mM, [$Zn(OAc)_2$] = 0 or 5 mM in 0.1 M NH_4OAc (pH = 7.0), under a N_2 atmosphere, and blue light irradiation (λ_{irr} = 450 nm, P = 15.8 mW, Φ_0 = 39.1 nmol/s).

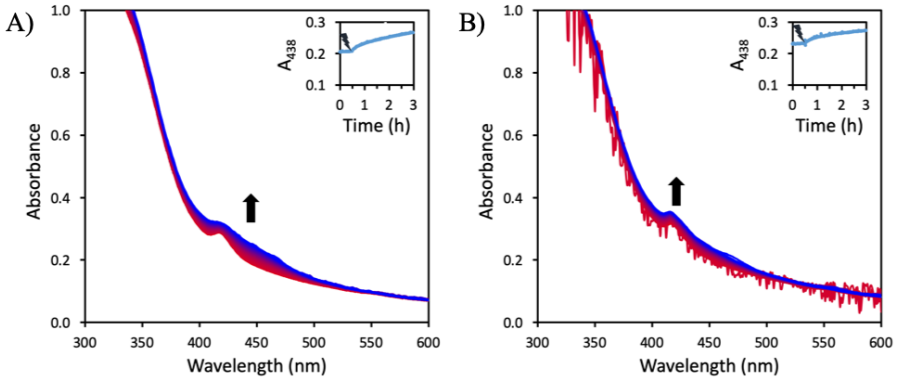

Figure B17. The change in absorbance due to the conversion of $WST1^-$ versus irradiation time for liposomes prepared from DPPC:NaDSPE-PEG2K:**WALP23-Re$_2$** (100:1:1) in absence (A) or in presence (B) of added $Zn(OAc)_2$ (5 mM). Experimental conditions: [DPPC] = 2.5 mM, [NaDSPE-PEG2K] = 25 µM, [**WALP23-Re$_2$**] = 25 µM, [$HEDTA^{3-}$] = 0.125 M (before SEC column), [$WST1^-$] = 0.33 mM, [$Zn(OAc)_2$] = 0 or 5 mM in 0.1 M NH_4OAc (pH = 7.0), under an air atmosphere, and blue light irradiation (λ_{irr} = 385 nm, P = 7.3 mW, Φ_0 = 13.1 nmol/s).

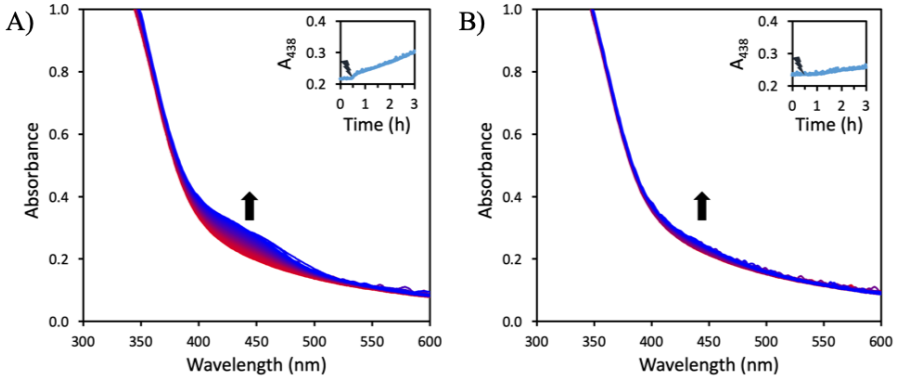

Figure B18. The change in absorbance due to the conversion of $WST1^-$ versus irradiation time for liposomes prepared from DPPC:NaDSPE-PEG2K:**WALP23-Re$_2$** (100:1:1) in absence (A) or in presence (B) of added $Zn(OAc)_2$ (5 mM). Experimental conditions: [DPPC] = 2.5 mM, [NaDSPE-PEG2K] = 25 µM, [**WALP23-Re$_2$**] = 25 µM, [$HEDTA^{3-}$] = 0.125 M (before SEC column), [$WST1^-$] = 0.33 mM, [$Zn(OAc)_2$] = 0 or 5 mM in 0.1 M NH_4OAc (pH = 7.0), under a N_2 atmosphere, and blue light irradiation (λ_{irr} = 410 nm, P = 8.9 mW, Φ_0 = 30.4 nmol/s).

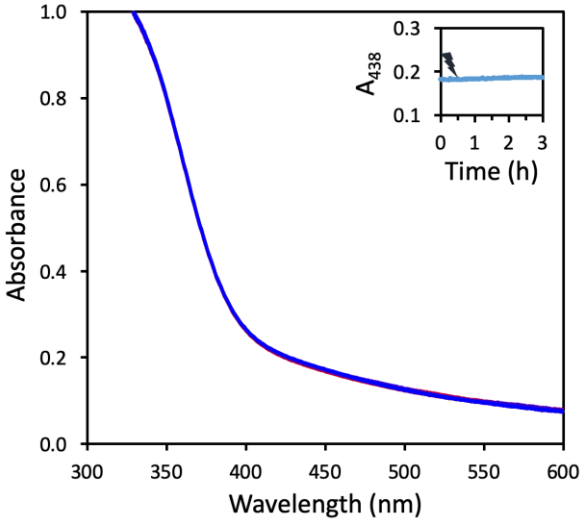

Figure B19. The change in absorbance due to the conversion of $WST1^{-}$ versus irradiation time for liposomes prepared from DPPC:NaDSPE-PEG2K:**WALP23-bpy$_2$** (100:1:1) in absence of added $Zn(OAc)_2$. Experimental conditions: [DPPC] = 2.5 mM, [NaDSPE-PEG2K] = 25 µM, [**WALP23-bpy$_2$**] = 25 µM, [$HEDTA^{3-}$] = 0.125 M (before SEC column), [$WST1^{-}$] = 0.33 mM in 0.1 M NH_4OAc (pH = 7.0), under a N_2 atmosphere, and blue light irradiation (λ_{irr} = 410 nm, P = 8.9 mW, Φ_0 = 30.4 nmol/s).

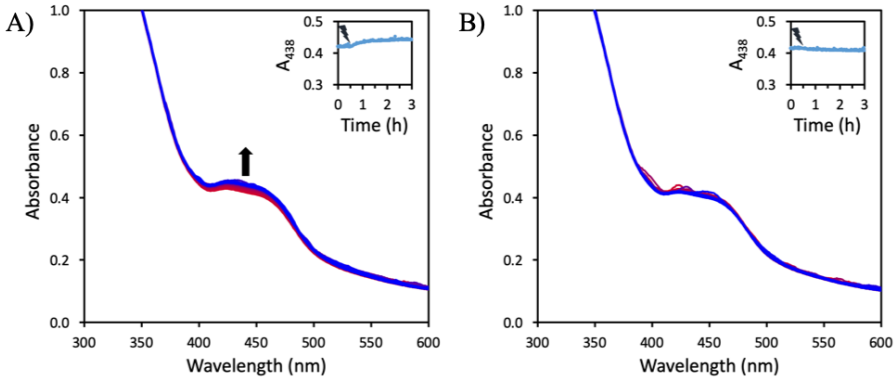

Figure B20. The change in absorbance due to the conversion of $WST1^{-}$ versus irradiation time for liposomes prepared from DPPC:NaDSPE-PEG2K:**RuC$_{15}$** (100:1:1) in absence (A) or in presence (B) of $Zn(OAc)_2$ (5 mM). Experimental conditions: [DPPC] = 2.5 mM, [NaDSPE-PEG2K] = 25 µM, [**RuC$_{15}$**] = 25 µM, [$HEDTA^{3-}$] = 0.125 M (before SEC column), [$WST1^{-}$] = 0.33 mM, [$ZnSO_4$] = 0 or 5 mM in 0.1 M NH_4OAc (pH = 7.0), under a N_2 atmosphere, and blue light irradiation (λ_{irr} = 450 nm, P = 15.8 mW, Φ_0 = 39.1 nmol/s).

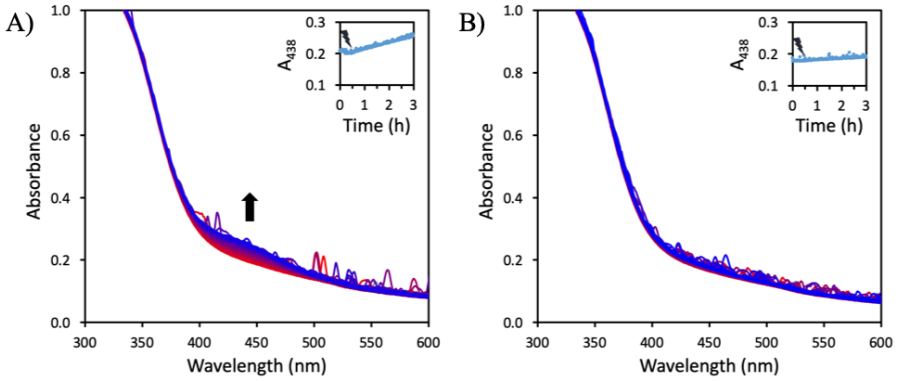

Figure B21. The change in absorbance due to the conversion of $WST1^{-}$ versus irradiation time for liposomes prepared from DPPC:NaDSPE-PEG2K:**ReC_{15}** (100:1:1) in absence (A) or in presence (B) of added $Zn(OAc)_2$ (5 mM). Experimental conditions: [DPPC] = 2.5 mM, [NaDSPE-PEG2K] = 25 µM, [**ReC_{15}**] = 25 µM, $[HEDTA^{3-}]$ = 0.125 M (before SEC column), $[WST1^{-}]$ = 0.33 mM, $[Zn(OAc)_2]$ = 0 or 5 mM in 0.1 M NH_4OAc (pH = 7.0), under a N_2 atmosphere, and blue light irradiation (λ_{irr} = 410 nm, P = 8.9 mW, Φ_0 = 39.1 nmol/s).

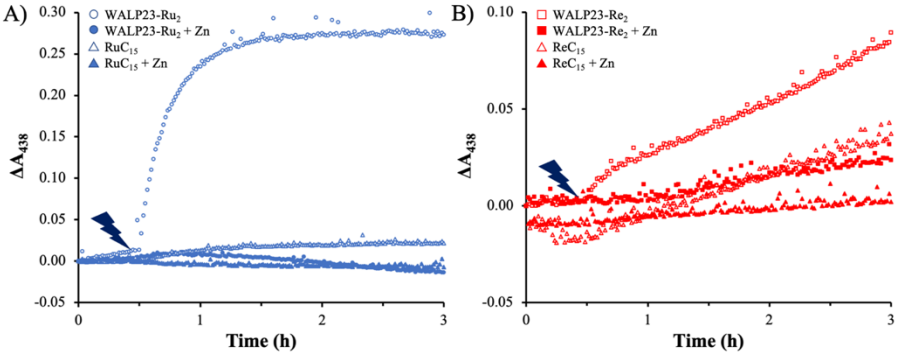

Figure B22. The formation of Fz^{2-} as monitored by a change in absorbance (λ_{max} = 438 nm) versus irradiation time for liposome systems containing **WALP23-Ru_2** or **RuC_{15}** (A) or **WALP23-Re_2** or **ReC_{15}** (B) with (open symbols) or without Zn (closed symbols). The data are based on the insets of Figures B16, B18, B20, and B21. Experimental conditions: [DPPC] = 2.5 mM, [NaDSPE-PEG2K] = 25 µM, [**WALP23-Ru_2**, **RuC_{15}**, **WALP23-Re_2** or **ReC_{15}**] = 25 µM, $[HEDTA^{3-}]$ = 0.125 M (before SEC column), $[WST1^{-}]$ = 0.33 mM, $[Zn(OAc)_2$ or $ZnSO_4]$ = 0 or 5 mM in 0.1 M NH_4OAc (pH = 7.0), under a N_2 atmosphere, and blue light irradiation (λ_{irr} = 450 nm, P = 15.8 mW, Φ_0 = 39.1 nmol/s for **WALP23-Ru_2** and **RuC_{15}**, λ_{irr} = 410 nm, P = 8.9 mW, Φ_0 = 30.4 nmol/s for **WALP23-Re_2** and **ReC_{15}**).

B. 7. Leakage studies

Protocol to determine the concentration of $HEDTA^{3-}$ in liposome samples: The concentration of $HEDTA^{3-}$ (both outside the liposomes, and in the whole sample) was determined by complexometry as described earlier.[28] In this work, we determined the concentration of $HEDTA^{3-}$ for three different cases: a) directly after liposome preparation; b) 3 h after liposome preparation, keeping the samples in the dark; and c) after irradiation experiments (0.5 h dark and 2.5 h light irradiation). In short, a cuvette (3 mL) was equipped with either 0.1 mL liposome stock solution (0.125 mM (metallo)peptide or metal complex) for case a and b, or 0.5 mL liposome solution (0.025 mM (metallo)peptide or metal complex) for case c. Afterwards an aqueous solution of NH_4OAc (pH = 7.0, p = 0.42 mOsm) was added to reach a total volume of 2.9 mL. Finally, a solution of murexide (9 mg of 250:1 K_2SO_4:murexide) in 0.1 mL NaOH (0.1 M) was added, resulting in bulk concentrations of 0.4167 mM DPPC, 4.167 µM NaDSPE-PEG2K, and 4.167 µM (metallo)peptide or metal complex respectively (30× dilution compared to the liposome stock solution). The murexide/liposome solution was titrated with an aqueous solution of $Cu(NO_3)_2$ (10 mM, 2 µL per addition), and a UV-Vis spectrum was recorded after each addition. The amount of $HEDTA^{3-}$ present in the aqueous bulk was determined as follows; when addition of one further drop of the copper solution led to a decrease in the absorbance at 525 nm (free murexide), it meant that all the $HEDTA^{3-}$ in the aqueous bulk was bound to Cu^{2+} and therefore that [Cu(murexide)] (λ = 468 nm) was formed (see Scheme B2). In a second step, the liposomes were destroyed by the addition of 5 µL 10% w/v% triton-X100, leading to a further increase in the absorbance at 525 nm, due to the release of $HEDTA^{3-}$ from the inner compartment of the liposome to the bulk, leading to a competitive complexation of copper. The $Cu(NO_3)_2$ titration of the murexide/destroyed liposome solutions was resumed (10 mM, 2 µL per addition). When addition of one drop of the copper solution led to a second decrease in the absorbance at 525 nm, all $HEDTA^{3-}$ (bulk + inner compartment) was bound to Cu^{2+}, which provided the total amount of $HEDTA^{3-}$ in the sample.

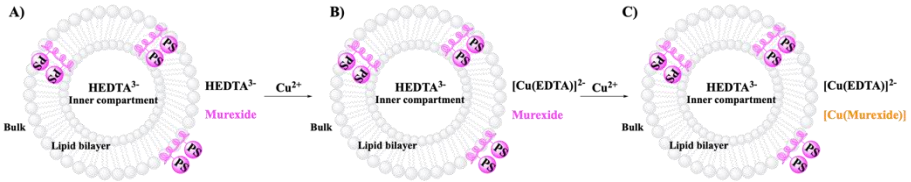

Scheme B2. Titration of $HEDTA^{3-}$ in asymmetric liposome samples using murexide and Cu^{2+}. **(A)** At the start of the experiment, the solution is purple (λ = 525 nm) due to the presence of unbound murexide. **(B)** Cu^{2+} will first react with $HEDTA^{3-}$ to form $[Cu(EDTA)]^{2-}$; the solution is still purple due to the presence of unbound murexide. **(C)** Addition of excess Cu^{2+} compared to $HEDTA^{3-}$ leads to the reaction between Cu^{2+} and murexide. The newly formed [Cu(murexide)] is orange (λ = 468 nm), leading to a decrease of the absorption at 525 nm, which is detected.

Table B5. Concentration of $HEDTA^{3-}$ in the bulk aqueous phase, $C_{outside}$, and the total amount of $HEDTA^{3-}$ present in the liposome sample after liposome disruption following addition of triton-X100, C_{total}, as determined by murexide titration following the absorbance at 525 nm.

Sample	$C_{outside}$ (mM)[a]	C_{total} (mM)[a]
WALP23-Ru_2 t = 0 h	0.0 – 0.2	0.4 – 0.6
WALP23-Ru_2 t = 3 h, dark	0.0 – 0.2	0.4 – 0.6
WALP23-Ru_2 t = 3 h, light	0.2 – 0.4	0.4 – 0.6
WALP23-Re_2 t = 0 h	0.0 – 0.2	1.4 – 1.6
WALP23-Re_2 t = 3 h, dark	0.0 – 0.2	1.4 – 1.6
WALP23-Re_2 t = 3 h, light	0.4 – 0.6	1.4 – 1.6
RuC_{15} before reaction[b]	0.4 – 0.6	2.0 – 2.2
RuC_{15} after reaction	0.4 – 0.6	2.0 – 2.2
ReC_{15} before reaction[b]	0.4 – 0.6	1.8 – 2.0
ReC_{15} after reaction	0.4 – 0.6	2.2 – 2.4
WALP23-bpy_2 before reaction[b]	0.0 – 0.1	0.9 – 1.0
WALP23-bpy_2 after reaction	n.d.	n.d.

[a] The concentrations of $HEDTA^{3-}$ given are the ones for the liposome stock solution; thus, the concentration of $HEDTA^{3-}$ determined by murexide titration was multiplied by 30 to take into account the dilution factor. A range is given for the concentrations; the first number corresponds to the amount of Cu^{2+} that was added without observing a change in the absorption at 525 nm, and the last number corresponds to the amount of Cu^{2+} that was needed to induce a decrease in the absorption at 525 nm. [b] Determined within 3 h after liposome preparation to minimise passive leakage of $HEDTA^{3-}$ across the lipid bilayer.

B. 8. References

1 D. M. Klein, S. Rodríguez-Jiménez, M. E. Hoefnagel, A. Pannwitz, A. Prabhakaran, M. A. Siegler, T. E. Keyes, E. Reisner, A. M. Brouwer and S. Bonnet, *Chem. Eur. J.*, 2021, **27**, 17203–17212.

2 C. G. Hatchard, C. A. Parker and E. J. Bowen, *Proc. R. Soc. Lond. Ser. Math. Phys. Sci.*, 1956, **235**, 518–536.

3 M. W. H. Hoorens, M. Medved', A. D. Laurent, M. Di Donato, S. Fanetti, L. Slappendel, M. Hilbers, B. L. Feringa, W. J. Buma and W. Szymanski, *Nat. Commun.*, 2019, **10**, 2390.

4 J. J. Snellenburg, S. Laptenok, R. Seger, K. M. Mullen and I. H. M. van Stokkum, *J. Stat. Softw.*, 2012, **49**, 1–22.

5 E. Krieger and G. Vriend, *Bioinformatics*, 2014, **30**, 2981–2982.

6 M. R. R. de Planque and J. A. Killian, *Mol. Membr. Biol.*, 2003, **20**, 271–284.

7 J. A. Killian, I. Salemink, M. R. R. de Planque, G. Lindblom, R. E. Koeppe and D. V. Greathouse, *Biochemistry*, 1996, **35**, 1037–1045.

8 K. J. Kise and B. E. Bowler, *Tetrahedron Asymmetry*, 1998, **9**, 3319–3324.

9 J. E. Collins, J. J. S. Lamba, J. C. Love, J. E. McAlvin, C. Ng, B. P. Peters, X. Wu and C. L. Fraser, *Inorg. Chem.*, 1999, **38**, 2020–2024.

10 K. J. Kise and B. E. Bowler, *Inorg. Chem.*, 2002, **41**, 379–386.

11 D. V. Greathouse, R. L. Goforth, T. Crawford, P. C. A. van der Wel and J. A. Killian, *J. Pept. Res.*, 2001, **57**, 519–527.

12 A. Juris, V. Balzani, F. Barigelletti, S. Campagna, P. Belser and A. von Zelewsky, *Coord. Chem. Rev.*, 1988, **84**, 85–277.

13 N. Ikuta, S. Y. Takizawa and S. Murata, *Photochem. Photobiol. Sci.*, 2014, **13**, 691–702.

14 M. J. Abraham, T. Murtola, R. Schulz, S. Páll, J. C. Smith, B. Hess and E. Lindahl, *SoftwareX*, 2015, **1–2**, 19–25.

15 E. J. Sorin and V. S. Pande, *Biophys. J.*, 2005, **88**, 2472–2493.

16 A. V. Marenich, S. V. Jerome, C. J. Cramer and D. G. Truhlar, *J. Chem. Theory Comput.*, 2012, **8**, 527–541.

17 P. Brandt, T. Norrby, B. Åkermark and P.-O. Norrby, *Inorg. Chem.*, 1998, **37**, 4120–4127.

18 P. Li and K. M. Merz, *J. Chem. Inf. Model.*, 2016, **56**, 599–604.

19 M. J. Frisch, G. W. Trucks, H. B. Schlegel, G. E. Scuseria, M. A. Robb, J. R. Cheeseman, G. Scalmani, V. Barone, G. A. Petersson, H. Nakatsuji, X. Li, M. Caricato, A. V. Marenich, J. Bloino, B. G. Janesko, R. Gomperts, B. Mennucci, H. P. Hratchian, J. V. Ortiz, A. F. Izmaylov, J. L. Sonnenberg, D. Williams-Young, F. Ding, F. Lipparini, F. Egidi, J. Goings, B. Peng, A. Petrone, T. Henderson, D. Ranasinghe, V. G. Zakrzewski, J. Gao, N. Rega, G. Zheng, W.

Liang, M. Hada, M. Ehara, K. Toyota, R. Fukuda, J. Hasegawa, M. Ishida, T. Nakajima, Y. Honda, O. Kitao, H. Nakai, T. Vreven, K. Throssell, J. A. Montgomery Jr., J. E. Peralta, F. Ogliaro, M. J. Bearpark, J. J. Heyd, E. N. Brothers, K. N. Kudin, V. N. Staroverov, T. A. Keith, R. Kobayashi, J. Normand, K. Raghavachari, A. P. Rendell, J. C. Burant, S. S. Iyengar, J. Tomasi, M. Cossi, J. M. Millam, M. Klene, C. Adamo, R. Cammi, J. W. Ochterski, R. L. Martin, K. Morokuma, O. Farkas, J. B. Foresman and D. J. Fox, Gaussian, Inc., Wallingford CT, 2016.

20 J. P. M. Jämbeck and A. P. Lyubartsev, *J. Phys. Chem. B*, 2012, **116**, 3164–3179.

21 W. L. Jorgensen, J. Chandrasekhar, J. D. Madura, R. W. Impey and M. L. Klein, *J. Chem. Phys.*, 1983, **79**, 926–935.

22 G. Bussi, D. Donadio and M. Parrinello, *J. Chem. Phys.*, 2007, **126**, 014101.

23 H. J. C. Berendsen, J. P. M. Postma, W. F. van Gunsteren, A. DiNola and J. R. Haak, *J. Chem. Phys.*, 1984, **81**, 3684–3690.

24 M. Parrinello and A. Rahman, *J. Appl. Phys.*, 1981, **52**, 7182–7190.

25 S. Nosé and M. L. Klein, *Mol. Phys.*, 1983, **50**, 1055–1076.

26 U. Essmann, L. Perera, M. L. Berkowitz, T. Darden, H. Lee and L. G. Pedersen, *J. Chem. Phys.*, 1995, **103**, 8577–8593.

27 A. Pannwitz, H. Saaring, N. Beztsinna, X. Li, M. A. Siegler and S. Bonnet, *Chem. Eur. J.*, 2021, **27**, 3013–3018.

28 B. Limburg, E. Bouwman and S. Bonnet, *Chem. Commun.*, 2015, **51**, 17128–17131.

29 J. N. Demas, W. D. Bowman, E. F. Zalewski and R. A. Velapoldi, *J. Phys. Chem.*, 1981, **85**, 2766–2771.

30 B. Limburg, E. Bouwman and S. Bonnet, *ACS Catal.*, 2016, **6**, 5273–5284.

31 A. Bahreman, M. Rabe, A. Kros, G. Bruylants and S. Bonnet, *Chem. Eur. J.*, 2014, **20**, 7429–7438.

32 M. Ishiyama, M. Shiga, K. Sasamoto, M. Mizoguchi and P. He, *Chem. Pharm. Bull.*, 1993, **41**, 1118–1122.

Appendix C

Supporting information for Chapter 3

C. 1. Methods

General methods. ^{1}H NMR and ^{13}C NMR spectra were recorded on a Bruker AV400 MHz spectrometer and ^{19}F NMR spectra on a Bruker AV500 MHz spectrometer. Chemical shift values (δ) are reported in ppm relative to the solvent. Electrospray ionisation mass spectrometry (ESI-MS) spectra were measured with a ThermoFischer Scientific MSQ Plus electrospray ionisation mass spectrometer with a 17 – 2000 *m/z* detection range and a resolution of approximately 0.5 *m/z*. High-resolution mass spectrometry (HRMS) was measured via direct injection on a Thermo Finnagan LTQ Orbitrap with electrospray ionisation. Elemental analysis was performed by Mikroanalytisches Laboratorium Kolbe in Oberhausen, Germany. UV-Vis absorption spectra were measured on a Varian Cary60 spectrophotometer equipped with a single cell Peltier temperature controller at 25 °C using either a 3 mL cuvette for standard solutions or a 0.6 mL cuvette for liposome solutions. Emission spectra were measured on a FLS900 spectrometer from Edinburgh Instruments Ltd. in a 3 mL cuvette at 22 °C using 380 nm as excitation source for the rhenium complexes and 450 nm as excitation source for the ruthenium complexes. Luminescence lifetimes were measured for rhenium complexes using the set-up for transient absorption spectroscopy described below, using an excitation wavelength of 380 nm. Instead of detecting the transmitted probe light, the spontaneous emission generated by the laser pulse was observed at different delay times determined by the electronically controlled detector gate (gate width = 5 ns), and the intensity versus time was modelled by a monoexponential decay using Glotaran.[1] Confocal microscopy images were taken on a Nikon Eclipse Ti microscope with 20x objective (0.75 NA, 1.00 WD) and confocal imaging with 488 nm laser and 640 – 680 nm detection wavelength. Images were processed with the Fiji version of ImageJ2.

Preparation of liposomes for immobilisation studies and photocatalysis. DMPC, DPPC, or DSPC lipids in chloroform, NaDSPE-PEG2K in chloroform, **RuC$_n$** in methanol, and/or **ReC$_n$** in chloroform were added in a pressure resistant tube. The organic solvents were evaporated under reduced pressure and the resulting lipid film was dried for at least 1 hour in *vacuo* to remove residual solvent. The film was then hydrated with NaH_2PO_4 buffer (4 mL, 0.1 M, pH = 7.7) with or without sodium ascorbate (0.1 M), followed by 10 freeze-thaw cycles in liquid N_2 and 50 °C water bath. Subsequently, the vesicles were extruded 11x with an Avanti Polar Lipids mini-extruder through a 0.2 µm polycarbonate membrane at 10 °C above the phase transition temperature of the lipid. Assuming no losses during preparation, the resulting liposomes consist of lipid:NaDSPE-PEG2K:**RuC$_n$**:**ReC$_n$** in the ratio 100:1.0:0.4:0.4 with expected bulk concentrations of 6.25 mM lipid, 0.625 mM NaDSPE-PEG2K, and 0.025 mM **RuC$_n$** and 0.025 mM **ReC$_n$**. Liposome samples were stored at RT and used within one week. For photocatalytic CO_2 reduction experiments, the liposome solutions were diluted ten-fold with the same buffer as that used for liposome preparation. The size distribution of the hydrodynamic diameter (Z_{ave}) and the polydispersity index (PDI) were measured at 25 °C by dynamic light scattering with a Zetasizer Nano-S from Malvern operating at 632.8 nm with a scattering angle of 173°; at this wavelength neither **RuC$_n$** nor **ReC$_n$** absorb light significantly.

Photocatalysis measurements. Before photocatalysis, the liposome-containing solution obtained right after extrusion (0.3 mL) was diluted 10-fold using an aqueous solution containing 0.1 M phosphate buffer and 0.1 M sodium ascorbate. It was then purged in triplicates for 20 min with CO_2, or N_2 for control experiments, containing in both cases 2% methane as internal standard for gas chromatography. After purging, the vials were kept in a water bath at 25 °C and irradiated for 3 h using a Newport Oriel Xenon 150 W solar light simulator (100 mW cm^{-2}, AM1.5G containing infrared water and ultraviolet (λ > 455 or 400 nm) filters).

Product quantification. The amount of produced H_2 and CO was monitored by headspace gas analysis using a Shimadzu Tracera GC-2010 Plus with a barrier discharge ionisation detector. The GC-2010 Plus was equipped with a

ShinCarbon micro-ST column (0.53 mm diameter) kept at 40 °C using helium carrier gas. Aliquots of 50 µL of the headspace gas were removed from the sealed photocatalytic vials using a gastight syringe (Hamilton) for gas chromatography analysis at hourly time intervals. Each different photocatalytic experiment was performed in triplicate, unless stated otherwise. Data are presented as mean ± standard error of the mean. The mean values and standard errors of the mean were calculated from the number of repeats of independent experiments.

Isotopic labelling experiment. Photocatalysis experiment with $^{13}CO_2$ as the headspace gas was performed. After three hours of simulated light irradiation, the vial headspace was transferred to an evacuated gas infrared cell (SpecAc, 10 cm path length, equipped with KBr windows) and a high-resolution transmission spectrum was collected on a Thermo Scientific Nicolet iS50 FT-IR spectrometer. To check whether formate had formed, an aliquot of the aqueous phase, together with a D_2O solution of trimethylsilylpropanoic acid as internal standard, was measured by ^1H NMR on a Bruker 400 MHz NMR spectrometer at room temperature.

Quantum yield measurements. One-millilitre solutions containing DPPC liposomes made of **ReC$_9$** and **RuC$_9$** (bulk concentration = 25 µM) were irradiated with monochromatic light (λ = 455 nm), using two different light intensities (I_1 = 10.5 mW cm^{-2}, and I_2 = 13.5 mW cm^{-2}), produced by a solar simulator (LOT LSN 254) equipped with a monochromator (LOT MSH 300). Duplicate experiments were performed for each light intensity and the averaged values of the produced mol of CO were utilised to determine the Φ_{CO} using Equation C1:

$$\Phi_{CO}\ (\%) = \frac{2\, n_{CO}\, N_A\, h\, c}{t_{irr}\, \lambda\, I\, A\, P} \cdot 100 \qquad \text{Equation C1}$$

where n_{CO} is the moles of photogenerated CO gas ($n_{CO,1}$ = 2.12 x 10^{-8} mol and $n_{CO,2}$ = 1.20 x 10^{-8} mol), N_A is the Avogadro constant in mol^{-1}, h is the Planck constant in J s, c the speed of light in m s^{-1}, t_{irr} is the irradiation time (3600 s), λ is the monochromatic light wavelength in m, I the light intensity in J s^{-1}

m^{-2}, and A is the irradiation cross-section (1 x 10^{-4} m^2). P is the probability of absorbing a photon by the photosensitiser, i.e. 1 – $10^{-(Abs@454nm)}$, where due to the high scattering of the DPPC liposomes the absorbance used (0.252) was calculated employing the bulk concentration (25 µM), the molar absorption coefficient (1.32 x 10^4 M^{-1} cm^{-1}), and the immobilisation correction factor (η_{immob} = 0.764) of photosensitiser **RuC$_9$**.

Protocol for cyclic voltammetry (CV) and differential pulse voltammetry (DPV). CV and DPV were recorded with an Autolab Pgstat 10 potentiostat controlled by GPES4 software in a customised glass cell, equipped with a 1 mM solution of **RuC$_n$** or **ReC$_n$** and 0.1 M Bu_4NPF_6 in 6 mL dry acetonitrile or dichloromethane. The solution was stirred and degassed with argon for 15 minutes before each measurement. At the end of each measurement, 5 mg (0.03 mmol) ferrocene was added as an internal reference. A glassy carbon working electrode, a Ag/AgCl reference electrode, and a platinum counter electrode were employed to obtain spectra typically from –2.0 V to 1.6 V, with a scan rate of 100 mV/s (CV) or 50 mV/s (DPV).

Protocol for studying immobilisation efficiency of metal complexes on liposomes. For the immobilisation efficiency tests, liposome samples (0.6 mL) were loaded in specialised safe-lock Eppendorfs (Thermo Scientific X100 Tube PA Microtubes, 1.5 mL) and placed within adapters from Beranek Laborgeräte (catalogue number 11044). Subsequently, the liposomes were spinned down by ultracentrifugation on a Beckman Coulter Optima XE-90 Ultracentrifuge, using a Ti70 rotor at 36000 rpm (max. 100.4 kG) and 4 °C. Afterwards, the supernatant was separated from the pellet containing liposomes and immobilised metal complexes. Both the liposome stock sample before ultracentrifugation, as well as the supernatant were subsequently studied by UV-Vis spectroscopy and ICP-MS analysis.

Protocol for ICP-MS analysis. The supernatant samples for ICP-MS were prepared by digesting 100 µL supernatant sample in 100 µL nitric acid (65%) in a 10 mL plastic tube overnight. Then 9.8 mL MilliQ water was added. The solutions still containing liposomes were prepared by adding 100 µL liposome sample to 80 µL 37% HCl and 120 µL 65% HNO_3 in a glass tube with

a glass marble on top and digesting for 48 hours at 90°C in the oven. After 48 hours the water had evaporated and 10 mL MilliQ water was added. The ruthenium and rhenium content of the samples were subsequently measured in triplicate using a NexION 2000 ICP mass spectrometer, a SC2 DX auto sampler, and Syngistix software from Perkin Elmer.

Nanosecond transient absorption spectroscopy. Nanosecond transient absorption was measured using an in-house assembled setup in which transient (ΔA) spectra were recorded as a function of delay time with respect to a laser pulse exciting the solution.[2] The excitation pulses at 450 nm (3.5 mJ/pulse; ca. 5 ns full width at half maximum) were generated using a tunable Nd:YAG-laser system (NT342B, Ekspla). The laser system was operated at a repetition rate of 5 Hz. The probe light, running at 10 Hz, was generated by a high-stability short arc xenon flash lamp (FX-1160, Excelitas Technologies) with a modified PS302 controller (EG&G). The probe light was split in a signal and a reference beam with a 50/50 beam splitter and focused on the entrance slit of a spectrograph (SpectraPro-150, Princeton Instruments). The probe beam (A = 1 mm^2) was passed through the sample cell and orthogonally overlapped with the excitation beam on a 1 mm × 1 cm area. The excitation power was recorded by measuring the excitation power at the back of an empty sample holder. The reference beam was used to normalise the signal for fluctuations in the flash lamp spectral intensity. Both beams were recorded simultaneously using a gated intensified CCD camera (PI-MAX3, Princeton Instruments) with an adjustable gate (gate width = 20 ns). The timing of the excitation pulse, the flash lamp, and the gate of the camera was achieved with a delay generator (DG645, Stanford Research Systems, Inc.). The setup was controlled by an in-house written program (LabView). Spectra were averaged from 490 to 540 nm (**RuC$_n^-$** absorption) and the ΔA_{av} values as a function of time were fitted with Equation 3.5 using Igor Pro version 8 (Wavemetrics).

Microcavity Support. The micropore array substrates for fluorescence correlation spectroscopy were prepared in polydimethylsiloxane (PDMS) as described previously.[3] First, mica sheets were cut in to 1 cm^2 area and glued to a cover glass slide. ~20 µL of ethanolic solution of 0.1% of 4.61 µm

polystyrene spheres was drop cast onto the flat mica sheet and after evaporation, PDMS was poured over the array of spheres, and cured at 90 °C for 1 h. On cooling, the PDMS was gently peeled off to create a thin chamber of identical dimensions of mica sheet thickness. The pores were generated by dissolving PS sphere from the PDMS substrate by immersion and sonication in tetrahydrofuran for 15 min. The substrates were then left to dry overnight. The PDMS substrates were then plasma cleaned using oxygen plasma for 5 min to make the surface hydrophilic and the microcavities were buffer filled by sonication and stored inside buffer prior to applying the bilayer.

Preparation of microcavity supported lipid bilayers. The lipid bilayers were prepared on the PDMS substrate containing 2 µm sized cavities through Langmuir-Blodgett technique followed by vesicle fusion methods.[3] The proximal lipid monolayer was transferred by Langmuir-Blodgett technique (KSV Nema) in the air-water interface. The lipid solution was left to evaporate for about 10 min at the sub-phase surface (MilliQ water, pH 7.4) and the lipid monolayer was transferred at a surface pressure of 40 mN/m. The liposomes were prepared by mixing DPPC:NaDSPE-PEG2K:**RuC$_n$** in the ratio 100:1: $4{\cdot}10^{-4}$ and then it was dried under nitrogen flow. It was kept under vacuum for 60 minutes and hydrated using phosphate buffer saline (pH 7.7) followed by vortex agitation. These vesicles were extruded with 0.2 µm polycarbonate membrane at 10 °C above the phase transition temperature of the lipid. These vesicles were injected to the microfluidic chamber of lipid monolayer. It was allowed to fuse for 90 min and the residual liposomes were removed by phosphate buffer saline wash.

Fluorescence lifetime correlation spectroscopy (FLCS). The diffusion coefficient of **RuC$_n$**-labelled supported lipid bilayers were obtained using FLCS, accomplished on a MicroTime 200 system (Picoquant GmBH, Berlin, Germany) consisting of an inverted Olympus X1-71 microscope with an Olympus UPlanSApo 60x/1.2 water immersion objective, a time correlated single photon counting (TCSPC) unit, and a dual single photo avalanche diode (SPAD). The **RuC$_n$** probes were excited with a 532 nm laser PicoTA from Toptica (Picoquant) with a pulse repetition rate of 20 MHz. 532 nm was

selected as the excitation wavelength as it gave superior S/N ratio in the time trace due to reflectance from the substrate at 440 nm. The excitation light was directed onto the sample through the objective lens by a 440/532rpc dichroic mirror. The emitted fluorescence was also collected through the same objective and filtered by the dichroic mirror and by a 580 nm interference filter. A 50 µm pinhole was used in order to confine the detection volume in the axial direction onto the SPAD. The autocorrelation functions (ACFs) were fitted using Equation C2:

$$G(\tau) = \left[\frac{1}{N}\right]\left[\frac{1}{1+\left(\frac{\tau}{\tau_{D1}}\right)^{\alpha_1}}\right] + \left[\frac{(1-c)}{\left(1+\frac{\tau}{\tau_{D2}}\right)^{\alpha_2}}\right] \qquad \text{Equation C2}$$

where G(τ) is the autocorrelation function of fluorescence fluctuations, N is the average number of diffusing fluorophores in the effective volume, τ is the delay time, τ_{D1} and τ_{D2} are the diffusion time of the molecules across the confocal volume of the 1st component and 2nd component respectively, α_1 and α_2 are the anomalous parameters of the 1st and 2nd components, respectively, and c is the contribution of the diffusing species. ACFs were fitted using the two-dimensional model of diffusion to determine the diffusion time and the diffusion coefficient was calculated using Equation C3:

$$D = \frac{\omega^2}{4\tau_D} \qquad \text{Equation C3}$$

where D is the diffusion coefficient and ω is the $1/e^2$ radius of the confocal volume. ω was measured using ATTO-532 (Atto TEC, GmbH) dye solution of known diffusion coefficient at 20 °C in water. All measurements were performed with a dye concentration of 10 nM. Three-dimensional diffusion of 10 nM **RuC_{19}** was recorded in acetonitrile and the ACF was fitted using the three-dimensional diffusion model:

$$G(\tau) = \left[\frac{1}{N}\right]\left[\frac{1}{1+\left(\frac{\tau}{\tau_D}\right)^{\alpha}}\right]\left[\frac{1}{\sqrt{1+\left(\frac{\tau}{\tau_D}\right)^{\alpha}K^2}}\right] \qquad \text{Equation C4}$$

where K is the length to diameter ratio of the confocal volume. The fluorescence lifetime image was also taken in the same MicroTime 200 system. Each sample was acquired for 360 s with a 512 x 512 resolution. Data was analysed using PicoQuant Symphotime software.

C. 2. Synthesis

Materials and reagents. Chemical reagents and solvents were purchased from commercial suppliers and were used without further purification. Sodium ascorbate (≥ 99%) and $NaH_2PO_4{\cdot}2H_2O$ were purchased from Merck. 2,2'-bipyridine (bpy), 4,4'-dionyl-bpy, $[Re(CO)_5Cl]$, and bpy-$(C_9)_2$ were purchased from Sigma Aldrich. The lipids (dry powder) 1,2-dimyristoyl-*sn*-glycero-3-phosphocholine (DMPC), 1,2-dipalmitoyl-*sn*-glycero-3-phosphocholine (DPPC), 1,2-distearoyl-*sn*-glycero-3-phosphocholine (DSPC) were purchased from Avanti Polar Lipids and stored at −20 °C. Sodium 1,2-distearoyl-*sn*-glycero-3-phosphoethanolamine N-(carbonyl-methoxypolyethylene glycol-2000) (NaDSPE-PEG2K) was purchased from Lipoid and stored at −20 °C. *cis*-$[Ru(bpy)_2Cl_2]$ was synthesised according to literature, while isolating $[Ru(bpy)_3](PF_6)_2$ as a side product after anion exchange with potassium hexafluorophosphate.[4] Phosphate buffer (1 L, 0.1 M, pH = 7.7) was prepared by dissolving $NaH_2PO_4{\cdot}2H_2O$ (12 g) in Milli-Q water (500 mL), adjusting the pH with NaOH (≈ 90 mL, 1 M), and diluting further with Milli-Q water up to 1 L. The Avanti Mini-Extruder including polycarbonate extrusion filter (pore size = 0.2 µm, diameter = 19 mm) and filter supports (10 mm) was purchased from Avanti Polar Lipids.

General procedure for the synthesis of 4,4'-$(C_nH_{2n+1})_2$-bpy. 4,4'-$(C_nH_{2n+1})_2$-bpy (n = 12, 15, 17, and 19) were synthesised according to a known procedure for **4,4'-$(C_9H_{19})_2$-bpy**.[5] Tetrahydrofuran was dried over 3 Å molecular sieves overnight and was deoxygenated under N_2 prior to use. To a solution of diisopropylamine (2.4 mM in tetrahydrofuran, 2.7 equiv.) was added a solution of *n*-butyllithium (1.6 M or 2.5 M in hexane, 2.7 equiv.) under N_2 atmosphere. After 1 h at 0 °C, 4,4'-dimethyl-2,2'-bipyridine (0.14 mM in tetrahydrofuran, 1.0 equiv.) was added dropwise to the yellow

solution. After another 3 h at 0 °C, 1-bromoundecane (1.4 mM in tetrahydrofuran, 2.7 equiv.) was added dropwise to the red solution and the solution was allowed to warm to room temperature. After 1 day, the reaction mixture was quenched with water. The aqueous phase was extracted with diethyl ether (3 x). The combined organic phases were dried over $MgSO_4$, the dried solution was filtered, and the filtrate was concentrated under reduced pressure. The crude product **4,4'-(C_nH_{2n+1})$_2$-bpy** was either recrystallised from pentane (n = 12, 15, and 17) or it was collected by filtration after it precipitated during extraction (n = 19).

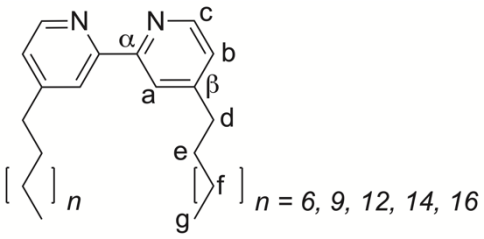

4,4'-didodecyl-2,2'-bipyridine (4,4'-($C_{12}H_{25}$)$_2$-bpy): method above, from 4,4'-dimethyl-2,2'-bipyridine (2.0 g, 10.9 mmol); white solid (yield: 3.2 g, 6.5 mmol, 60%). R_f = 0.7 (SiO_2, DCM/MeOH 9:1). ^{1}H NMR (400 MHz, $CDCl_3$): δ = 8.58 (d, *J* = 5.0 Hz, 2H, *c*), 8.26 (s, 2H, *a*), 7.16 (dd, *J* = 5.0, 1.5 Hz, 2H, *b*), 2.71 (t, *J* = 7.6 Hz, 4H, *d*), 1.71 (p, *J* = 7.6 Hz, 4H, *e*), 1.27 (m, 36H, *f*), 0.90 (t, *J* = 6.7 Hz, 6H, *g*). ^{13}C NMR (100 MHz, $CDCl_3$): δ = 156.09 (C_q, *α*), 153.20 (C_q, *β*), 149.00 (CH, *c*), 124.08 (CH, *b*), 121.51 (CH, *a*), 35.69 (CH_2, *d*), {32.05, 30.60, 29.79 – 29.45, 22.82 (CH_2, *e+f*)}, 14.25 (CH_3, *g*). HRMS (ESI) *m/z* found (calcd): 493.45146 (493.45163, [*M*+H]$^+$). Elemental analysis calcd (%) for $C_{34}H_{56}N_2 \cdot H_2O$: C 79.94, H 11.44, N 5.48; found: C 80.47, H 11.37, N 5.31.

4,4'-dipentadecyl-2,2'-bipyridine (4,4'-($C_{15}H_{31}$)$_2$-bpy): method above, from 4,4'-dimethyl-2,2'-bipyridine (1.0 g, 5.4 mmol); white solid (yield: 1.2 g, 2.0 mmol, 37%). ^{1}H NMR (400 MHz, $CDCl_3$): δ = 8.56 (d, *J* = 5.0 Hz, 2H, *c*), 8.26 (s, 2H, *a*), 7.15 (dd, *J* = 5.0, 1.5 Hz, 2H, *b*), 2.69 (t, *J* = 7.8 Hz, 4H, *d*), 1.69 (p, *J* = 7.8 Hz, 4H, *e*), 1.25 (m, 48H, *f*), 0.87 (t, *J* = 6.8 Hz, 6H, *g*). ^{13}C NMR (100 MHz, $CDCl_3$): δ = 155.77 (C_q, *α*), 153.51 (C_q, *β*), 148.85 (CH, *c*), 124.19 (CH, *b*), 121.69 (CH, *a*), 35.72 (CH_2, *d*), {32.07, 30.59, 29.85-29.45, 22.84 (CH_2, *e+f*)}, 14.27

(CH_3, *g*). HRMS (ESI) *m/z* found (calcd): 577.54527 (577.54553, [*M*+H]$^+$). Elemental analysis calcd (%) for $C_{40}H_{68}N_2$: C 83.27, H 11.88, N 4.86; found: C 83.23, H 11.94, N 4.82.

4,4'-diheptadecyl-2,2'-bipyridine (4,4'-($C_{17}H_{35}$)$_2$-bpy): method above, from 4,4'-dimethyl-2,2'-bipyridine (2.0 g, 10.9 mmol); white solid (yield: 2.2 g, 3.5 mmol, 32%). ^{1}H NMR (400 MHz, $CDCl_3$): δ = 8.55 (d, *J* = 5.3 Hz, 2H, *c*), 8.23 (d, *J* = 1.5 Hz, 2H, *a*), 7.13 (dd, *J* = 5.3, 1.5 Hz, 2H, *b*), 2.68 (t, *J* = 6.8 Hz, 4H, *d*), 1.68 (p, *J* = 6.5 Hz, 4H, *e*), 1.25 (m, 56H, *f*), 0.87 (t, *J* = 6.7 Hz, 6H, *g*). ^{13}C NMR (100 MHz, $CDCl_3$): δ = 156.23 (C_q, α), 153.14 (C_q, β), 149.07 (CH, *c*), 124.07 (CH, *b*), 121.49 (CH, *a*), 35.70 (CH_2, *d*), {32.07, 30.62, 29.84, 29.82, 29.80, 29.78, 29.68, 29.58, 29.51, 29.48, 22.84 (CH_2, *e+f*)}, 14.27 (CH_3, *g*). MS (ESI) *m/z* found (calcd): 633.6 (633.6, [*M*+H]$^+$). Elemental analysis calcd (%) for $C_{44}H_{76}N_2$: C 83.47, H 12.10, N 4.42; found: C 83.43, H 12.07, N 4.39. Colourless single crystals of **4,4'-($C_{17}H_{35}$)$_2$-bpy** were obtained by evaporation of the solvent $CDCl_3$ at room temperature. The structure and refinement data are shown in the section on single crystal X-ray crystallography (Appendix C.9).

4,4'-dinonadecyl-2,2'-bipyridine (4,4'-($C_{19}H_{39}$)$_2$-bpy): method above, from 4,4'-dimethyl-2,2'-bipyridine (2.0 g, 10.9 mmol); white solid (yield: 3.5 g, 5.0 mmol, 46%). R_f = 0.4 (SiO_2, pentane/EtOAc 10:1). ^{1}H NMR (400 MHz, $CDCl_3$): δ = 8.56 (d, *J* = 5.0 Hz, 2H, *c*), 8.24 (s, 2H, *a*), 7.14 (dd, *J* = 5.0, 1.7 Hz, 2H, *b*), 2.69 (t, *J* = 7.6 Hz, 4H, *d*), 1.68 (p, *J* = 7.6 Hz, 4H, *e*), 1.25 (m, 64H, *f*), 0.86 (t, *J* = 6.8 Hz, 6H, *g*). ^{13}C NMR (100 MHz, $CDCl_3$): δ = 156.02 (C_q, α), 153.31 (C_q, β), 148.98 (CH, *c*), 124.12 (CH, *b*), 121.57 (CH, *a*), 35.71 (CH_2, *d*), {32.07, 30.61, 29.86-29.46, 22.84 (CH_2, *e+f*)}, 14.27 (CH_3, *g*). HRMS (ESI) *m/z* found (calcd): 689.66953 (689.67073, [*M*+H]$^+$). Elemental analysis calcd (%) for $C_{48}H_{84}N_2 \cdot 0.5\ H_2O$: C 82.57, H 12.27, N 4.01; found: C 82.60, H 12.12, N 3.99.

General procedure for the synthesis of [Re(4,4'-(C_nH_{2n+1})$_2$-bpy)(CO)$_3$Cl] (ReC$_n$): The compounds were synthesised according to known procedures.[6,7] To a solution of $[Re(CO)_5Cl]$ (typically 0.028 mM in dry toluene, 1.0 equiv. or 1.5 equiv., respectively, in case of **ReC$_{19}$**) was added **4,4'-(C_nH_{2n+1})$_2$-bpy** (1.0 equiv.) under inert atmosphere and the yellow mixture was heated to reflux. After 3 – 48 h, the orange solution was concentrated under reduced

pressure. The residue was redissolved in a minimum amount of diethyl ether and the solution was carefully concentrated until the desired product started to precipitate, which was collected by vacuum filtration. Due to the alkyl chain length, different procedures were followed from this point. For **ReC$_9$** and **ReC$_{12}$**, concentration of the filtrate resulted in additional solids, which were reprecipitated by dissolving in acetone and evaporation under reduced pressure. For **ReC$_{15}$** and **ReC$_{17}$**, the precipitate was washed with 3 x 20 mL acetone and vacuum dried. For **ReC$_{19}$**, the precipitate was washed with 3 x 20 mL Et_2O and vacuum dried.

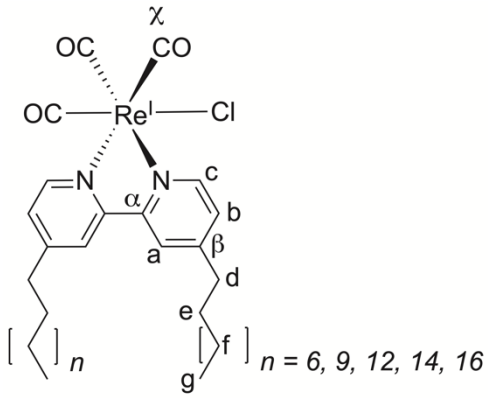

[Re(bpy)(CO)$_3$Cl] (ReC$_0$): from [Re(CO)$_5$Cl] (81 mg, 0.22 mmol) and bpy (35 mg, 0.22 mmol); yellow solid (yield: 86 mg, 0.19 mmol, 83%). Elemental analysis calcd (%) for $C_{13}H_8N_2O_3ReCl$: C 33.81, H 1.75, N 6.07; found: C 33.67, H 1.74, N 5.99.

[Re(4,4'-(C$_9$H$_{19}$)$_2$-bpy)(CO)$_3$Cl] (ReC$_9$): from [Re(CO)$_5$Cl] (100 mg, 0.28 mmol) and **4,4'-(C$_9$H$_{19}$)$_2$-bpy** (113 mg, 0.28 mmol); yellow solid **ReC$_9$** (yield: 195 mg, 0.27 mmol, 99%). ^{1}H NMR (400 MHz, $CDCl_3$): δ = 8.88 (d, *J* = 5.7 Hz, 2H, *c*), 7.95 (s, 2H, *a*), 7.32 (dd, *J* = 5.7, 1.6 Hz, 2H, *b*), 2.78 (t, *J* = 7.7 Hz, 4H, *d*), 1.70 (p, *J* = 7.7 Hz, 4H, *e*), 1.28 (m, 24H, *f*), 0.88 (t, *J* = 6.7 Hz, 6H, *g*). ^{13}C NMR (100 MHz, $CDCl_3$): δ = 197.44 (CO), 190.05 (CO), 156.00 (C_q, *α*), 155.63 (C_q, *β*), 152.77 (CH, *c*), 127.23 (CH, *b*), 123.13 (CH, *a*), 35.84 (CH_2, *d*), {31.95, 30.33, 29.55, 29.48, 29.38, 22.77 (CH_2, *e+f*)}, 14.23 (CH_3, *g*). UV-Vis ($CHCl_3$): λ_{max} (ε): 382 nm (3.86×10^3 $mol^{-1}dm^3cm^{-1}$). Phosphorescence ($CHCl_3$): λ_{ex} = 380 nm,

λ_{em} = 582 nm, τ = 76 ns. HRMS (ESI) *m/z* found (calcd): 679.28924 (679.29039, [*M*-Cl]$^+$), 720.31590 (720.31699, [*M*-Cl+CH_3CN]$^+$), 732.29069 (732.29350, [*M*+NH_4]$^+$), 737.24709 (737.24824, [*M*+Na]$^+$). Elemental analysis calcd (%) for $C_{31}H_{44}N_2O_3ReCl$: C 52.12, H 6.21, N 3.92; found: C 52.10, H 6.22, N 3.94.

[Re(4,4'-($C_{12}H_{25}$)$_2$-bpy)(CO)$_3$Cl] (ReC$_{12}$): from [Re(CO)$_5$Cl] (100 mg, 0.28 mmol) and **4,4'-($C_{12}H_{25}$)$_2$-bpy** (136 mg, 0.28 mmol); yellow solid **ReC$_{12}$** (yield: 146 mg, 0.18 mmol, 67%). ^{1}H NMR (400 MHz, $CDCl_3$): δ = 8.88 (d, *J* = 5.7 Hz, 2H, *c*), 7.96 (s, 2H, *a*), 7.32 (dd, *J* = 5.7, 1.7 Hz, 2H, *b*), 2.78 (t, *J* = 7.6 Hz, 4H, *d*), 1.70 (p, *J* = 7.6 Hz, 4H, *e*), 1.27 (m, 36H, *f*), 0.87 (t, *J* = 6.7 Hz, 6H, *g*). ^{13}C NMR (100 MHz, $CDCl_3$): δ = 197.45 (CO), 190.02 (CO), 156.01 (C_q, *α*), 155.61 (C_q, *β*), 152.74 (CH, *c*), 127.22 (CH, *b*), 123.14 (CH, *a*), 35.83 (CH_2, *d*), {32.02, 30.32, 29.75, 29.73, 29.60, 29.48, 29.46, 29.39, 22.80 (CH_2, *e+f*)}, 14.24 (CH_3, *g*). UV-Vis ($CHCl_3$): λ_{max} (ε): 383 nm (3.98 $\times$ 10^3 $mol^{-1}dm^3cm^{-1}$). Phosphorescence ($CHCl_3$): λ_{ex} = 380 nm, λ_{em} = 588 nm, τ = 74 ns. HRMS (ESI) *m/z* found (calcd): 763.38378 (763.38434, [*M*-Cl]$^+$), 804.41072 (804.41088, [*M*-Cl+CH_3CN]$^+$), 816.38649 (816.38752, [*M*+NH_4]$^+$), 821.34191 (821.34219, [*M*+Na]$^+$). Elemental analysis calcd (%) for $C_{37}H_{56}N_2O_3ReCl \cdot 2\ C_3H_6O$: C 56.47, H 7.49, N 3.06; found: C 56.19, H 7.37, N 3.08.

[Re(4,4'-($C_{15}H_{31}$)$_2$-bpy)(CO)$_3$Cl] (ReC$_{15}$): from [Re(CO)$_5$Cl] (107 mg, 0.30 mmol) and **4,4'-($C_{15}H_{31}$)$_2$-bpy** (170 mg, 0.30 mmol); yellow solid **ReC$_{15}$** (yield: 92 mg, 0.10 mmol, 35%). ^{1}H NMR (400 MHz, $CDCl_3$): δ = 8.89 (d, *J* = 5.7 Hz, 2H, *c*), 7.95 (s, 2H, *a*), 7.32 (dd, *J* = 5.7, 1.6 Hz, 2H, *b*), 2.78 (t, *J* = 7.7 Hz, 4H, *d*), 1.70 (p, *J* = 7.6 Hz, 4H, *e*), 1.26 (m, *J* = 6.6 Hz, 48H, *f*), 0.87 (t, *J* = 6.7 Hz, 6H, *g*). ^{13}C NMR (100 MHz, $CDCl_3$): δ = 197.44 (CO), 190.05 (CO), 155.99 (C_q, *α*), 155.63 (C_q, *β*), 152.79 (CH, *c*), 127.23 (CH, *b*), 123.13 (CH, *a*), 35.86 (CH_2, *d*), {32.05, 30.34, 29.82, 29.80, 29.79, 29.77, 29.75, 29.62, 29.49, 29.41, 22.82 (CH_2, *e+f*)}, 14.10 (CH_3, *g*). UV-Vis ($CHCl_3$): λ_{max} (ε): 382 nm (3.80 $\times$ 10^3 $mol^{-1}dm^3cm^{-1}$). Phosphorescence ($CHCl_3$): λ_{ex} = 380 nm, λ_{em} = 585 nm, τ = 74 ns. HRMS (ESI) *m/z* found (calcd): 847.47678 (847.47820, [*M*-Cl]$^+$), 888.50452 (888.50475, [*M*-Cl+CH_3CN]$^+$), 900.48034 (900.48142, [*M*+NH_4]$^+$), 905.43608 (905.43682, [*M*+Na]$^+$). Elemental analysis calcd (%) for $C_{43}H_{68}N_2O_3ReCl$: C 58.51, H 7.76, N 3.17; found: C 58.47, H 7.82, N 3.14.

[Re(4,4'-($C_{17}H_{35}$)$_2$-bpy)(CO)$_3$Cl] (ReC$_{17}$): from [Re(CO)$_5$Cl] (88 mg, 0.24 mmol) and **4,4'-($C_{17}H_{35}$)$_2$-bpy** (153 mg, 0.24 mmol); yellow solid **ReC$_{17}$** (yield: 194 mg, 0.21 mmol, 85%). ^{1}H NMR (400 MHz, $CDCl_3$): δ = 8.89 (d, *J* = 5.8 Hz, 2H, *c*), 7.95 (s, 2H, *a*), 7.32 (dd, *J* = 5.7, 1.1 Hz, 2H, *b*), 2.78 (t, *J* = 7.8 Hz, 4H, *d*), 1.71 (p, *J* = 7.8 Hz, 4H, *e*), 1.26 (m, 56H, *f*), 0.88 (t, *J* = 6.9 Hz, 6H, *g*). ^{13}C NMR (100 MHz, $CDCl_3$) δ = 197.43 (CO), 190.06 (CO), 155.98 (C_q, α), 155.63 (C_q, β), 152.79 (CH, *c*), 127.23 (CH, *b*), 123.12 (CH, *a*), 35.86 (CH_2, *d*), {32.06, 30.19, 29.83, 29.81, 29.79, 29.76, 29.63, 29.50, 29.41, 22.82 (CH_2, *e+f*)}, 14.10 (CH_3, *g*). UV-Vis ($CHCl_3$): λ_{max} (ε): 383 nm (3.83 $\times$ 10^3 $mol^{-1}dm^3cm^{-1}$). Phosphorescence ($CHCl_3$): λ_{ex} = 380 nm, λ_{em} = 581 nm, τ = 74 ns. HRMS (ESI) *m/z* found (calcd): 903.53904 (903.54109, [*M*-Cl]$^+$), 944.56588 (944.56766, [*M*-Cl+CH_3CN]$^+$), 956.54294 (956.54341, [*M*+NH_4]$^+$), 961.49829 (961.49881, [*M*+Na]$^+$). Elemental analysis calcd (%) for $C_{47}H_{76}N_2O_3ReCl$: C 60.13, H 8.16, N 2.98; found: C 60.15, H 8.22, N 2.95.

[Re(4,4'-($C_{19}H_{39}$)$_2$-bpy)(CO)$_3$Cl] (ReC$_{19}$): from [Re(CO)$_5$Cl] (157 mg, 0.44 mmol) and **4,4'-($C_{19}H_{39}$)$_2$-bpy** (200 mg, 0.29 mmol); yellow solid **ReC$_{19}$** (yield: 161 mg, 0.16 mmol, 56%). ^{1}H NMR (400 MHz, $CDCl_3$): δ = 8.87 (d, *J* = 5.7 Hz, 2H, *c*), 7.96 (s, 2H, *a*), 7.31 (dd, *J* = 5.7, 1.4 Hz, 2H, *b*), 2.77 (t, *J* = 7.6 Hz, 4H, *d*), 1.70 (p, *J* = 7.6 Hz, 4H, *e*), 1.25 (m, 64H, *f*), 0.87 (t, *J* = 6.7 Hz, 6H, *g*). ^{13}C NMR (100 MHz, $CDCl_3$): δ = 197.45 (CO), 189.99 (CO), 156.01 (C_q, α), 155.59 (C_q, β), 152.69 (CH, *c*), 127.19 (CH, *b*), 123.16 (CH, *a*), 35.80 (CH_2, *d*), {32.02, 30.30, 29.80, 29.76, 29.73, 29.60, 29.47, 29.37, 22.79 (CH_2, *e+f*)}, 14.23 (CH_3, *g*). UV-Vis ($CHCl_3$): λ_{max} (ε): 381 nm (3.80 $\times$ 10^3 $mol^{-1}dm^3cm^{-1}$). HRMS (ESI) *m/z* found (calcd): 1007.56265 (1007.56146, [*M*+Na]$^+$), 1002.60725 (1002.60606, [*M*+NH_4]$^+$). Elemental analysis calcd (%) for $C_{51}H_{84}ClN_2O_3Re$: C 61.57, H 8.51, N 2.82; found: C 60.93, H 8.38, N 2.76.

General procedure for [Ru(4,4'-(C_nH_{2n+1})$_2$-bpy)(bpy)$_2$](PF$_6$)$_2$ (RuC$_n$): The synthesis for **RuC$_n$** was followed as reported in literature for a similar compound with some modifications.[5] To a solution of *cis*-[Ru(bpy)$_2$Cl$_2$] (typically 0.014 mM in deoxygenated water/ethanol = 1:1 for **RuC$_9$** and **RuC$_{12}$** or water/ethanol/chloroform = 1:1:1 for **RuC$_{15}$**, **RuC$_{17}$**, and **RuC$_{19}$**, 1.0 equiv.) was added the respective **4,4'-(C_nH_{2n+1})$_2$-bpy** (1.0 equiv.) and the reaction

mixture was heated to reflux at 110 °C under inert atmosphere. After 1 – 4 days, the reaction mixture was concentrated under reduced pressure. The crude product was purified as described in the following protocols.

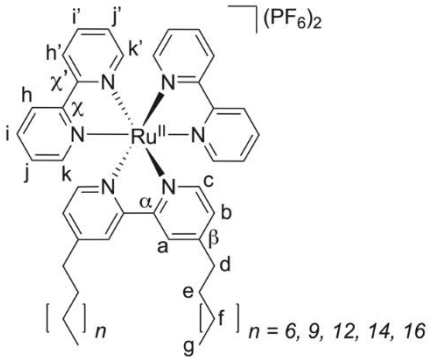

[Ru(bpy)$_3$](PF$_6$)$_2$ (RuC$_0$): Elemental analysis calcd (%) for $C_{30}H_{24}F_{12}N_6P_2Ru$: C 41.92, H 2.81, N 9.78; found: C 41.56, H 2.84, N 9.72.

[Ru(4,4'-(C$_9$H$_{19}$)$_2$-bpy)(bpy)$_2$](PF$_6$)$_2$ (RuC$_9$): from *cis*-[Ru(bpy)$_2$Cl$_2$] (0.22 g, 0.44 mmol) and **4,4'-(C$_9$H$_{19}$)$_2$-bpy** (0.18 g, 0.44 mmol). For purification, the crude product was dissolved in a minimum amount of water. Saturated aqueous potassium hexafluorophosphate was added and the resulting orange precipitate was collected by vacuum filtration. The precipitate was dried by co-evaporation with toluene and *in vacuo*. **RuC$_9$** was obtained as a red solid (yield: 450 mg, 0.40 mmol, 91%). R_f = 0.6 (SiO_2, acetone/water/saturated KNO_3 100:10:1). ^{1}H NMR (400 MHz, CD_3CN): δ = 8.49 (d, *J* = 8.2 Hz, 4H, *h+h'*), 8.37 (s, 2H, *a*), 8.04 (t, *J* = 8.0, 2.9 Hz, 4H, *i+i'*), 7.72 (d, *J* = 5.2 Hz, 4H, *k+k'*), 7.54 (d, *J* = 5.5 Hz, 2H, *c*), 7.39 (q, *J* = 6.7 Hz, 4H, *j+j'*), 7.22 (d, *J* = 5.5 Hz, 2H, *b*), 2.79 (t, *J* = 7.8 Hz, 4H, *d*), 1.68 (p, *J* = 7.0 Hz, 4H, *e*), 1.27 (m, 24H, *f*), 0.87 (t, *J* = 6.4 Hz, 6H, *g*). ^{13}C NMR (100 MHz, CD_3CN): δ = 157.97 (C_q), 157.55 (C_q), 155.76 (C_q), 152.59 (CH, *k or k'*), 152.41 (CH, *k or k'*), 151.78 (CH, *c*), 138.51 (CH, *i+i'*), 128.46 (CH, *b, j or j'*), 128.42 (CH, *b, j or j'*), 128.40 (CH, *b, j or j'*), 125.15 (CH, *a*), 125.10 (CH, *h or h'*), 35.64 (CH_2, *d*), {32.51, 30.81, 30.08, 29.93, 29.90, 29.74, 23.30 (CH_2, *e+f*)}, 14.32 (CH_3, *g*). ^{19}F NMR (471 MHz, CD_3CN): δ = -72.77 (d, *J* = 706.7 Hz). UV-Vis (CH_3CN): λ_{max} (ε): 453 nm (1.32×10^4 $mol^{-1}dm^3cm^{-1}$). Phosphorescence (CH_3CN): λ_{ex} = 450 nm, λ_{em} = 617 nm.

HRMS (ESI) *m/z* found (calcd): 411.19560 (411.19585, $[M\text{-}2(PF_6)]^{2+}$). Elemental analysis calcd (%) for $C_{48}H_{60}F_{12}N_6P_2Ru \cdot 3\ H_2O$: C 49.44, H 5.70, N 7.21; found: C 49.67, H 5.40, N 7.23.

[Ru(4,4'-($C_{12}H_{25}$)$_2$-bpy)(bpy)$_2$](PF_6)$_2$ (RuC$_{12}$): from *cis*-[Ru(bpy)$_2$Cl$_2$] (0.20 g, 0.41 mmol) and **4,4'-($C_{12}H_{25}$)$_2$-bpy** (0.20 g, 0.41 mmol. For purification, the procedure for **RuC$_9$** was followed. The orange precipitate was further purified by column chromatography on silica gel (dichloromethane/methanol = 99:1 to 90:10). The solvents were removed under reduced pressure and the remaining solids were dried *in vacuo*. **RuC$_{12}$** was obtained as a red solid (yield: 176 mg, 0.15 mmol, 36%). R_f = 0.6 (SiO_2, acetone/water/saturated KNO_3 100:10:1). ^{1}H NMR (400 MHz, CD_3CN): δ = 8.48 (dd, *J* = 8.2, 1.9 Hz, 4H, *h+h'*), 8.37 (d, *J* = 1.8 Hz, 2H, *a*), 8.04 (tq, *J* = 8.0, 2.8, 1.5 Hz, 4H, *i+i'*), 7.71 (dd, *J* = 5.2, 1.2 Hz, 4H, *k+k'*), 7.53 (d, *J* = 5.8 Hz, 2H, *c*), 7.38 (dq, *J* = 7.2, 5.6, 1.3 Hz, 4H, *j+j'*), 7.22 (dd, *J* = 5.8, 1.8 Hz, 2H, *b*), 2.78 (t, *J* = 7.6 Hz, 4H, *d*), 1.68 (p, *J* = 7.4 Hz, 4H, *e*), 1.25 (m, 36H, *f*), 0.87 (t, *J* = 6.9 Hz, 6H, *g*). ^{13}C NMR (100 MHz, CD_3CN): δ = 158.00 (C_q), 157.98 (C_q), 157.56 (C_q), 155.78 (C_q), 152.61 (CH, *k or k'*), 152.42 (CH, *k or k'*), 151.80 (CH, *c*), 138.53 (CH, *i+i'*), 128.50 (CH, *b, j or j'*) 128.44 (CH, *b, j or j'*), 125.15 (CH, *a*), 125.11 (CH, *h+h'*), 35.65 (CH_2, *d*), {32.58, 30.81, 30.32, 30.30, 30.24, 30.12, 30.02, 29.93, 29.74, 23.33 (CH_2, *e+f*)}, 14.35 (CH_3, *g*). ^{19}F NMR (471 MHz, CD_3CN): δ = -72.33 (d, *J* = 706.2 Hz). UV-Vis (CH_3CN): λ_{max} (ε): 453 nm (1.35×10^4 $mol^{-1}dm^3cm^{-1}$). Phosphorescence (CH_3CN): λ_{ex} = 450 nm, λ_{em} = 616 nm. HRMS (ESI) *m/z* found (calcd): 453.24253 (453.24289, $[M\text{-}2(PF_6)]^{2+}$). Elemental analysis calcd (%) for $C_{54}H_{72}F_{12}N_6P_2Ru$: C 54.22, H 6.07, N 7.03; found: C 53.67, H 6.04, N 6.82.

[Ru(4,4'-($C_{15}H_{31}$)$_2$-bpy)(bpy)$_2$](PF_6)$_2$ (RuC$_{15}$): from *cis*-[Ru(bpy)$_2$Cl$_2$] (0.21 g, 0.43 mmol) and **4,4'-($C_{15}H_{31}$)$_2$-bpy** (0.25 g, 0.43 mmol). For purification, the crude product was purified via chromatography on silica gel (acetone/water/brine = 8:4:1). The solvents were removed under reduced pressure and the red solid was extracted with chloroform (3 x). The combined organic layers were dried over $MgSO_4$ and the solvents were evaporated under reduced pressure. Methanol was added and the white precipitate was filtered off. Henceforth, the procedure for **RuC$_9$** was followed. The orange

precipitate was collected by dissolving in acetone and dried by evaporation under reduced pressure and *in vacuo*. The yield in crude product before addition of hexafluorophosphate was 56% (258 mg, 0.24 mmol). From 105 mg of such crude product, KPF_6 reprecipitation afforded **RuC_{15}** as a red solid in 36% overall yield (82 mg, 0.064 mmol). ^{1}H NMR (400 MHz, CD_3CN): δ = 8.49 (d, *J* = 8.3 Hz, 4H, *h+h'*), 8.36 (d, *J* = 1.8 Hz, 2H, *a*), 8.04 (tt, *J* = 8.0, 1.8 Hz, 4H, *i+i'*), 7.71 (dd, *J* = 5.7, 1.4 Hz, 4H, *k+k'*), 7.53 (d, *J* = 5.8 Hz, 2H, *c*), 7.38 (dq, *J* = 6.7, 6.5, 1.2 Hz, 4H, *j+j'*), 7.22 (dd, *J* = 5.9, 1.8 Hz, 2H, *b*), 2.78 (t, *J* = 7.8 Hz, 4H, *d*), 1.68 (p, *J* = 7.2 Hz, 4H, *e*), 1.26 (m, 48H, *f*), 0.87 (t, *J* = 6.6 Hz, 6H, *g*). ^{13}C NMR (100 MHz, CD_3CN): δ = 158.00 (C_q), 157.98 (C_q), 157.55 (C_q), 155.78 (C_q), 152.61 (CH, *k or k'*), 152.31 (CH, *k or k'*), 151.80 (CH, *c*), 138.52 (CH, *i+i'*), 128.50 (CH, *b, j or j'*), 128.43 (CH, *b, j or j'*), 125.11 (CH, *a+h+h'*), 35.63 (CH_2, *d*), {32.58, 30.79, 30.34, 30.32, 30.29, 30.22, 30.10, 30.02, 29.90, 29.70, 23.33 (CH_2, *e+f*)}, 14.34 (CH_3, *g*). ^{19}F NMR (471 MHz, CD_3CN): δ = -72.43 (d, *J* = 706.6 Hz). UV-Vis (CH_3CN): λ_{max} (ε): 453 nm (1.32 $\times$ 10^4 $mol^{-1}dm^3cm^{-1}$). Phosphorescence (CH_3CN): λ_{ex} = 450 nm, λ_{em} = 613 nm. HRMS (ESI) *m/z* found (calcd): 495.29007 (495.29032, [*M*-2(PF_6)]$^{2+}$), 1135.54224 (1135.54474, [*M*-PF_6]$^+$). Elemental analysis calcd (%) for $C_{60}H_{84}F_{12}N_6P_2Ru$: C 56.29, H 6.61, N 6.56; found: C 57.49, H 7.01, N 6.31.

[Ru(4,4'-($C_{17}H_{35}$)$_2$-bpy)(bpy)$_2$](PF_6)$_2$ (RuC_{17}): from *cis*-[Ru(bpy)$_2$$Cl_2$] (0.75 g, 1.56 mmol) and **4,4'-($C_{17}H_{35}$)$_2$-bpy** (0.98 g, 1.54 mmol). For purification, the crude product was purified via chromatography on silica gel (1st column: acetone/water/brine = 8:4:1, 2nd column: acetone/water/saturated KNO_3 = 100:10:1). The organic solvents were removed under reduced pressure and the red solid was extracted with chloroform (3 x). The combined organic layers were dried over $MgSO_4$ and the solvent was removed under reduced pressure. The red solid was taken up in methanol and subjected to ion exchange column with Amberlite (50 g, pre-soaked with brine and washed 10 x with water and 3 x with methanol). The solvent was removed under reduced pressure and the obtained red solid was redissolved in a mixture of chloroform and brine. The phases were separated, and the aqueous phase was extracted with chloroform (2 x). The combined organic layers were dried over $MgSO_4$ and the solvent was evaporated *in vacuo*. Trituration of the solid

in acetone (100 mL) followed by removal of 50 mL of acetone on the rotary evaporator, cooling to room temperature, filtration, and washing with acetone (50 mL) yielded the compound as chloride salt [Ru(4,4'-($C_{17}H_{35}$)$_2$-bpy)(bpy)$_2$](Cl)$_2$·NaCl·3 H_2O. The filtrate was poured into saturated aqueous hexafluorophosphate to yield an orange precipitate that was filtered and washed with water and collected from the frit with acetone. Removal of the solvent in vacuo yielded **RuC$_{17}$** as a red solid (yield: 0.32 g, 0.22 mmol, 14%.). ^{1}H NMR (400 MHz, CD_3CN): δ = 8.49 (d, J = 8.2 Hz, 4H, *h+h'*), 8.36 (d, J = 1.8 Hz, 2H, *a*), 8.04 (ddt, J = 8.1, 2.3, 1.5 Hz, 4H, *i+i'*), 7.71 (td, J = 5.7, 0.7 Hz, 4H, *k+k'*), 7.54 (d, J = 5.8 Hz, 2H, *c*), 7.39 (m, J = 7.2, 5.8, 1.3 Hz, 4H, *j+j'*), 7.22 (dd, J = 5.8, 1.8 Hz, 2H, *b*), 2.78 (t, J = 7.4 Hz, 4H, *d*), 1.68 (p, J = 7.2 Hz, 4H, *e*), 1.25 (m, 56H, *f*), 0.86 (t, J = 6.7 Hz, 6H, *g*). ^{13}C NMR (100 MHz, CD_3CN): δ = 157.97 (C_q), 157.94 (C_q), 157.51 (C_q), 155.74 (C_q), 152.57 (CH, *k or k'*), 152.36 (CH, *k or k'*), 151.77 (CH, *c*), 138.50 (CH, *i+i'*), 128.48 (CH, *b, j or j'*), 128.42 (CH, *b, j or j'*), 128.39 (CH, *b, j or j'*), 125.09 (CH, *a+h+h'*), 35.60 (CH_2, *d*), {32.56, 30.75, 30.31, 30.29, 30.20, 30.07, 29.99, 29.87, 29.68, 23.31 (CH_2, *e+f*)}, 14.32 (CH_3, *g*). UV-Vis (CH_3CN): λ_{max} (ε): 453 nm (1.69×10^4 $mol^{-1}dm^3cm^{-1}$). Phosphorescence (CH_3CN): λ_{ex} = 450 nm, λ_{em} = 615 nm. HRMS (ESI) *m/z* found (calcd): 523.32126 (523.32168, [*M*-2PF_6]$^{2+}$). Elemental analysis calcd (%) for $C_{64}H_{92}F_{12}N_6P_2Ru$ · 2 C_3H_6O: C 57.88, H 7.22, N 5.79; found: C 57.84, H 7.08, N 5.71.

[Ru(4,4'-($C_{19}H_{39}$)$_2$-bpy)(bpy)$_2$](PF_6)$_2$ (RuC$_{19}$): from *cis*-[Ru(bpy)$_2$$Cl_2$] (0.10 g, 0.21 mmol) and **4,4'-($C_{19}H_{39}$)$_2$-bpy** (0.20 g, 0.29 mmol). The crude product was purified via chromatography on silica gel (acetone/water/saturated KNO_3 = 100:10:1). After removing all solvents under reduced pressure, the procedure for **RuC$_9$** was carried out. **RuC$_{19}$** was finally obtained as a red solid (yield: 36 mg, 0.026 mmol, 8.9%). R_f = 0.2 (SiO_2, acetone/water/saturated KNO_3 100:10:1). ^{1}H NMR (400 MHz, CD_3CN): δ = 8.49 (dd, J = 8.2, 1.7 Hz, 4H, *h+h'*), 8.36 (d, J = 1.8 Hz, 2H, *a*), 8.04 (tq, J = 7.9, 1.8 Hz, 4H, *i+i'*), 7.71 (d, J = 5.7, 1.4 Hz, 4H, *k+k'*), 7.54 (d, J = 5.8 Hz, 2H, *c*), 7.39 (dq, J = 6.1, 5.7, 1.6, 1.2 Hz, 4H, *j+j'*), 7.22 (dd, J = 5.8, 1.8 Hz, 2H, *b*), 2.78 (t, J = 7.9 Hz, 4H, *d*), 1.68 (p, J = 7.0 Hz, 4H, *e*), 1.25 (m, 64H, *f*), 0.87 (t, J = 6.5 Hz, 6H, *g*). ^{13}C NMR (100 MHz, CD_3CN): δ = 158.01 (C_q), 157.98 (C_q), 157.55 (C_q), 155.78 (C_q), 152.61

(CH, *k or k'*), 152.40 (CH, *k or k'*), 151.81 (CH, *c*), 138.54 (CH, *i+i'*), 128.52 (CH, *b, j or j'*) 128.45 (CH, *b, j or j'*), 128.42 (CH, *b, j or j'*) 125.12 (CH, *a+h+h'*), 35.64 (CH_2, *d*), {32.59, 30.79, 30.32, 30.23, 30.10, 30.03, 29.90, 29.71, 23.34 (CH_2, *e+f*)}, 14.35 (CH_3, *g*). UV-Vis (CH_3CN): λ_{max} (ε): 453 nm (1.39×10^4 $mol^{-1}dm^3cm^{-1}$). Phosphorescence (CH_3CN): λ_{ex} = 450 nm, λ_{em} = 615 nm. HRMS (ESI) *m/z* found (calcd): 551.35195 (551.35304, $[M\text{-}2(PF_6)]^{2+}$), 1247.66904 (1247.67080, $[M\text{-}PF_6]^+$). Elemental analysis calcd (%) for $C_{68}H_{100}F_{12}N_6P_2Ru^{2+}$: C 58.65, H 7.24, N 6.04; found: C 58.13, H 7.23, N 5.91.

C. 3. Liposome preparation

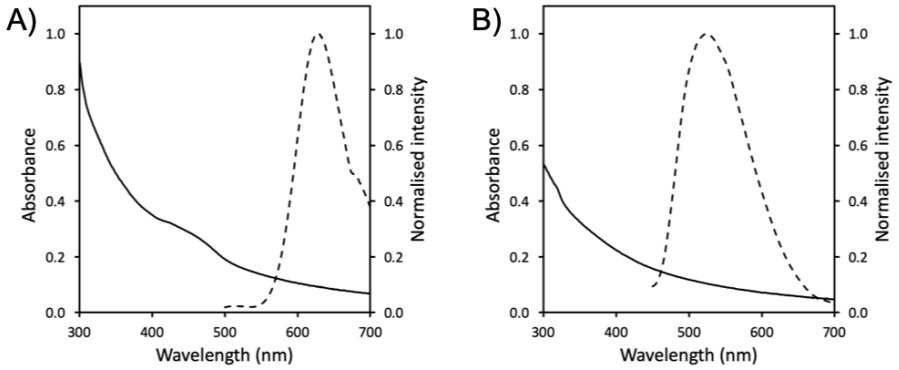

Figure C1. The absorption (solid line) and emission spectrum (dashed line, λ_{exc} = 450 nm for Ru and 380 nm for Re) of A) DSPC:NaDSPE-PEG2K 100:1 liposomes functionalised with **RuC_{15}** in 0.1 M NaH_2PO_4 buffer and B) DPPC:NaDSPE-PEG2K 100:1 liposomes functionalised with **ReC_9** in 0.1 M NaH_2PO_4 buffer. Experimental conditions: [DPPC or DSPC] = 6.25 mM, [NaDSPE-PEG2K] = 62.5 µM, and [**RuC_{15}** or **ReC_9**] = 25 µM.

Table C1. Diameter size (d), polydispersity index (PDI), absorption maxima ($\lambda_{abs.}$), and emission maxima (λ_{em}) of liposomes prepared from lipids, NaDSPE-PEG2K, and **RuCn** or **ReCn** in a ratio of 100:1.0:0.4.

	DMPC				DPPC				DSPC		
Sample[a]	d (nm)	PDI[b]	λ_{abs}[c] (nm)	λ_{em} (nm)	d (nm)	PDI[b]	λ_{abs}[c] (nm)	λ_{em} (nm)	d (nm)	PDI[b]	λ_{abs}[c] (nm)
RuC0	119	0.09	449	608	147	0.10	420	610	149	0.10	-
RuC9	124	0.17	425	635	138	0.11	425	629	164	0.09	456
RuC12	126	0.15	427	632	143	0.11	427	629	170	0.08	425
RuC15	134	0.13	425	633	134	0.10	425	627	154	0.10	420
RuC17	126	0.16	425	634	142	0.11	427	630	157	0.09	-
RuC19	137	0.15	425	633	143	0.10	424	629	149	0.10	465
ReC0	142	0.14	-	553	149	0.09	-	554	153	0.10	-
ReC9	143	0.13	-	523	148	0.07	-	525	154	0.09	-
ReC12	140	0.14	-	520, 552	144	0.07	-	-	163	0.08	-
ReC15	132	0.12	-	531, 551	148	0.10	-	531, 553	153	0.11	-
ReC17	143	0.14	-	510, 552	149	0.08	-	554	148	0.07	-
ReC19	141	0.13	-	554	144	0.08	-	554	152	0.10	-

[a] Experimental conditions: [DMPC, DPPC, or DSPC] = 6.25 mM, [NaDSPE-PEG2K] = 62.5 µM, and [**RuCn**] or [**ReCn**] = 25 µM in 0.1 M NaH_2PO_4 buffer. Bulk concentrations [**ReCn**] and [**RuCn**] indicate theoretical concentrations (before extrusion). [b] Liposome size is considered to be uniformly distributed when PDI < 0.2. [c] λ_{abs} could not be determined for rhenium complexes, due to the high levels of lipid scattering at λ_{abs} of the rhenium complexes.

Table C2. Diameter size (d), polydispersity index (PDI), absorption maxima (λ_{abs}), and emission maxima (λ_{em}) of photocatalytic liposomes $\mathbf{C_n}$ prepared from DPPC, NaDSPE-PEG2K, $\mathbf{RuC_n}$, and $\mathbf{ReC_n}$ in a ratio of 100:1.0:0.4:0.4.

Samples [a]	d (nm)[b]	PDI[b]	λ_{em} (nm)
C_0	130 ± 3	0.066 ± 0.005	601[c], 607[d]
C_9	143 ± 9	0.083 ± 0.001	555[c], 627[c], 632[d]
C_{12}	128 ± 5	0.072 ± 0.016	556[c], 628[c], 630[d]
C_{15}	138 ± 2	0.080 ± 0.012	556[c], 626[c], 628[d]
C_{17}	137 ± 11	0.094 ± 0.006	556[c], 627[c], 627[d]
C_{19}	139 ± 3	0.077 ± 0.003	555[c], 627[c], 628[d]

[a] Experimental conditions: [DPPC] = 6.25 mM, [NaDSPE-PEG2K] = 62.5 μM, [$\mathbf{RuC_n}$] = 25 μM, and [$\mathbf{ReC_n}$] = 25 μM in 0.1 M NaH_2PO_4 buffer. Bulk concentrations [$\mathbf{ReC_n}$] and [$\mathbf{RuC_n}$] indicate theoretical concentrations (before extrusion). [b] Average over two independent liposome preparations. Liposome size is considered to be uniformly distributed when PDI < 0.2. [c] Excited at 380 nm, [d] excited at 450 nm.

Table C3. Summary of DLS results obtained before and after light irradiation (t_{irr} = 3 h, λ > 455 nm) for photocatalytic liposomes $\mathbf{C_n}$ prepared from DPPC, NaDSPE-PEG2K, $\mathbf{RuC_n}$, and $\mathbf{ReC_n}$ in a ratio of 100:1.0:0.4:0.4.

	Before irradiation		After irradiation	
Sample[a]	d (nm)[b]	PDI[b]	d (nm)[b]	PDI[b]
C_0	161 ± 4	0.12 ± 0.01	171 ± 5	0.13 ± 0.01
C_9	157 ± 5	0.11 ± 0.02	172 ± 5	0.18 ± 0.02
C_{12}	150 ± 4	0.12 ± 0.01	164 ± 4	0.16 ± 0.01
C_{15}	119 ± 4	0.11 ± 0.02	131 ± 4	0.17 ± 0.01
C_{17}	158 ± 6	0.10 ± 0.04	165 ± 8	0.11 ± 0.02
C_{19}	155 ± 6	0.10 ± 0.01	162 ± 6	0.14 ± 0.02

[a] Experimental conditions: [DPPC] = 625 μM, [NaDSPE-PEG2K] = 6.25 μM, [$\mathbf{RuC_n}$] = 2.5 μM, and [$\mathbf{ReC_n}$] = 2.5 μM in 0.1 M $NaHCO_3$ and 0.1 M NaHAsc solutions at 25 °C. Bulk concentrations [$\mathbf{ReC_n}$] and [$\mathbf{RuC_n}$] indicate theoretical concentrations (before extrusion). [b] Average over three independent liposome preparations.

Table C4. Diameter size (d) and polydispersity index (PDI) of photocatalytic liposomes prepared from DPPC, NaDSPE-PEG2K, **RuC$_n$** and **ReC$_n$** in a ratio of 100:1.0:0.4:X with X = 0.0, 0.4, and 1.6, which were used for time-resolved spectroscopy measurements.

Samples [a]	d (nm)[b]	PDI[b]
RuC_9 and 0.0 % ReC_9	146	0.09
RuC_9 and 0.4 % ReC_9	114	0.10
RuC_9 and 1.6 % ReC_9	108	0.18
RuC_{19} and 0.0 % ReC_{19}	136	0.08
RuC_{19} and 0.4 % ReC_{19}	142	0.06
RuC_{19} and 1.6 % ReC_{19}	129	0.09

[a] Experimental conditions: [DPPC] = 6.25 mM, [NaDSPE-PEG2K] = 62.5 µM, [**RuC$_n$**] = 25 µM, and [**ReC$_n$**] = 0, 25 or 100 µM in CO_2-saturated 0.1 M NaHAsc aqueous solution. Bulk concentrations [**ReC$_n$**] and [**RuC$_n$**] indicate theoretical concentrations (before extrusion). [b] Liposome size is considered to be uniformly distributed when PDI < 0.2.

C. 4. Photocatalysis

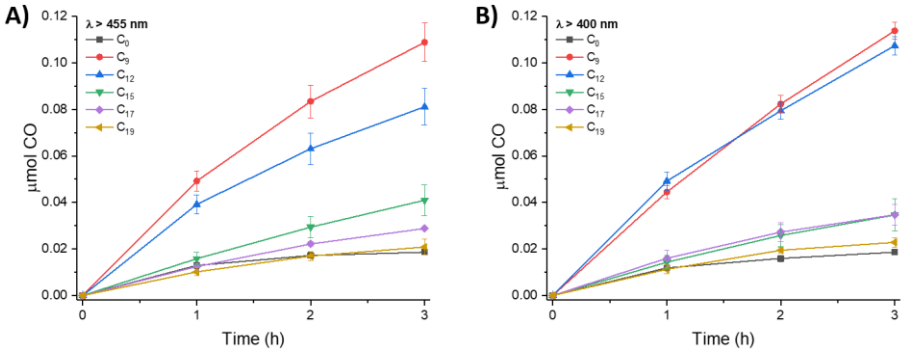

Figure C2. Photocatalytic CO formation after three hours of simulated solar light irradiation (AM 1.5G, 100 mW cm^{-2}) at (A) λ > 455 nm or (B) λ > 400 nm as a function of alkyl chain length for DPPC:NaDSPE-PEG2K 100:1 photocatalytic liposomes **C$_n$** containing **ReC$_n$**-**RuC$_n$** with the same n. Experimental conditions: [DPPC] = 625 µM, [NaDSPE-PEG2K] = 6.25 µM, [**RuC$_n$**] = 2.5 µM, and [**ReC$_n$**] = 2.5 µM in CO_2-saturated 0.1 M NaH_2PO_4 and 0.1 M NaHAsc aqueous solution (3 mL, pH ≈ 6.3) at 25 °C. Bulk concentrations [**ReC$_n$**] and [**RuC$_n$**] indicate theoretical concentrations (before extrusion). Experiments were performed in triplicates.

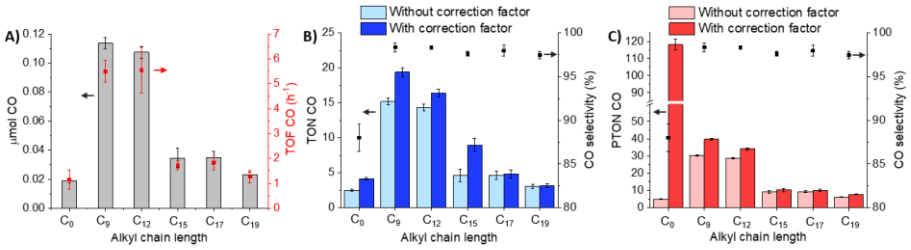

Figure C3. Photocatalytic activity after three hours of simulated solar light irradiation (λ > 400 nm, AM 1.5G, 100 mW cm^{-2}) as a function of alkyl chain length for DPPC:NaDSPE-PEG2K 100:1 photocatalytic liposomes **C$_n$** containing **ReC$_n$-RuC$_n$** with the same n: (A) evolved µmol of CO and uncorrected TOF CO; (B) (light blue) uncorrected and (dark blue) corrected TON CO and CO selectivity; (C) (light red) uncorrected and (dark red) corrected turnover number of CO produced per mol of photosensitiser (PTON CO) and CO selectivity. The TONs and TOFs were obtained after three hours and one hour, respectively. The applied correction (η_{immob}) can be found in Figure 3.4 and Table C9. Experimental conditions: [DPPC] = 625 µM, [NaDSPE-PEG2K] = 6.25 µM, [**ReC$_n$**] = 2.5 µM and [**RuC$_n$**] = 2.5 µM; CO_2-saturated 0.1 M NaH_2PO_4 and 0.1 M NaHAsc aqueous solution (3 mL, pH ≈ 6.3) at 25 °C. Bulk concentrations [**ReC$_n$**] and [**RuC$_n$**] indicate theoretical concentrations (before extrusion). Experiments were performed in triplicates.

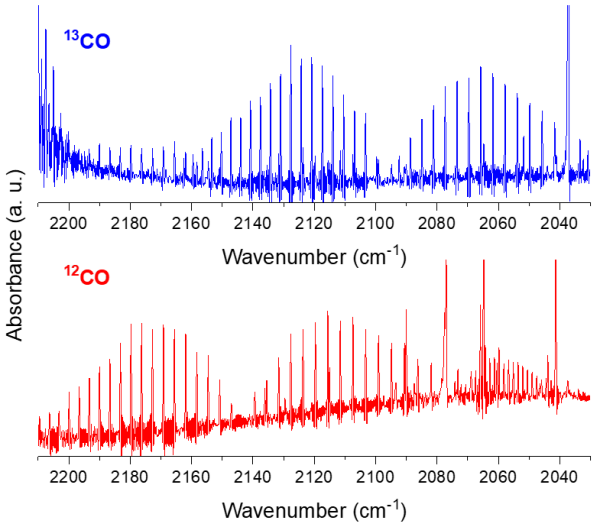

Figure C4. IR absorbance spectra of CO gas obtained from isotopic labelling control experiments using (blue) $^{13}CO_2$ and (red) $^{12}CO_2$ as the headspace gas after three hours of photocatalysis with DPPC:NaDSPE-PEG2K 100:1 photocatalytic liposomes **C$_9$** containing **ReC$_9$** and **RuC$_9$**. Experimental conditions: [DPPC] = 6.25 mM, [NaDSPE-PEG2K] = 62.5 µM, [**RuC$_9$**] = 25 µM, and [**ReC$_9$**] = 25 µM in 0.1 M NaH_2PO_4 and 0.1 M NaHAsc. Bulk concentrations [**ReC$_n$**] and [**RuC$_n$**] indicate theoretical concentrations (before extrusion).

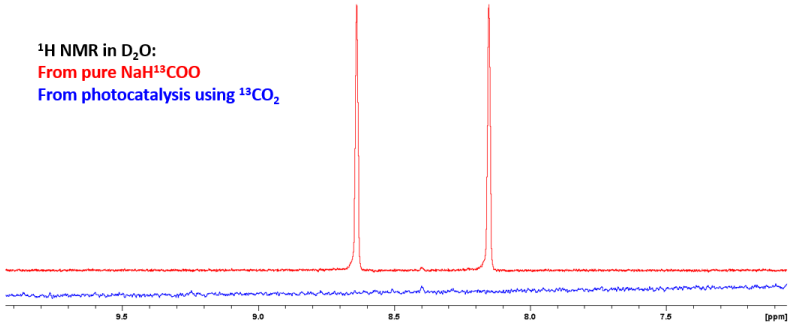

Figure C5. ^{1}H NMR spectra of (red) isotopic labelled sodium formate and (blue) formate obtained from isotopic labelling control experiments using $^{13}CO_2$ as the headspace gas after three hours of photocatalysis using DPPC:NaDSPE-PEG2K 100:1 photocatalytic liposomes **C_9** containing **ReC_9** and **RuC_9**. Experimental conditions: [DPPC] = 6.25 mM, [NaDSPE-PEG2K] = 62.5 µM, [**RuC_9**] = 25 µM, and [**ReC_9**] = 25 µM in 0.1 M NaH_2PO_4 and 0.1 M NaHAsc. Bulk concentrations [**ReC_n**] and [**RuC_n**] indicate theoretical concentrations (before extrusion).

Table C5. Summary of photocatalysis results obtained from all alkyl chain lengths in DPPC:NaDSPE-PEG2K 100:1 photocatalytic liposomes **C_n** containing **ReC_n** and **RuC_n** with the same n. All experiments were carried out in CO_2-saturated 0.1 M NaH_2PO_4 and 0.1 M NaHAsc solutions at 25 °C for three hours under visible light (λ > 400 or 455 nm), and in triplicates. In addition to CO and H_2 no other photocatalytic products were detected. TOF and PTOF values were calculated by averaging the obtained values of each hour.

Alkyl chain length	λ (nm)	CO (nmol)	H_2 (nmol)	TON CO	TON H_2	PTON CO	PTON H_2	TOF CO (h^{-1})	TOF H_2 (h^{-1})	PTOF CO (h^{-1})	PTOF H_2 (h^{-1})	CO selectivity (%)
C_0	400	18.6 ± 1.0	2.9 ± 1.2	2.5 ± 0.1	0.4 ± 0.2	5.0 ± 0.1	0.8 ± 0.2	1.2 ± 0.4	0.2 ± 0.1	2.3 ± 0.8	0.3 ± 0.1	88 ± 2
	455	18.6 ± 0.9	0.9 ± 0.1	2.5 ± 0.1	0.1 ± 0.1	5.0 ± 0.1	0.3 ± 0.1	1.2 ± 0.5	< 0.1	2.5 ± 0.9	0.2 ± 0.1	94 ± 1
C_9	400	113.8 ± 3.7	2.5 ± 0.5	15.2 ± 0.5	0.3 ± 0.1	30.3 ± 0.5	0.7 ± 0.1	5.5 ± 0.4	0.1 ± 0.1	11.0 ± 0.9	0.2 ± 0.1	98 ± 1
	455	108.8 ± 8.3	1.1 ± 0.1	14.5 ± 1.1	0.2 ± 0.1	29.0 ± 1.1	0.3 ± 0.1	5.7 ± 0.9	< 0.1	11.3 ± 1.7	0.1 ± 0.1	99 ± 1
C_{12}	400	107.4 ± 3.9	2.0 ± 0.6	14.3 ± 0.5	0.3 ± 0.1	28.6 ± 0.5	0.5 ± 0.1	5.5 ± 0.9	0.1 ± 0.1	11.1 ± 1.8	0.2 ± 0.1	98 ± 1
	455	81.1 ± 7.8	1.4 ± 0.4	10.8 ± 1.0	0.2 ± 0.1	21.6 ± 1.0	0.4 ± 0.1	4.3 ± 0.8	0.1 ± 0.1	8.7 ± 1.6	0.2 ± 0.1	98 ± 1
C_{15}	400	34.6 ± 0.7	0.7 ± 0.2	4.6 ± 0.9	0.1 ± 0.1	9.2 ± 0.9	0.2 ± 0.1	1.7 ± 0.2	< 0.1	3.4 ± 0.4	< 0.1	98 ± 1
	455	40.9 ± 6.6	0.8 ± 0.3	5.5 ± 0.9	0.1 ± 0.1	10.9 ± 0.9	0.2 ± 0.1	2.0 ± 0.1	< 0.1	3.9 ± 0.3	< 0.1	98 ± 1
C_{17}	400	34.7 ± 4.4	1.0 ± 0.3	4.6 ± 0.6	0.1 ± 0.1	9.2 ± 0.6	0.3 ± 0.1	1.8 ± 0.3	< 0.1	3.7 ± 0.6	< 0.1	98 ± 1
	455	28.8 ± 0.3	0.5 ± 0.1	3.8 ± 0.1	< 0.1	7.7 ± 0.1	< 0.1	1.5 ± 0.2	< 0.1	2.9 ± 0.4	< 0.1	97 ± 2
C_{19}	400	22.8 ± 2.0	0.5 ± 0.1	3.0 ± 0.3	< 0.1	6.1 ± 0.3	0.1 ± 0.1	1.3 ± 0.2	< 0.1	2.5 ± 0.5	< 0.1	97 ± 1
	455	20.8 ± 3.3	0.5 ± 0.1	2.8 ± 0.4	< 0.1	5.5 ± 0.4	0.1 ± 0.1	1.1 ± 0.2	< 0.1	2.3 ± 0.4	< 0.1	98 ± 1

Table C6. Summary of photocatalysis results for CO gas obtained from all alkyl chain lengths in DPPC:NaDSPE-PEG2K 1001 photocatalytic liposomes **C_n** containing **ReC_n** and **RuC_n** with the same n before and after applying h_{immob} as correction factor (Table C9). Non-corrected data is also shown in Table C5.

Alkyl chain length	λ (nm)	TON CO	^{corr}TON CO	PTON CO	^{corr}PTON CO	TOF CO (h^{-1})	^{corr}TOF CO (h^{-1})	PTOF CO (h^{-1})	^{corr}PTOF CO (h^{-1})
C_0	400	2.5 ± 0.1	4.1 ± 0.2	5.0 ± 0.1	118.1 ± 3.2	1.2 ± 0.4	1.9 ± 0.6	2.3 ± 0.8	55.0 ± 18.4
	455	2.5 ± 0.1	4.1 ± 0.2	5.0 ± 0.1	118.2 ± 3.0	1.2 ± 0.5	2.1 ± 0.8	2.5 ± 0.9	68.3 ± 21.6
C_9	400	15.2 ± 0.5	19.4 ± 0.6	30.3 ± 0.5	39.7 ± 0.7	5.5 ± 0.4	7.0 ± 0.6	11.0 ± 0.9	14.4 ± 1.1
	455	14.5 ± 1.1	18.6 ± 1.4	29.0 ± 1.1	38.0 ± 1.4	5.7 ± 0.9	7.2 ± 1.1	11.3 ± 1.7	14.8 ± 2.3
C_{12}	400	14.3 ± 0.5	16.4 ± 0.6	28.6 ± 0.5	34.2 ± 0.6	5.5 ± 0.9	6.3 ± 1.0	11.1 ± 1.8	13.2 ± 2.2
	455	10.8 ± 1.0	12.4 ± 1.2	21.6 ± 1.0	25.8 ± 1.2	4.3 ± 0.8	5.0 ± 0.9	8.7 ± 1.6	10.4 ± 1.9
C_{15}	400	4.6 ± 0.9	6.3 ± 1.3	9.2 ± 0.9	10.9 ± 1.1	1.7 ± 0.2	2.4 ± 0.3	3.4 ± 0.4	4.1 ± 0.4
	455	5.5 ± 0.9	7.5 ± 1.2	10.9 ± 0.9	12.9 ± 1.0	2.0 ± 0.1	2.7 ± 0.2	3.9 ± 0.3	4.6 ± 0.3
C_{17}	400	4.6 ± 0.6	4.8 ± 0.6	9.2 ± 0.6	10.2 ± 0.7	1.8 ± 0.3	1.9 ± 0.3	3.7 ± 0.6	4.0 ± 0.7
	455	3.8 ± 0.1	4.0 ± 0.1	7.7 ± 0.1	8.5 ± 0.1	1.5 ± 0.2	1.5 ± 0.2	2.9 ± 0.4	3.2 ± 0.4
C_{19}	400	3.0 ± 0.3	3.1 ± 0.3	6.1 ± 0.3	7.8 ± 0.3	1.3 ± 0.2	1.3 ± 0.3	2.5 ± 0.5	3.3 ± 0.6
	455	2.8 ± 0.4	2.9 ± 0.5	5.5 ± 0.4	7.1 ± 0.6	1.1 ± 0.2	1.2 ± 0.2	2.3 ± 0.4	2.9 ± 0.6

Table C7. Summary of photocatalysis experiments obtained from all alkyl chain lengths in DPPC:NaDSPE-PEG2K 100:1 photocatalytic liposomes **C_n**. All experiments were conducted in CO_2- or N_2- saturated 0.1 M NaH_2PO_4 and 0.1 M NaHAsc buffer solutions for three hours at 25 °C under visible light (λ > 455 nm) and in duplicates, except for the first row in C_9 system whose experiments were performed as triplicates. Symbols "✓" and "-" stand for "included" and "not included" respectively, and "n. d." stands for "not detected".

Alkyl chain length	Components				Gaseous products after three-hour experiments				
	Catalyst	Photosensitiser	Sodium ascorbate	CO_2	CO (nmol)	H_2 (nmol)	TON CO	TON H_2	CO selectivity (%)
C_0	✓	-	✓	✓	n. d.	n. d.	-	-	-
	-	✓	✓	✓	0.1 ± 0.1	0.1 ± 0.1	-	-	-
C_9	✓	✓	✓	✓	108.9 ± 8.3	1.1 ± 0.1	14.5 ± 1.1	0.2 ± 0.1	99 ± 1
	✓	✓	✓	✓[a]	n. d.	n. d.	-	-	-
	✓	✓	-	✓	n. d.	n. d.	-	-	-
	✓	✓	✓	-[b]	n. d.	n. d.	-	-	-
	✓	-	✓	✓	n. d.	n. d.	-	-	-
	-	✓	✓	✓	0.2 ± 0.1	n. d.	-	-	-
C_{12}	✓	-	✓	✓	0.2 ± 0.1	n. d.	-	-	-
	-	✓	✓	✓	n. d.	n. d.	-	-	-
C_{15}	✓	-	✓	✓	n. d.	n. d.	-	-	-
	-	✓	✓	✓	0.3 ± 0.1	n. d.	-	-	-
C_{17}	✓	-	✓	✓	0.3 ± 0.1	0.3 ± 0.1	-	-	-
	-	✓	✓	✓	n. d.	n. d.	-	-	-
C_{19}	✓	-	✓	✓	0.1 ± 0.1	n. d.	-	-	-
	-	✓	✓	✓	0.3 ± 0.1	n. d.	-	-	-

[a] Experiments were carried out in the dark. [b] Experiments were carried out in N_2-saturated solutions.

C. 5. Electrochemistry

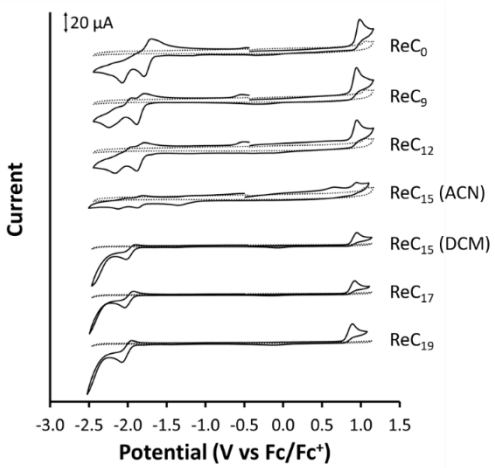

Figure C6. Cyclic voltammograms of solutions of **ReC$_n$** (1 mM) in degassed acetonitrile (**ReC$_0$**, **ReC$_9$**, **ReC$_{12}$**, and **ReC$_{15}$**) or degassed dichloromethane (**ReC$_{15}$**, **ReC$_{17}$**, and **ReC$_{19}$**) with 0.1 M Bu_4NPF_6 electrolyte, measured at 25 °C. The voltammograms were obtained at a scanning rate of 100 mV s^{-1} with a glassy carbon working electrode, Ag/AgCl reference electrode, and a Pt wire auxiliary electrode.

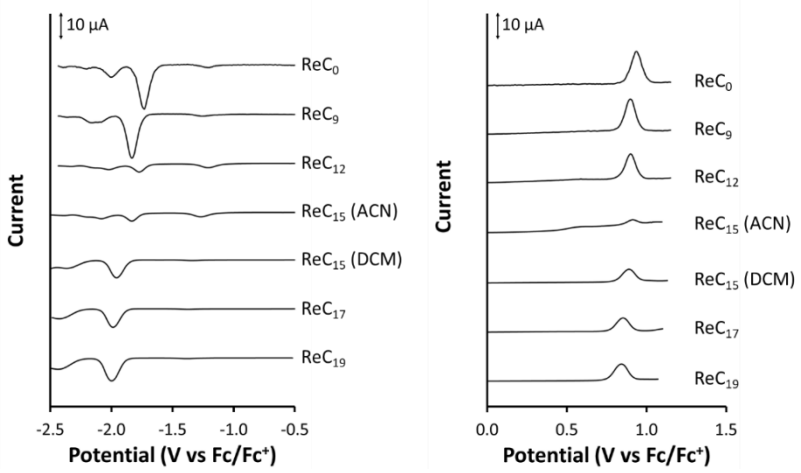

Figure C7. Differential pulse voltammograms of solutions of **ReC$_n$** (1 mM) in degassed acetonitrile (**ReC$_0$**, **ReC$_9$**, **ReC$_{12}$**, and **ReC$_{15}$**) or degassed dichloromethane (**ReC$_{15}$**, **ReC$_{17}$**, and **ReC$_{19}$**) with 0.1 M Bu_4NPF_6 electrolyte, measured at 25 °C. The voltammograms were obtained at a scanning rate of 50 mV s^{-1} with a glassy carbon working electrode, Ag/AgCl reference electrode, and a Pt wire auxiliary electrode.

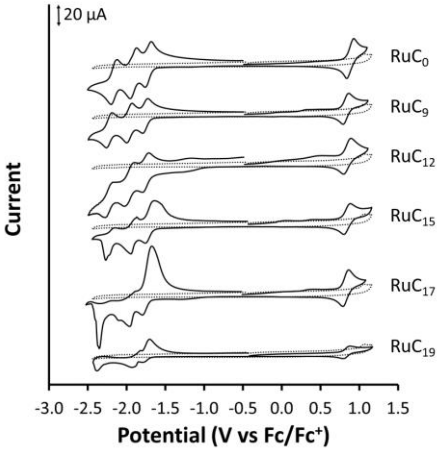

Figure C8. Cyclic voltammograms of solutions of **RuC_n** (1 mM) in degassed acetonitrile with 0.1 M Bu_4NPF_6 electrolyte, measured at 25 °C. The voltammograms were obtained at a scanning rate of 100 mV s^{-1} with a glassy carbon working electrode, Ag/AgCl reference electrode, and a Pt wire auxiliary electrode.

Table C8. Redox potentials of **RuC_n** and **ReC_n** complexes.[a]

Metal complex	$E_{1/2}$ (oxdn) in V *vs.* Fc^+/Fc	$E_{1/2}$ (redn) in V *vs.* Fc^+/Fc
RuC_0	0.88	–1.72, –1.92, –2.16
RuC_9	0.83	–1.76, –1.97, –2.22
RuC_{12}	0.84	–1.70, –1.91, –2.20
RuC_{15}	0.84	–1.70, –1.91, –2.20
RuC_{17}	0.80	–1.76, –1.92, –2.26
RuC_{19}	0.83	–1.74, –1.87, –2.35
ReC_0	0.94	–1.73, –2.00
ReC_9	0.90	–1.83, –2.15
ReC_{12}	0.90	–1.83, –2.12
ReC_{15}	0.91[b]	–1.83[b], –2.08[b]
	0.89[c]	–1.96[c], –2.37[c]
ReC_{17}	0.85[c]	–1.99[c], –2.43[c]
ReC_{19}	0.84[c]	–2.00[c], –2.44[c]

[a] These values were obtained at 25 °C in degassed acetonitrile solutions containing 0.1 M tetrabutylammonium hexafluorophosphate and 1 mM metal complex. [b] **ReC_{15}** was partially soluble in acetonitrile. [c] These values were measured in degassed dichloromethane.

C. 6. Liposome immobilisation efficiency

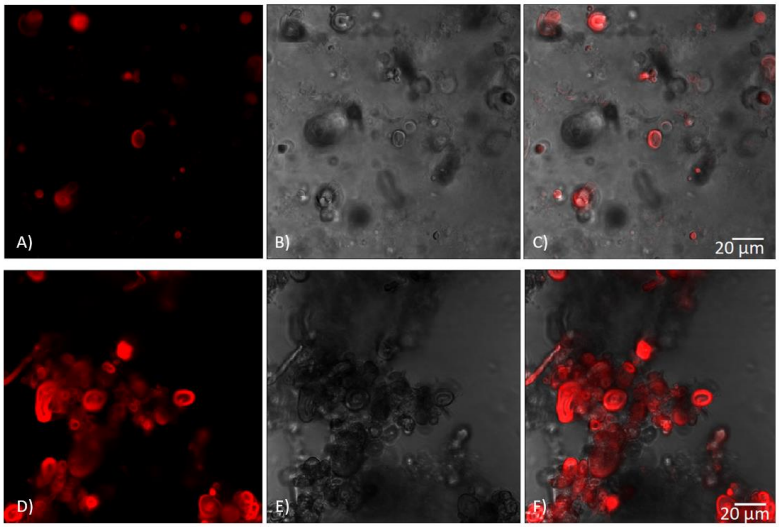

Figure C9. Confocal microscopy of DPPC (A, B, C) and DMPC (D, E, F) giant vesicles containing 2% **RuC_{12}** in 0.1 M NaH_2PO_4 buffer (pH = 7.7). Figures C9A and C9D are fluorescence images, Figures C9B and C9E are transmission images, and Figures C9C and C9F are overlay images. Images were taken with a Nikon Ti2 microscope at 80x total zoom, 488 nm excitation, and 640 – 680 nm emission.

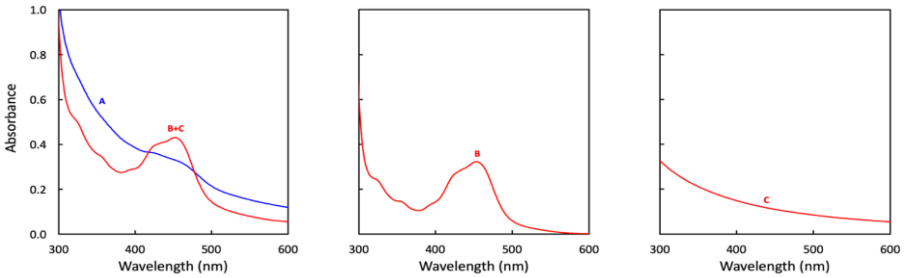

Figure C10. UV-Vis absorption spectra of A) DSPC:NaDSPE-PEG2K 100:1 liposomes functionalised with **RuC_{12}** in 0.1 M NaH_2PO_4 buffer (blue line), B) **RuC_{12}** in acetonitrile (no liposomes), C) DSPC:NaDSPE-PEG2K 100:1 liposomes (without **RuC_{12}**) in 0.1 M NaH_2PO_4 buffer. Red curve in A shows the addition of the absorption spectra of B and C; it obviously does not superpose to the absorption spectrum of the Ru-functionalised liposomes (blue line), illustrating the limits of UV-Vis spectroscopy for quantifying the **RuC_{12}** concentration in liposomes. Experimental conditions: [DSPC] = 6.25 mM, [NaDSPE-PEG2K] = 62.5 µM, and [RuC_{12}] = 25 µM.

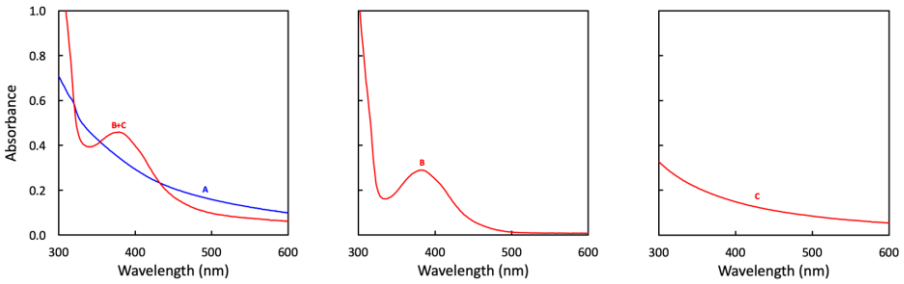

Figure C11. UV-Vis absorption spectra of A) DSPC:NaDSPE-PEG2K 100:1 liposomes functionalised with **ReC$_{12}$** in 0.1 M NaH_2PO_4 buffer, B) **ReC$_{12}$** in chloroform (no liposomes), C) DSPC:NaDSPE-PEG2K 100:1 liposomes (without **ReC$_{12}$**) in 0.1 M NaH_2PO_4 buffer. Red curve in A shows the addition of the absorption spectra of B and C; it obviously does not superpose with the absorption spectrum of the Re-functionalised liposomes (blue line), illustrating the limits of UV-Vis spectroscopy for quantifying the **ReC$_{12}$** concentration in liposomes. Experimental conditions: [DSPC] = 6.25 mM, [NaDSPE-PEG2K] = 62.5 µM, and [ReC_{12}] = 25 µM.

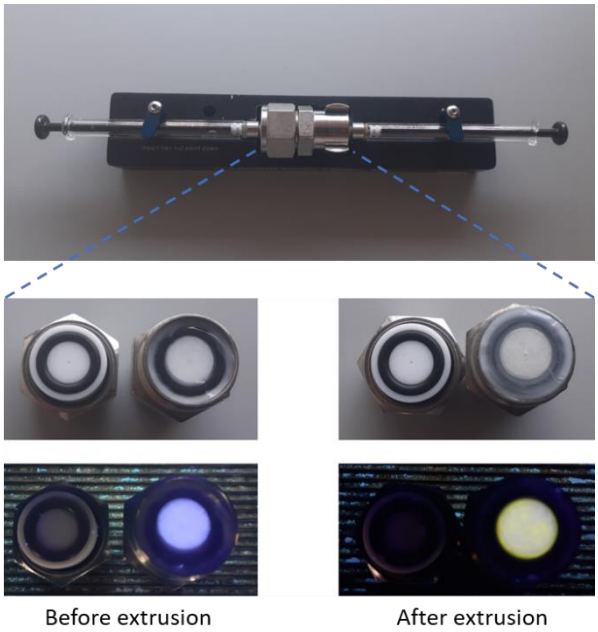

Figure C12. The Avanti Polar Lipids mini-extruder used to prepare liposomes (in this case DPPC:PEG2K:**RuC$_9$**:**ReC$_9$** in a ratio 100:1.0:0.4:0.4) and the internal membrane supports including the filter supports and the polycarbonate membrane (0.2 µm) before and after extrusion. A deposit was observed on the filter after extrusion, which coloured brightly yellow under UV light (λ = 366 nm), which indicated that some **ReC$_9$** (λ_{abs} = 380 nm and λ_{em} = 582 nm in chloroform) was present on the filter.

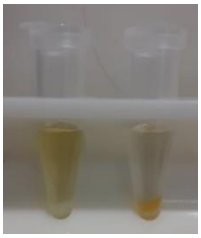

Figure C13. Solutions of **RuC_0-ReC_0** liposomes (left) and **RuC_9-ReC_9** liposomes (right) after ultracentrifugation.

Table C9. Immobilisation efficiencies, determined by ICP-MS, for photocatalytic liposomes **C_n** prepared from DPPC, NaDSPE-PEG2K, **RuC_n**, and **ReC_n** (100:1.0:0.4:0.4).[a]

Metal complex	η_{extr}[b]	η_{encap}[b]	η_{immob}[b]
RuC_0	94.9 ± 5.1%	4.2 ± 4.2%	3.8 ± 3.8%
RuC_9	80.3 ± 1.1%	95.0 ± 0.8%	76.3 ± 1.7%
RuC_{12}	86.4 ± 0.2%	97.0 ± 0.5%	83.8 ± 0.3%
RuC_{15}	85.2 ± 6.3%	99.6 ± 0.3%	84.9 ± 6.0%
RuC_{17}	91.2 ± 5.1%	99.5 ± 0.2%	90.7 ± 5.2%
RuC_{19}	78.6 ± 2.7%	99.2 ± 0.1%	78.0 ± 2.6%
ReC_0	95.1 ± 4.9%	62.0 ± 5.5%	59.3 ± 8.2%
ReC_9	80.2 ± 10.9%	97.5 ± 0.8%	78.1 ± 10.0%
ReC_{12}	86.1 ± 14.0%	97.4 ± 0.6%	83.7 ± 13.1%
ReC_{15}	75.2 ± 22.3%	97.2 ± 0.6%	73.2 ± 22.2%
ReC_{17}	96.2 ± 3.8%	98.4 ± 1.0%	94.7 ± 4.7%
ReC_{19}	99.3 ± 0.7%	96.9 ± 0.4%	96.2 ± 1.1%

[a] Experimental conditions: [DPPC] = 6.25 mM, [NaDSPE-PEG2K] = 62.5 µM, [**RuC_n**] = 25 µM, and [**ReC_n**] = 25 µM in 0.1 M NaH_2PO_4 buffer. Bulk concentrations [**ReC_n**] and [**RuC_n**] indicate theoretical concentrations (before extrusion). [b] The errors are based on two independent liposome preparations.

C. 7. Transient absorption spectroscopy

C. 7. 1. Supplementary figures

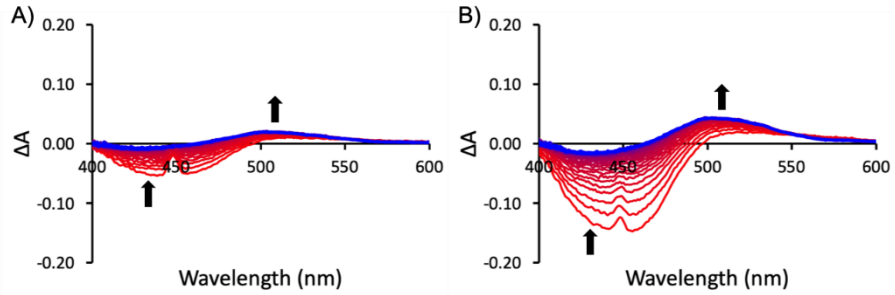

Figure C14. Time-resolved absorption spectroscopy data after laser excitation (λ_{exc} = 450 nm, 3.5 mJ per pulse) on a 2 µs timescale (timestep = 0.04 µs) for DPPC-NaDSPE-PEG2K liposome systems $\mathbf{C_n}$ consisting of A) $\mathbf{RuC_9}$ and 0.0% $\mathbf{ReC_9}$ and B) $\mathbf{RuC_{19}}$ and 0.0% $\mathbf{ReC_{19}}$. Experimental conditions: [DPPC] = 6.25 mM, [NaDSPE-PEG2K] = 62.5 µM, and [$\mathbf{RuC_n}$] = 25 µM in CO_2-saturated 0.1 M NaHAsc aqueous solution. Bulk concentration [$\mathbf{RuC_n}$] indicates theoretical concentration (before extrusion). The observed artefact in the data at 450 nm is due to the scattering of laser light.

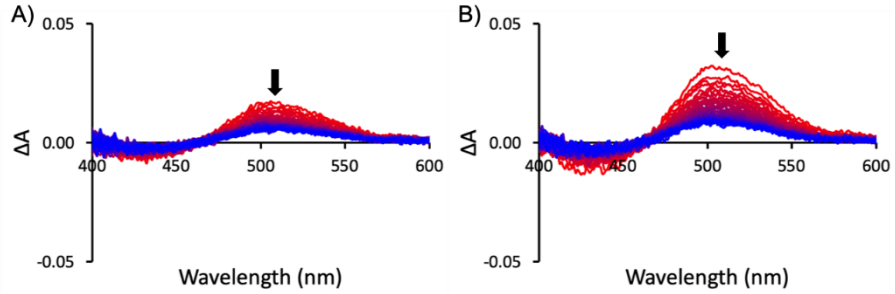

Figure C15. Time-resolved absorption spectroscopy data after laser excitation (λ_{exc} = 450 nm, 3.5 mJ per pulse) on a 2 ms timescale (timestep = 0.04 ms) for DPPC-NaDSPE-PEG2K liposome systems $\mathbf{C_n}$ consisting of A) $\mathbf{RuC_9}$ and 0.0% $\mathbf{ReC_9}$ and B) $\mathbf{RuC_{19}}$ and 0.0% $\mathbf{ReC_{19}}$. Experimental conditions: [DPPC] = 6.25 mM, [NaDSPE-PEG2K] = 62.5 µM, and [$\mathbf{RuC_n}$] = 25 µM in CO_2-saturated 0.1 M NaHAsc aqueous solution. Bulk concentration [$\mathbf{RuC_n}$] indicates theoretical concentration (before extrusion).

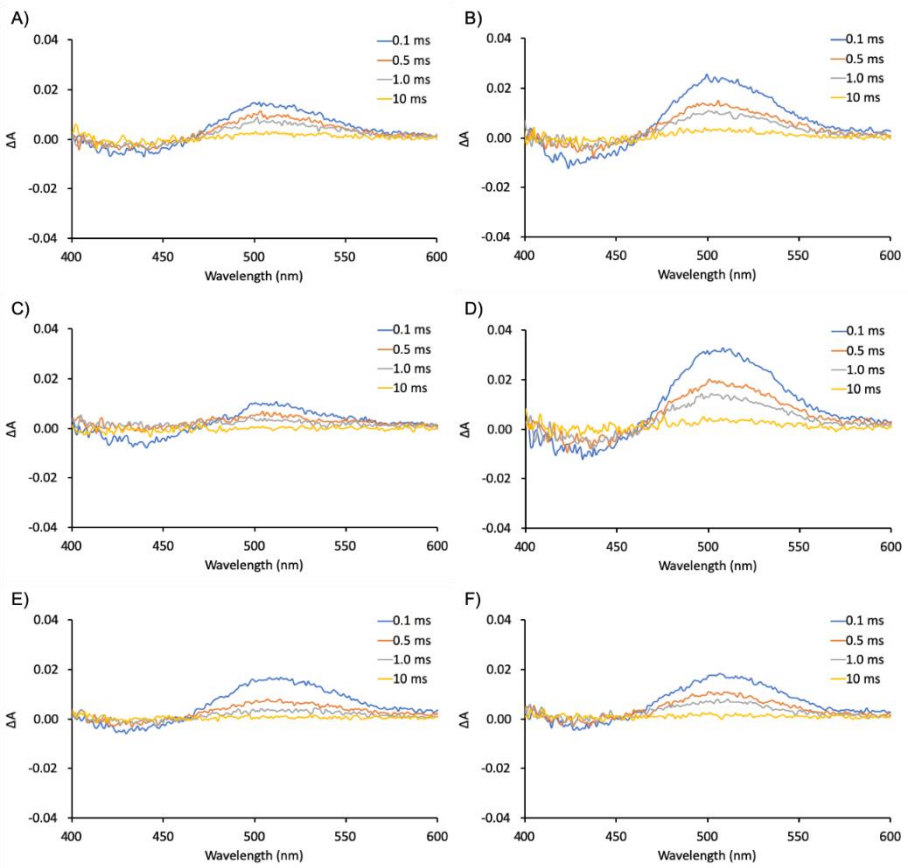

Figure C16. Time-resolved absorption spectroscopy data after laser excitation (λ_{exc} = 450 nm, 3.5 mJ per pulse) on a 10 ms timescale (timestep = 0.1 ms) for DPPC-NaDSPE-PEG2K liposome systems $\mathbf{C_n}$ consisting of A) $\mathbf{RuC_9}$ and 0.0% $\mathbf{ReC_9}$, B) $\mathbf{RuC_{19}}$ and 0.0% $\mathbf{ReC_{19}}$, C) $\mathbf{RuC_9}$ and 0.4% $\mathbf{ReC_9}$, D) $\mathbf{RuC_{19}}$ and 0.4% $\mathbf{ReC_{19}}$, E) $\mathbf{RuC_9}$ and 1.6% $\mathbf{ReC_9}$, and F) $\mathbf{RuC_{19}}$ and 1.6% $\mathbf{ReC_{19}}$. Experimental conditions: [DPPC] = 6.25 mM, [NaDSPE-PEG2K] = 62.5 µM, [$\mathbf{RuC_n}$] = 25 µM, and [$\mathbf{ReC_n}$] = 0, 25 or 100 µM in CO_2-saturated 0.1 M NaHAsc aqueous solution. Bulk concentrations [$\mathbf{ReC_n}$] and [$\mathbf{RuC_n}$] indicate theoretical concentrations (before extrusion).

C. 7. 2. Kinetic model

In the absence of quencher $\mathbf{ReC_n}$, the rate equation for $\mathbf{RuC_n^-}$ is a combination of the formation of $\mathbf{RuC_n^-}$ due to reductive quenching of $\mathbf{RuC_n^*}$ by $HAsc^-$ and the decay of $\mathbf{RuC_n^-}$ due to the second-order charge recombination of $\mathbf{RuC_n^-}$ and $HAsc^\bullet$ (Equation C5). The disappearance of $\mathbf{RuC_n^*}$ is very fast (µs) in comparison to the disappearance of $\mathbf{RuC_n^-}$ (ms). The TA spectroscopy measurements were performed in the ms timescale (10 ms with a timestep

of 0.1 ms) and thus the rate equation for **RuC$_n^-$** simplifies to Equation C6. Assuming that [**RuC$_n^-$**]$_0$ equals [HAsc$^\bullet$]$_0$ leads to a standard second order rate law (Equation C7) with its solution (Equation C8), which can be rewritten to Equation 3.4.

$$\frac{d[\mathrm{RuC}_n^-]}{dt} = k_{\mathrm{RQ}}[\mathrm{RuC}_n^*][HAsc^-] - k_{\mathrm{CR}}[\mathrm{RuC}_n^-][HAsc^\bullet] \quad \text{Equation C5}$$

$$\frac{d[\mathrm{RuC}_n^-]}{dt} = -k_{\mathrm{CR}}[\mathrm{RuC}_n^-][HAsc^\bullet] \quad \text{Equation C6}$$

$$\frac{d[\mathrm{RuC}_n^-]}{dt} = -k_{\mathrm{CR}}[\mathrm{RuC}_n^-]^2 \quad \text{Equation C7}$$

$$\frac{1}{[\mathrm{RuC}_n^-]} = \frac{1}{[\mathrm{RuC}_n^-]_0} + k_{\mathrm{CR}}t \quad \text{Equation C8}$$

In the presence of quencher **ReC$_n$**, the rate equation for **RuC$_n^-$** is a combination of the decay of **RuC$_n^-$** due to second-order charge recombination of **RuC$_n^-$** and HAsc$^\bullet$ and due to first-order quenching by **ReC$_n$** (Equation C9). Equation C9 can be solved according to Limburg et al.[8] to give Equation 3.6 in the main text.

$$\frac{d[\mathrm{RuC}_n^-]}{dt} = -k_{\mathrm{CR}}[\mathrm{RuC}_n^-][HAsc^\bullet] - k_{\mathrm{Q}}[ReC_n] \quad \text{Equation C9}$$

C. 7. 3. Data fitting

The average absorbance between 490 – 540 nm was fitted using Equation C10 and C11, which is derived from Equation 3.5 in Chapter 3 using the Lambert-Beer law. At these wavelengths the concentration and absorption of **RuC$_n^-$** are strictly proportional to the optical pathlength (l = 1 cm) and the molar absorption coefficient ($\varepsilon_{505\mathrm{nm}}$ = 1.2 x 10^4 M^{-1}cm^{-1} for [Ru(bpy)$_3$]$^+$ in acetonitrile[9] was used).

$$A(t) = \frac{A_0}{1 + k' A_0 t} + A_\infty \quad \text{Equation C10}$$

$$k' = \frac{k_{CR}}{\varepsilon_{505}\, l} \quad \text{Equation C11}$$

Table C10. Fitting parameters used to fit the data in Figure 3.5 using Equation C10.

Sample	A_0	$k'\varepsilon_{505}c_0l$ (μs^{-1})	A_∞ (10^3)
RuC_9 and 0.0 % **ReC_9**	0.011 ± 0.003	131 ± 7	1.26 ± 0.07
RuC_9 and 0.4 % **ReC_9**	0.012 ± 0.003	651 ± 103	0.60 ± 0.09
RuC_9 and 1.6 % **ReC_9**	0.022	334 ± 12	–0.20 ± 0.04
RuC_{19} and 0.0 % **ReC_{19}**	0.019 ± 0.004	100 ± 4	1.79 ± 0.07
RuC_{19} and 0.4 % **ReC_{19}**	0.0286 ± 0.0004	73 ± 2	1.50 ± 0.06
RuC_{19} and 1.6 % **ReC_{19}**	0.0160 ± 0.0003	149 ± 5	0.54 ± 0.05

C. 8. Fluorescence correlation spectroscopy

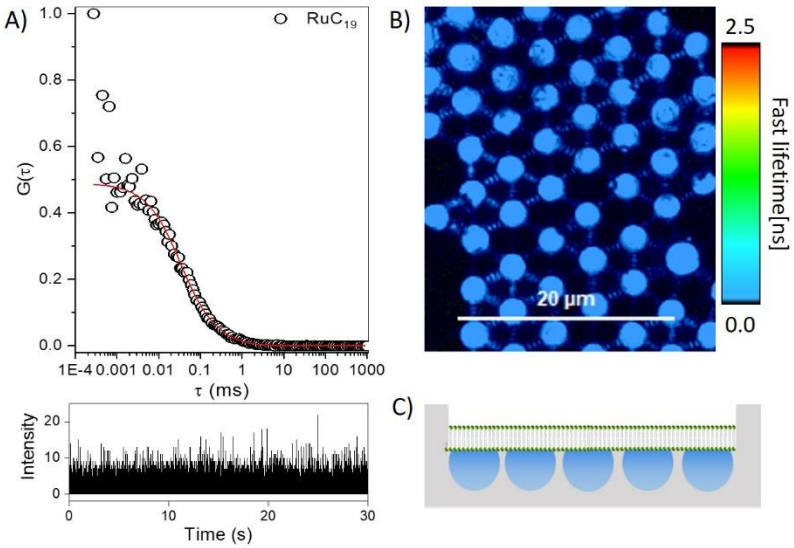

Figure C17. A) top ACF and bottom time trace for diffusion of **RuC_{19}** in acetonitrile. The diffusion coefficient in solution was measured by fitting this curve to a three-dimensional model with D equals 199 ± 149 $\mu m^2 s^{-1}$ with an α value of 0.99 ± 0.08. B) Fluorescence lifetime image of MSLBs comprised of DPPC:NaDSPE-PEG2K in a ratio of 100:1. The membrane is labelled with 10 nM DOPE-ATTO 655 and the image shows the fluorescence from the ATTO probe above the pores of the arrays confirming that the bilayer has formed. C) Schematic illustration of aqueous filled microcavity supported lipid bilayer. Note we have included the organic probe to image the bilayer, because the much lower quantum yield of the Ru compound makes it difficult to see it in fluorescence lifetime imaging above the pores against background/scatter from the substrate.

C. 9. Single crystal X-ray crystallography of 4,4'-$(C_{17}H_{35})_2$-bpy

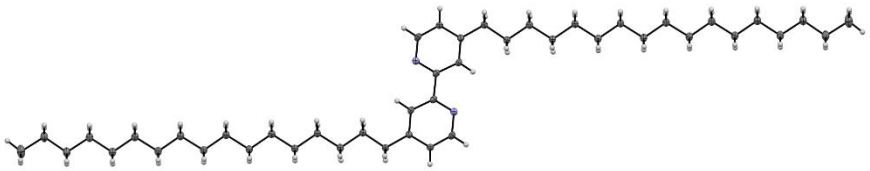

Figure C18. Displacement ellipsoid plots (50% probability level) of **4,4'-$(C_{17}H_{35})_2$-bpy** at 110(2) K.

Colourless single crystals of **4,4'-$(C_{17}H_{35})_2$-bpy** were obtained by evaporation of the solvent $CDCl_3$ at room temperature. The supplementary crystallographic data of **4,4'-$(C_{17}H_{35})_2$-bpy** can be found under deposition number 2062217 (https://www.ccdc.cam.ac.uk/structures). These data are provided free of charge by the joint Cambridge Crystallographic Data Centre and Fachinformationszentrum Karlsruhe.

All reflection intensities were measured at 110(2) K using a SuperNova diffractometer (equipped with Atlas detector) with Cu Kα radiation (λ = 1.54178 Å) under the program CrysAlisPRO (Version CrysAlisPro 1.171.39.29c, Rigaku OD, 2017, Oxford Diffraction / Agilent Technologies UK Ltd, Yarnton, England). The same program was used to refine the cell dimensions and for data reduction. The structure was solved with the program SHELXS-2018/3[10] and was refined on F^2 with SHELXL-2018/3[10]. Analytical numeric absorption correction using a multifaceted crystal model was applied using CrysAlisPro. The temperature of the data collection was controlled using the system Cryojet (manufactured by Oxford Instruments). The H atoms were placed at calculated positions using the instruction AFIX 23, AFIX 43 or AFIX 137 with isotropic displacement parameters having values 1.2 or 1.5 *U*eq of the attached C atoms.

The structure is ordered. The crystal that was mounted on the diffractometer was a composite of two crystals stuck together (most crystals were significantly twinned). The two crystals are related by a rotation of *ca.* 3.74°

around the b direction. The refinement was carried out using the HKLF5 instruction, and the BASF scale factor refines to 0.135(2).

	xs2388a
Crystal data	
Chemical formula	$C_{44}H_{76}N_2$
M_r	633.06
Crystal system, space group	Triclinic, *P*-1
Temperature (K)	110
a, *b*, *c* (Å)	6.4931 (4), 7.0030 (4), 21.8388 (11)
α, β, γ (°)	80.932 (4), 86.310 (5), 86.295 (4)
V (Å^3)	977.10 (10)
Z	1
Radiation type	Cu *K*α
m (mm^{-1})	0.45
Crystal size (mm)	0.29 × 0.09 × 0.02
Data collection	
Diffractometer	SuperNova, Dual, Cu at zero, Atlas
Absorption correction	Analytical CrysAlis PRO 1.171.39.29c (Rigaku OD, 2017) Analytical numeric absorption correction using a multifaceted crystal model based on expressions derived by R.C. Clark & J.S. Reid.[11] Empirical absorption correction using spherical harmonics, implemented in SCALE3 ABSPACK (An Oxford Diffraction Program (1.0.4, gui:1.0.3) © 2005 Oxford Diffraction Ltd.) scaling algorithm.
T_{min}, T_{max}	0.929, 0.991
No. of measured, independent and observed [$I > 2s(I)$] reflections	11246, 3934, 1773
R_{int}	0.030
$(\sin \theta/l)_{max}$ (Å^{-1})	0.598
Refinement	
$R[F^2 > 2s(F^2)]$, $wR(F^2)$, *S*	0.036, 0.093, 0.71
No. of reflections	3934
No. of parameters	210
H-atom treatment	H-atom parameters constrained
$\Delta\rho_{max}$, $\Delta\rho_{min}$ (e Å^{-3})	0.15, -0.18

Computer programs: CrysAlis PRO 1.171.39.29c (Rigaku OD, 2017), SHELXS2018/3[10], SHELXL2018/3[10], SHELXTL v6.10[12].

C. 10. References

1 J. J. Snellenburg, S. Laptenok, R. Seger, K. M. Mullen and I. H. M. van Stokkum, *J. Stat. Softw.*, 2012, **49**, 1–22.

2 M. W. H. Hoorens, M. Medved', A. D. Laurent, M. Di Donato, S. Fanetti, L. Slappendel, M. Hilbers, B. L. Feringa, W. J. Buma and W. Szymanski, *Nat. Commun.*, 2019, **10**, 2390.

3 G. B. Berselli, N. K. Sarangi, S. Ramadurai, P. V Murphy and T. E. Keyes, *ACS Appl. Bio Mater.*, 2019, **2**, 3404–3417.

4 J. E. Collins, J. J. S. Lamba, J. C. Love, J. E. McAlvin, C. Ng, B. P. Peters, X. Wu and C. L. Fraser, *Inorg. Chem.*, 1999, **38**, 2020–2024.

5 K. Neuthe, F. Bittner, F. Stiemke, B. Ziem, J. Du, M. Zellner, M. Wark, T. Schubert and R. Haag, *Dyes Pigm.*, 2014, **104**, 24–33.

6 L. A. Worl, R. Duesing, P. Chen, L. Della Ciana and T. J. Meyer, *J. Chem. Soc. Dalt. Trans.*, 1991, 849–858.

7 N. Ikuta, S. Y. Takizawa and S. Murata, *Photochem. Photobiol. Sci.*, 2014, **13**, 691–702.

8 B. Limburg, E. Bouwman and S. Bonnet, *J. Phys. Chem. B*, 2016, **120**, 6969–6975.

9 R. S. Khnayzer, V. S. Thoi, M. Nippe, A. E. King, J. W. Jurss, K. A. El Roz, J. R. Long, C. J. Chang and F. N. Castellano, *Energy Environ. Sci.*, 2014, **7**, 1477–1488.

10 G. M. Sheldrick, *Acta Crystallogr. Sect. C*, 2015, **71**, 3–8.

11 R. C. Clark and J. S. Reid, *Acta Crystallogr. Sect. A*, 1995, **51**, 887–897.

12 G. M. Sheldrick, *Acta Crystallogr. Sect. A*, 2008, **64**, 112–122.

Appendix D

Supporting information for Chapter 4

D.1. EPR Spectroscopy

Figure D1 shows the EPR spectrum of **CoC_{12}** at 10 K. The broad and highly anisotropic signal indicates the presence of a high spin Co(II) species, with examples present in literature.[1,2] Simulations were performed with a g tensor of g = [g_{xx} g_{yy} g_{zz}] = [4.79 4.25 1.99] and a hyperfine splitting due to the coupling with ^{59}Co nucleus (I = 7/2) of A_{zz} = 340 MHz, which can be seen as eight lines at 350 mT (g_{zz} direction), see Figure D1. As line broadening an H-strain was used with the components 1500 MHz, 4800 MHz, and 240 MHz in the respective g tensor directions.

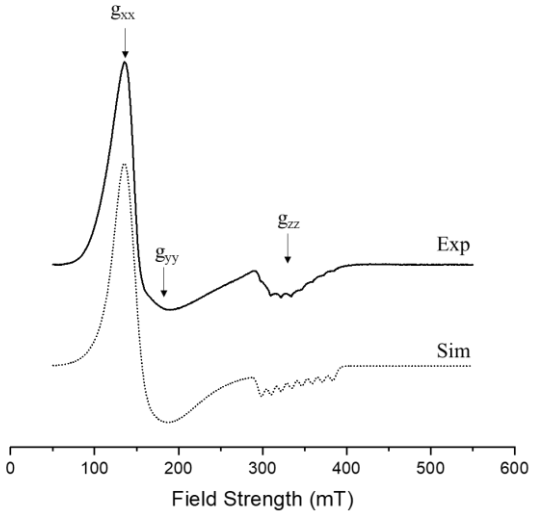

Figure D1. EPR spectrum (solid line) obtained from the frozen solution state of **CoC_{12}** in acetonitrile at 10 K and the corresponding simulation (dotted line). Experimental conditions: microwave frequency 9.502 GHz, microwave power 20 mW, modulation frequency 100 kHz, modulation amplitude 10 G. Simulation parameters: g = [g_{xx} g_{yy} g_{zz}] = [4.79 4.25 1.99], H-strain (MHz) = [1500 4800 240], hyperfine coupling A_{zz} of 340 MHz.

D.2. Local concentration calculation

When the bulk concentration of the photosensitiser or catalyst is known (i.e. 50 µM **RuC_{12}** and 5 µM **CoC_{12}**), the local concentration in the membrane can be calculated as follows[3]:

- The average area of DPPC lipid equals 0.7 nm^2/molecule.[4]
- Knowing the lipid bulk concentration (5 mM) and the sample volume (3 mL), the number of mole of lipid molecules in the sample is 15 µmol, from which we can deduct the full surface of all lipid bilayers in the sample, knowing there are two faces on a bilayer: the full bilayer surface is 0.7 nm^2 * 15 x 10^{-6} mol * 6.022 x 10^{-23} mol^{-1} / 2 = 3.15 x 10^{18} nm^2.
- From the total area of bilayer and the average liposome diameter by DLS (177.9 nm), we can calculate the area of one liposome ($4\pi(d/2)^2$), and the number of liposomes, hence the liposome concentration (in M): d = 177.9 nm, area of one liposome = $4\pi r^2$ → r = 177.9/2 = 88.95 nm. The area of one liposome is 9.94 x 10^4 nm^2.
- Total numbers of liposomes = 3.15 x 10^{18} nm^2/9.94 x 10^4 nm^2 = 0.32 x 10^{14}.
- Knowing the thickness of a bilayer (4 nm), the area of a liposome ($4\pi r^2$), calculate the volume of the bilayer of one liposome (thickness x $4\pi r^2$): Volume of bilayer of one liposome = 9.94 x 10^4 nm^2 * 4 nm = 3.98 x 10^5 nm^3.
- From the volume of the bilayer of one liposome and the total number of liposomes in the sample, we can calculate the total volume of all bilayers in the sample: 0.32 x 10^{14} x 3.98 x 10^5 nm^3 = 1.26 x 10^{19} nm^3 = 1.26 x 10^{-8} m^3 = 1.26 x 10^{-5} L = 1.26 x 10^{-2} mL = 0.0126 mL
- Knowing the ratio of total bilayer volume vs. bulk volume (3 mL), we can calculate the local concentration of each species in the volume of the bilayer: ratio between bulk and local concentration is 3 mL / 0.0126 mL = 238, local concentration of **RuC_{12}** = 50 µM x 238 = **11.9 mM** and local concentration **CoC_{12}** = 5 µM x 238 = **1.19 mM**.

D.3. Electrochemistry

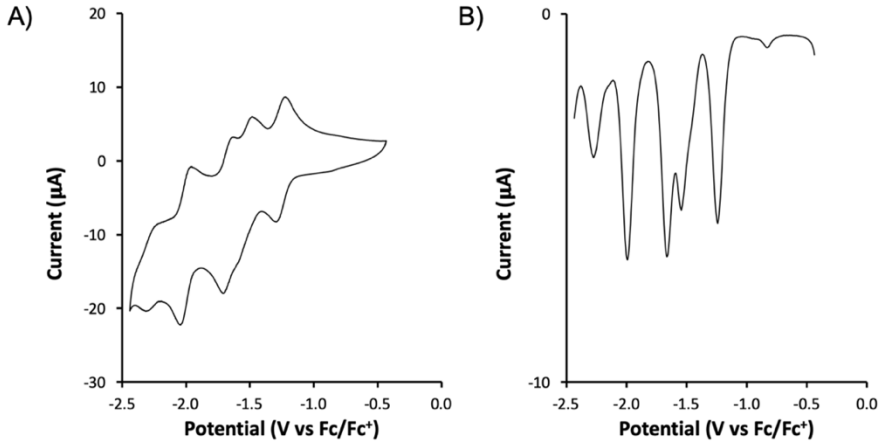

Figure D2. Cyclic voltammogram (A) and differential pulse voltammogram (B) of a solution of **CoC_{12}** (1 mM) in degassed acetonitrile with 0.1 M Bu_4NPF_6 electrolyte, measured at 25 °C. The cyclic voltammogram and the differential pulse voltammogram were obtained at a scanning rate of 100 mV s^{-1} and 50 mV s^{-1} respectively, with a glassy carbon working electrode, Ag/AgCl reference electrode, and a Pt wire auxiliary electrode. The reductive redox potentials of **CoC_{12}** were found to be –1.24, –1.54, –1.66, –1.99, and –2.27 V vs Fc/Fc^+.

D.4. Dynamic light scattering

Table D1. Summary of DLS results obtained of the liposome stock and after three independent light irradiation experiments (t_{irr} = 19 h, λ_{irr} = 450 nm) of photocatalytic liposomes prepared from DPPC, NaDSPE-PEG2K, **RuC_{12}**, and **CoC_{12}**. The control experiments (one of the components missing) were performed once.

					Before irradiation[a]			After irradiation[b]		
Lipid	**[NaHAsc]**	**[TCEP]**	**[RuC_{12}]**	**[CoC_{12}]**	**pH**	**d (nm)**	**PDI**	**pH[c]**	**d (nm)[c]**	**PDI[c]**
DPPC	0.1 M	0.1 M	50 µM	50 µM	5.0	154.7	0.089	4.8 ± 0.0	154.6 ± 1.9	0.083 ± 0.010
DPPC	0.1 M	0.1 M	50 µM	25 µM	5.0	159.3	0.140	4.7 ± 0.1	161.0 ± 1.6	0.161 ± 0.014
DPPC	0.1 M	0.1 M	50 µM	5 µM	5.0	177.9	0.122	4.8 ± 0.0	171.1 ± 2.5	0.136 ± 0.034
DPPC	0.1 M	0.1 M	50 µM	1 µM	5.0	172.1	0.109	4.8 ± 0.1	165.9 ± 1.4	0.109 ± 0.020
DPPC	0.1 M	0.1 M	50 µM	5 µM	3.0	146.5	0.125	2.6 ± 0.2	147.0 ± 1.5	0.145 ± 0.027
DPPC	0.1 M	0.1 M	50 µM	5 µM	4.0	166.5	0.116	4.0 ± 0.0	156.2 ± 0.1	0.115 ± 0.011
DPPC	0.1 M	0.1 M	50 µM	5 µM	6.0	205.3	0.148	6.3 ± 0.0	> 1000	0.466 ± 0.033
DPPC	0.1 M	0.1 M	25 µM	5 µM	5.0	161.4	0.120	4.9 ± 0.1	157.8 ± 3.6	0.138 ± 0.026
DMPC	0.1 M	0.1 M	50 µM	5 µM	4.0	158.8	0.155	3.9 ± 0.0	151.7 ± 0.9	0.142 ± 0.008
DSPC	0.1 M	0.1 M	50 µM	5 µM	4.0	171.0	0.101	3.8 ± 0.1	168.8 ± 8.3	0.156 ± 0.021
DPPC	0.1 M	0.1 M	50 µM	-	5.0	177.8	0.118	4.7	188.8	0.187
DPPC	0.1 M	0.1 M	-	25 µM	5.0	183.8	0.116	4.7	187.2	0.116
DPPC	0.1 M	-	50 µM	25 µM	5.0	157.2	0.120	5.1	165.1	0.156
DPPC	-	0.1 M	50 µM	25 µM	5.0	162.7	0.120	5.1	237.3	0.220

[a] Experimental conditions of the liposome stock solutions: [DPPC] = 17.5 mM, [NaDSPE-PEG2K] = 175 µM, [**RuC_{12}**] = 175 µM, and [**CoC_{12}**] = 3.5, 17.5, 87.5, or 175 µM in 0.1 M TCEP and 0.1 M NaHAsc solutions at 25 °C. The concentrations [**RuC_{12}**] and [**CoC_{12}**] indicate theoretical concentrations (before extrusion). [b] Experimental conditions for the photocatalytic liposome samples after irradiation: [DPPC] = 5 mM, [NaDSPE-PEG2K] = 50 µM, [**RuC_{12}**] = 50 µM, and [**CoC_{12}**] = 1, 5, 25, or 50 µM in 0.1 M TCEP and 0.1 M NaHAsc solutions at 25 °C. [c] Average and the mean absolute deviation over three independent irradiation experiments.

D.5. Control experiments

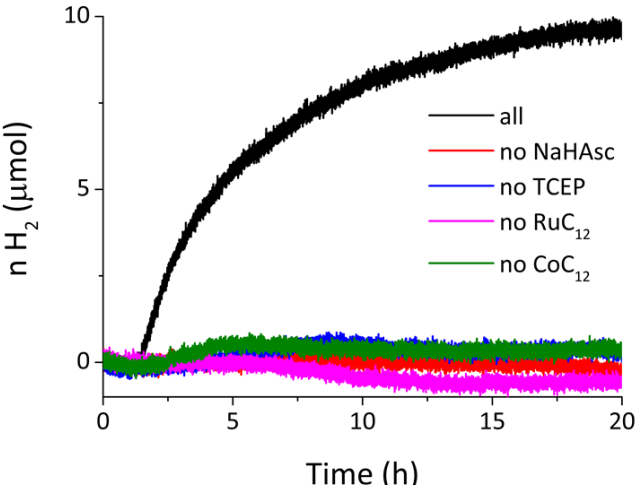

Figure D3. Photocatalytic H_2 generation with liposomes prepared from DPPC, NaDSPE-PEG2K, NaHAsc, TCEP, **RuC$_{12}$**, and **CoC$_{12}$** (black curve) and liposomes prepared in absence of one of the components (NaHAsc; red curve, TCEP; blue curve, **RuC$_{12}$**; pink curve, or **CoC$_{12}$**; green curve). The samples were left in the dark for 1 h and then irradiated with blue light for 19 h. Experimental conditions: [DPPC] = 5 mM, [NaDSPE-PEG2K] = 50 µM, [**RuC$_{12}$**] = 0 or 50 µM, [**CoC$_{12}$**] = 0 or 25 µM; argon-saturated 0 or 0.1 M NaHAsc and 0 or 0.1 M TCEP aqueous solution, pH = 5, volume 3.5 mL, temperature 25 °C, λ_{irr} = 450 nm, P = 10.6 mW, Φ_0 = 13.7 nmol/s. Bulk concentrations [**RuC$_{12}$**] and [**CoC$_{12}$**] indicate theoretical concentrations assuming no losses during liposome preparation.

D.6. Quantum yield determination

The quantum yield (QY) for the photocatalytic proton reduction reaction for the fully optimised system (DPPC lipid, 5 µM CoC_{12}, 50 µM RuC_{12}, pH 4) was obtained using the following equation:

$$QY = \frac{\#\ \text{photochemical events}}{\#\ \text{photons absorbed by photoactive molecule}} = \frac{TOF_{max}\, n_{CoC12}}{\Phi_0\,(1-10^{-A_{ref}})} \qquad \text{Equation D1}$$

In Equation D1, TOF_{max} is the maximum rate of H_2 formation per catalyst molecule in s^{-1} (TOF_{max} = 81 h^{-1} = 0.0225 s^{-1}, Table 4.1) and n_{CoC12} is amount

of catalyst molecules in nmol (5 µM CoC_{12} in a 3.5 mL solutions equals 17.5 nmol), Φ_0 the photon flux of the LED in nmol/s, and $(1 - 10^{-A_{ref}})$ equals the probability of photon absorption by the liposome solution at the irradiation wavelength. Ferrioxalate actinometry was performed to quantify Φ_0 provided by the light source (13.7 nmol/s derived from Figure D4).[5,6] In this particular system, A_{ref} was not measured experimentally but calculated using the molar absorption coefficients of **RuC_{12}** ($\varepsilon = 1.32 \times 10^4$ M^{-1} cm^{-1} at λ = 450 nm in MeOH)[7], the pathlength of the photochemical reactor (2.6 cm), and the bulk concentration (50 µM) of **RuC_{12}**. Indeed, the experimentally measured absorbance of the photocatalytic liposome solution had a significant deviation from the Beer-Lambert law generated by the scattering due to the presence of the liposomes, in particular in the near-UV domain.[7] Using these values, the QY for electron transfer was determined to be 0.029 at the maximum rate of the reaction.

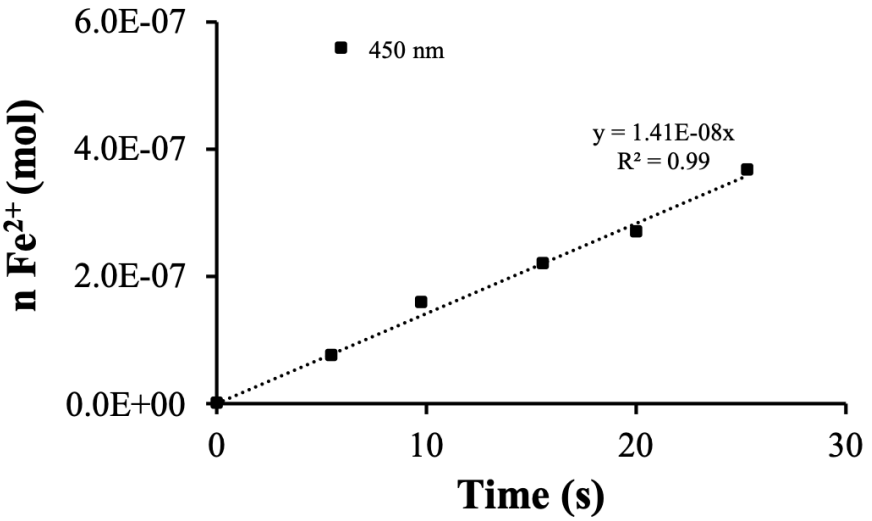

Figure D4. Ferrioxalate actinometry was performed to determine the photon flux Φ_0 (13.7 nmol/s) of the used light source (λ = 450 nm, P = 10.6 mW) within the photocatalysis setup.[5,6]

D.7. References

1 J.-S. Park, T.-J. Park, K.-H. Kim, K. Oh, M.-S. Seo, H.-I. Lee, M.-J. Jun, W. Nam and K.-M. Kim, *Bull. Korean Chem. Soc.*, 2006, **27**, 193–194.

2 D. Skrzypek, I. Madejska and J. Habdas, *Solid State Sci.*, 2007, **9**, 295–302.

3 A. Pannwitz and S. Bonnet, in *Supramolecular Catalysts — Design, Fabrication, and Applications*, 2020, pp. 495–528.

4 D. Marsh, *Handbook of Lipid Bilayers*, CRC Press, 2013.

5 C. G. Hatchard, C. A. Parker and E. J. Bowen, *Proc. R. Soc. Lond. Ser. Math. Phys. Sci.*, 1956, **235**, 518–536.

6 J. N. Demas, W. D. Bowman, E. F. Zalewski and R. A. Velapoldi, *J. Phys. Chem.*, 1981, **85**, 2766–2771.

7 D. M. Klein, S. Rodríguez-Jiménez, M. E. Hoefnagel, A. Pannwitz, A. Prabhakaran, M. A. Siegler, T. E. Keyes, E. Reisner, A. M. Brouwer and S. Bonnet, *Chem. Eur. J.*, 2021, **27**, 17203–17212.